



# **CHARACTERIZATION OF SENSING REPAIR MATERIALS**

**A Thesis**

**Presented to**

**the Faculty of the Department of Civil and Environmental Engineering**

**University of Houston**

**In Partial Fulfillment**

**of the Requirements for the Degree**

**Master of Science**

**in Civil Engineering**

**by**

**Srisothinathan Pakeetharan**

**August 2012**

# CHARACTERIZATION OF SENSING REPAIR MATERIALS

---

Srisothinathan Pakeetharan

Approved:

---

Chair of the Committee  
Cumaraswamy Vipulanandan, Professor,  
Civil and Environmental Engineering

Committee Members:

---

Ashraf S. Ayoub, Associate Professor,  
Civil and Environmental Engineering

---

Gangbing Song, Professor,  
Mechanical Engineering

---

Suresh K. Khator,  
Associate Dean,  
Cullen College of Engineering

---

Abdeldjelil "DJ" Belarbi,  
Professor and Chairman,  
Civil and Environmental Engineering

## ACKNOWLEDGEMENTS

This thesis would not have been possible without the guidance and the help of several individuals. First and foremost, I would like to express my sincere gratitude to Dr. Cumaraswamy “Vipu” Vipulanandan for his valuable guidance, kindness, and encouragement throughout the course of this study. His support will never be forgotten. I would also like to extend my appreciations to Dr. Ashraf Ayoub and Dr. Gangbing Song for serving on my thesis committee and sharing their valuable suggestions.

I am indebted to the members of the GEM group, especially Siva Sunder, Ahmed Mohammed, Jeannot Ahossin Guezo, Aram Mohammed, AbdelKader Zerrouk, Jia Liu, Lifang Wang, Wei Qiao, Dongmei Pan, Saravanan Ravichandran, Navid Salehi, Burak Kazez, Siva Vinay Moturi, Deepthi Naveen, Kalaiarasi Vembu, Prashanth Puvirajasingam Navarathinarajah Sivaruban, and Danistan Joseph, for their assistance, companionship, and encouragement. Special thanks are extended to my colleagues in the department for their support and friendship.

I owe my deepest gratitude to the faculty and the staff of Civil and Environmental Engineering Department at the University of Houston for their support and encouragement. Special thanks are due to Cherish Wallace, Stephanie Davis, Stephanie Woods, and Justin Burton. The help extended by Jeffrey Miller and Gerald McTigret through their technical expertise is also gratefully acknowledged.

The financial support provided by the CIGMAT, THC-IT, and the Department of Civil and Environmental Engineering at the University of Houston is gratefully acknowledged. Finally, I would like to thank my parents, siblings, friends, and relatives for their understanding, unconditional help, endless patience, and encouragement when it was most required. This thesis is dedicated to my parents who have supported me throughout my life.

# **CHARACTERIZATION OF SENSING REPAIR MATERIALS**

**An Abstract**

**of a**

**Thesis**

**Presented to**

**the Faculty of the Department of Civil and Environmental Engineering**

**University of Houston**

**In Partial Fulfillment**

**of the Requirements for the Degree**

**Master of Science**

**in Civil Engineering**

**by**

**Srisothinathan Pakeetharan**

**August 2012**

## **ABSTRACT**

In order to monitor construction, repairs, and maintenance of various types of structures, it is critical to develop materials used for structural applications with sensing capabilities. In this study, polymer and cement based structural grouting materials with compressive strengths in the range of 30 to 70 MPa were modified to have sensing capabilities. Piezoresistivity was considered as the sensing property and materials were tested under various service conditions in terms of strength and sensitivity. In addition, real-time application of such smart materials for low stress disaster monitoring was investigated. Also a cementitious repair material typically used in steel pipes as protective coating was investigated to evaluate the field performance in terms of shrinkage, water absorption, and strength characteristics.

For the piezoresistive cementitious and polymeric materials the resistivity change was over 10 times more than the engineering strain. A specially designed polymeric composite cantilever beam detected applied pressure as small as 1.4 kPa (~0.2 psi). The compressive stress-strain relationships of the polymer and cementitious composite were modeled using a non-linear relationship and the constitutive behavior of the piezoresistive material was modeled using incremental nonlinear stress-resistivity relationship.

# TABLE OF CONTENTS

ACKNOWLEDGEMENTS .....	iv
ABSTRACT .....	vi
TABLE OF CONTENTS .....	vii
LIST OF FIGURES .....	xii
LIST OF TABLES .....	xvi
CHAPTER 1 INTRODUCTION .....	1
1.1 Problem Statement .....	1
1.2 Objectives .....	2
1.3 Organization.....	2
CHAPTER 2 BACKGROUND AND LITERATURE REVIEW .....	4
2.1 Piezoresistivity Concept .....	4
2.1.1 Electrical Conductivity .....	4
2.1.2 Percolation Theory .....	5
2.1.3 Piezoresistivity .....	6
2.1.4 Measurement .....	7
2.2 Piezoresistive Repair Materials .....	8
2.2.1 Cementitious Material .....	8
2.2.2 Polymeric Composites.....	8
2.2.3 Additives .....	9
2.2.4 Fiber Dispersion and Modification.....	10

2.2.5 Environmental Effects .....	10
2.2.6 Curing Monitoring .....	11
2.3 Self-Sensing .....	14
2.3.1 Self-Sensing Material .....	14
2.3.2 Real Time Disaster Monitoring .....	14
2.3.3 Low Stress Monitoring .....	14
2.3.4 Piezoresistive Sensors .....	15
2.4 Tack coat .....	17
2.5 Material Modification .....	18
2.6 Shrinkage .....	20
<b>CHAPTER 3 CHARACTERIZATION OF BULK REPAIR MATERIALS .....</b>	<b>21</b>
3.1 Introduction .....	21
3.2 Materials and Methods .....	22
3.2.1 Materials .....	22
3.2.2 Mixing and Curing Conditions .....	24
3.2.3 Compression test (ASTM C39) .....	24
3.2.4 Tensile Bonding Strength Test (CIGMAT CT-3, modified ASTM C321) .....	25
3.2.5 Double Shear Bonding Strength Test (CIGMAT AC 3-08) .....	28
3.3 Stress-Strain Characterization .....	28
3.3.1 Epoxy Grout .....	28
3.3.2 Cement Grout .....	30

3.3.3 Concrete .....	33
3.3.4 Patch Material .....	34
3.4 Bonding characterization.....	36
3.4.1 Initial Characterization .....	36
3.4.2 Tensile Bonding Strength .....	37
3.4.3 Shear Bonding Strength.....	47
CHAPTER 4 SELF MONITORING BEHAVIOR OF BULK REPAIR MATERIALS .....	50
4.1 Materials and Methods .....	50
4.1.1 Materials .....	50
4.1.2 Modification and Optimization of Fiber .....	50
4.1.3 Specimen preparation .....	51
4.1.4 Compression Test .....	51
4.1.5 Tensile Test .....	51
4.1.6 Flexural Test .....	53
4.2 Piezoresistive behavior.....	55
4.2.1 Compression.....	55
4.2.2 Tension.....	61
4.2.3 Flexure .....	62
4.3 Shape Effect on Piezoresistivity .....	63
4.3.1 Slab .....	63
4.3.2 Thin Disk .....	64

4.4	Service Conditions .....	65
4.4.1	Flowability .....	65
4.4.2	Temperature cycling.....	67
4.4.3	Curing Conditions .....	73
4.4.4	Creep.....	74
4.4.5	Real Time Wireless Monitoring .....	77
4.5	Material Modification .....	79
4.5.1	Effect of Fly Ash.....	79
4.6	Low Stress Monitoring.....	80
4.6.1	Cantilever Model Design.....	80
4.6.2	Results and Discussion.....	81
4.7	Piezoresistive Structural Sensors (PRSS).....	85
4.7.1	Hollow Cylindrical Sensor .....	85
CHAPTER 5 CHARACTERIZATION OF COATING MATERIALS.....		89
5.1	Materials and Methods.....	89
5.1.1	Lab Specimens .....	89
5.1.2	Field Samples .....	90
5.2	Results and Discussion.....	91
5.2.1	Laboratory specimens .....	91
5.2.2	Field Samples .....	97
5.3	Comparison.....	99

CHAPTER 6	MODELING THE BEHAVIOR OF REPAIR MATERIALS .....	102
6.1	Stress-Strain Model.....	102
6.1.1	p-q model .....	102
6.1.2	Stress-Strain Model for Epoxy Grout.....	104
6.2	Piezoresistive Model .....	106
6.2.1	Analytical model (Sett, 2003).....	106
6.2.2	Piezoresistive Behavior Model for Epoxy Grout.....	109
CHAPTER 7	CONCLUSIONS AND RECOMMENDATIONS.....	113
7.1	Conclusions.....	113
7.2	Recommendations .....	116
REFERENCES	.....	118
APPENDIX	.....	124
A-1	Bonding Failure Modes.....	124
A-2	Impedance Spectroscopy (IS).....	125
A-3	Effect of Environmental Conditions on Piezoresistivity .....	127
(a)	Materials and Methods.....	127
(b)	Testing.....	127
(c)	Results .....	129

## LIST OF FIGURES

Figure 3-1: Particle size distribution of the dry mixes of used composites.....	23
Figure 3-2: Experimental set up for uniaxial compression testing .....	25
Figure 3-3: One type of tested crossed brick specimen .....	26
Figure 3-4: Experimental setup of tensile bonding strength test.....	27
Figure 3-5: Specimen under tensile loading .....	27
Figure 3-6: Specimen under double shear loading .....	28
Figure 3-7: Effect of fiber on stress-strain behavior of epoxy grout.....	29
Figure 3-8: Stress-strain behavior of fiber reinforced epoxy grout.....	30
Figure 3-9: Effect of fiber on stress-strain behavior of cement grout.....	31
Figure 3-10: Stress-strain behavior of fiber reinforced cement grout .....	31
Figure 3-11: Stress-Strain relationship of cement grout specimens at different curing conditions	33
Figure 3-12: Stress-Strain behavior of concrete due to material modification and fiber addition.	34
Figure 3-13: Variation of Stress Strain relationship for patch material with curing time .....	35
Figure 3-14: Compressive strength development of patch material .....	36
Figure 3-15: Comparison of Tensile bonding strength of series 1 specimens.....	37
Figure 3-16: One day tensile bonding strength of Concrete-Patch-Concrete specimens .....	40
Figure 3-17: One day tensile bonding strength of Concrete-Asphalt-Concrete specimens.....	41
Figure 3-18: One day tensile bonding strength of Patch-Asphalt-Patch specimens.....	43
Figure 3-19: Tensile bonding strength of Concrete-Patch+Asphalt+Patch-Concrete specimens..	44
Figure 3-20: Average 1day tensile bonding strength of series-2 bonding specimens .....	45
Figure 3-21: Failed specimen after subjecting to double shear.....	48
Figure 4-1: Experimental setup for compressive piezoresistive testing.....	52
Figure 4-2: Experimental setup for compressive piezoresistive testing .....	52
Figure 4-3: Experimental setup for flexural piezoresistive test .....	53

Figure 4-4: Testing Cement grout slab under 3 point bending loading.....	54
Figure 4-5: Experimental setup for testing thin disk under bending .....	54
Figure 4-6: Effect of fiber modification on Stress-Resistivity relationship for epoxy grout.....	55
Figure 4-7: Piezoresistive behavior of epoxy grout at different curing ages .....	56
Figure 4-8: Comparison of resistivity and strain for epoxy grout.....	57
Figure 4-9: Stress-Resistivity relationship of epoxy grout .....	58
Figure 4-10: Effect of fiber on stress-resistivity relationship of cement grout .....	59
Figure 4-11: Stress-resistivity relationship of cement grout.....	59
Figure 4-12: Comparison of stress-resistivity relationship of repair materials .....	60
Figure 4-13: Piezoresistive behavior of repair materials with percentage of strength .....	61
Figure 4-14: Stress-Resistivity relationship of epoxy grout under tension .....	61
Figure 4-15: Schematic of location of conductive cables in the beam.....	62
Figure 4-16: Piezoresistive behavior under flexural loading .....	62
Figure 4-17: Schematic diagram of the casted cement grout slab .....	63
Figure 4-18: Load-resistivity relationship in cement grout slab under bending loading.....	64
Figure 4-19: Stress-Resistivity relationship for thin disk under bending.....	65
Figure 4-20: Flow test for fiber reinforced cement grout using flow table .....	66
Figure 4-21: Stress-Resistivity behavior of epoxy grout specimens after subjected to different curing conditions .....	69
Figure 4-22: Variation of resistance and mass of cement grout specimens after water cured.....	71
Figure 4-23: Variation of resistance and mass of cement grout specimens after heat cured.....	71
Figure 4-24: Stress-Resistivity behavior of cement grout specimens after subjected to different curing conditions .....	72
Figure 4-25: Curing monitoring from time of casting for cement grout .....	73
Figure 4-26: Monitoring curing of patch material .....	74
Figure 4-27: Experimental setup for creep testing along with resistance measurement .....	75

Figure 4-28: Relationship between creep strain and change in resistance with time .....	76
Figure 4-29: Creep strain in each stage of loading .....	76
Figure 4-30: Experimental setup for real time wireless monitoring .....	77
Figure 4-31: Piezoresistive behavior of cement grout specimen monitored using wireless method .....	78
Figure 4-32: Real time health monitoring of cement grout specimen.....	78
Figure 4-33: Effect of Fly Ash and fiber on initial resistance of concrete .....	79
Figure 4-34: Piezoresistive behavior of concrete with and without fly ash .....	80
Figure 4-35: Stress distribution along the compression sides of stepped beam and solid beam ...	83
Figure 4-36: Schematic diagram of the stepped beam.....	83
Figure 4-37: Comparison of piezoresistive response at different locations of stepped beam .....	84
Figure 4-38: Comparison of resistivity in bending with pure compression .....	84
Figure 4-39: Schematic diagram of hollow cylindrical sensor .....	85
Figure 4-40: Piezoresistive behavior of hollow cylindrical sensor .....	86
Figure 4-41: Comparison of piezoresistive behavior of PRSS .....	87
Figure 5-1: Comparison of compressive strength of series-2 laboratory coating specimens .....	93
Figure 5-2: Strength gain of coating specimens with curing age.....	94
Figure 5-3: Shrinkage measurement on beam (0.17 w/d, #B1) .....	94
Figure 5-4: Monitoring the change in mass of beams made of the coating material.....	95
Figure 5-5: Properties of beams .....	96
Figure 5-6: Failed Geospray beams after subjecting to four point flexural loading.....	96
Figure 5-7: Mapping of thickness of series-2 field samples .....	98
Figure 5-8: Water absorption test for field coating samples (series #2) .....	99
Figure 5-9: Comparison of unit weight of field and lab coating specimens .....	100
Figure 5-10: Comparison of PWV measured across depth/thickness in coating specimens .....	100
Figure 5-11: Relationship between PWV and unit weight for coating specimens .....	101

Figure 6-1: Optimization of parameter $p$ .....	103
Figure 6-2: Typical stress-strain prediction for epoxy grout .....	104
Figure 6-3: Stress-Strain model for epoxy grout .....	105
Figure 6-4: Model prediction for stress-strain behavior of epoxy grout .....	106
Figure 6-5: Modeling piezoresistive behavior of epoxy grout.....	110
Figure 6-6: Piezoresistive behavior model for epoxy grout.....	111
Figure 6-7: Typical piezoresistive behavior model of epoxy grout .....	111
Figure A-1: Equivalent circuit representing piezoresistive structural sensor.....	125
Figure A-2: Schematic diagram of the IS testing arrangement with ohm meter.....	126
Figure A-3: Variation of Mass in cement grout specimens under temperature cycles.....	130
Figure A-4: Variation of Mass in epoxy grout specimens under temperature cycles .....	130
Figure A-5: Variation of Mass in cement grout specimens under wet-dry cycles .....	131
Figure A-6: Variation of Mass in epoxy grout specimens under wet-dry cycles .....	131
Figure A-7: Variation of electrical resistance in cement grout specimens under temperature cycles .....	132
Figure A-8: Variation of electrical resistance in epoxy grout specimens under temperature cycles .....	133
Figure A-9: Variation of electrical resistance in cement grout specimens under wet-dry cycles	133
Figure A-10: Variation of electrical resistance in epoxy grout specimens under wet-dry cycles	134
Figure A-11: Stress-Resistivity relationship for cement grout specimens after temperature cycles .....	135
Figure A-12: Stress-Resistivity relationship for cement grout specimens after wet-dry cycles..	136
Figure A-13: Stress-Resistivity relationship for epoxy grout specimens after temperature cycles .....	136
Figure A-14: Stress-Resistivity relationship for epoxy grout specimens after wet-dry cycles....	137

## LIST OF TABLES

Table 2-1: Summary of literature related to piezoresistivity .....	12
Table 2-2: Summary of literature related to piezoresistivity (continued) .....	13
Table 2-3: Recent studies on piezoresistivity in polymer & cement composites .....	16
Table 2-4: Summary of studies related to tack coat.....	19
Table 3-1: Type of materials studied.....	22
Table 3-2: Particle size distribution of dry mixes.....	23
Table 3-3: Different curing conditions applied for cement grout specimens .....	32
Table 3-4: Summary of Compressive strength of patch material with curing time.....	35
Table 3-5: Tensile bonding test results for first series .....	37
Table 3-6: List of specimens for series 2.....	38
Table 3-7: Test results for Concrete-Patch-Concrete specimens (all Type-3 Failure) .....	39
Table 3-8: Test results for Concrete-Asphalt-Concrete specimens.....	41
Table 3-9: Test results for Patch-Asphalt-Patch specimens (All Type-2 Failure) .....	42
Table 3-10: Test results for Concrete-(Patch+Asphalt+Patch)-Concrete specimens .....	44
Table 3-11: Summary of testing program and results for 2nd series studies of patch.....	45
Table 3-12: Types of failures observed in tensile bonding test .....	46
Table 4-1: Flow measurement for fiber loaded cement grout.....	66
Table 4-2: Different curing conditions applied for epoxy grout specimens.....	67
Table 4-3: Variation of initial resistance of epoxy grout at various curing conditions .....	68
Table 4-4: Variation of mass of epoxy grout at various curing conditions .....	68
Table 4-5: Variation of initial resistance of cement grout at various curing conditions .....	70
Table 4-6: Variation of mass of cement grout at various curing conditions .....	70
Table 5-1: Characterization of series-2 laboratory coating specimens .....	92
Table 5-2: Summary of results for test on beams made of the coating material .....	95

Table 5-3: Characterization of series-1 field coating samples .....	97
Table 6-1: Stress-strain model parameters for epoxy grout .....	105
Table 6-2: Piezoresistive coefficients of epoxy grout.....	112
Table A-1: Failure modes in tensile bonding strength test (Liu and Vipulanandan, 2005).....	124
Table A-2: Testing conditions for the piezoresistive grout specimens .....	127
Table A-3: Summary of cement grout (MM) specimens tested for piezoresistivity .....	128
Table A-4: Summary of epoxy grout (LL) specimens tested for piezoresistivity .....	128
Table A-5: Summary of strength ( $\sigma$ ) and changes in resistance ( $\Delta R$ ) and mass ( $\Delta M$ ) after 7 cycles.....	129
Table A-6: Change in resistivity at certain percentage of strength for epoxy grout and cement grout specimens after subjecting to temperature cycles and wet-dry cycles .....	138

# CHAPTER 1 INTRODUCTION

## 1.1 Problem Statement

The ability of a material to self-sense while sustaining its structural properties such as strength or toughness makes it unique. In other words the material monitoring itself depending on its intrinsic electrical resistivity makes it an ideal candidate for ‘smart material’ where no embedded or externally attached sensor is required for the structural health monitoring. Hence piezoresistive property of carbon fiber reinforced composites are being studied by many researchers for numerous applications including stress/strain sensing, damage monitoring, and health monitoring of structures.

Smart materials have been studied by researchers around the world, however, mainly in the context as a construction material. Nowadays maintenance and rehabilitation of civil engineering structures, especially aging bridges and buildings, are of increasing importance. Hence, repair materials, either bulk materials such as polymeric composites or cementitious composites or coating materials, capture a lot of interest. If the repair material can be made self-sensing, it will aid in monitoring the repaired component for its own health in addition to providing structural compatibility and performance. Hence, it is important to optimize the composition of the materials and also experimental characterization of such repair materials under different loading and service conditions needs to be done.

It is critical to monitor structures during disaster events to study the effect of different intensity loadings. Considering hurricanes, since the pressure applied by the wind on structures is small, the sensors should be made highly sensitive to detect it (ASCE 7-10). Very limited information is available in the literature on structural materials that can sense that small stress. Prashanth and Vipulanandan (2010) reported small pressures in the order of 38 kPa (5.4 psi) detected by a piezoresistive structural sensor (PRSS). This current study attempts to measure even

smaller pressures (1.4 kPa) by piezoresistivity of polymeric composite material in order for disaster monitoring.

## **1.2 Objectives**

The main objective of this research was to characterize repair materials for infrastructure applications. The specific objectives are as follows:

- 1) Investigate the effect of carbon fibers on the mechanical behavior of bulk repair materials.
- 2) Quantify the bonding ability of a cementitious repair material to concrete and asphalt.
- 3) Characterize a coating material in terms of strength, water absorption, and shrinkage properties.
- 4) Investigate the effect of shape, service conditions and material modification on piezoresistive behavior, and design and test stepped cantilever beam to measure pressure of the order of 1.4 kPa (0.2 psi).
- 5) Model the nonlinear behavior of repair material, comprising stress-strain and stress-resistivity relationships.

## **1.3 Organization**

This thesis is organized into seven chapters, Chapter 1 is the introduction. Chapter 2 summarizes the background and literature review related to characterization of polymeric and cementitious repair materials. Especially, studies related to self-sensing ability of materials is reviewed. Structural behavior of repair materials with and without carbon fiber is presented in Chapter 3. Mainly compressive behavior of bulk repair materials and bonding behavior of a cementitious repair material are presented. In Chapter 4, the experimental characterization of self-monitoring behavior of carbon fiber reinforced bulk repair materials under compressive, tensile and flexural loadings are summarized. Effect of shape, service conditions, and material

modification on piezoresistive behavior is also included. In addition the ability of the polymeric composite to sense low stress during disaster was investigated. Characterization of coating material in terms of strength, water absorption, and shrinkage properties is included in Chapter 5. Modeling of nonlinear material behavior, comprising stress-strain, and stress-resistivity relationships, is included in Chapter 6. Finally, the conclusions and recommendations of this research have been summarized in Chapter 7.

## CHAPTER 2 BACKGROUND AND LITERATURE REVIEW

### Introduction

The main purpose of this chapter is to provide a comprehensive review on the topics that are closely related to the proposed research. In view of characterization of sensing repair materials, this chapter summarizes the past and present research on repair materials and recent developments on self-sensing behavior. Furthermore studies on application of self-sensing materials, especially structural health monitoring, are reviewed.

### 2.1 Piezoresistivity Concept

#### 2.1.1 Electrical Conductivity

Electrical resistivity (often referred as resistivity or volume resistivity) is a measure of how strongly a material opposes the flow of electric current. A low resistivity indicates a material that readily allows the movement of electric charge. Resistivity,  $\rho$  is given by

$$\rho = RA/l \quad (2-1)$$

where  $R$  is the electrical resistance (measured in  $\Omega$ ),  $l$  and  $A$  are length and cross-sectional area of the specimen respectively. Conductivity (or specific conductance) is a measure of a composite's ability to conduct electricity. Conductivity,  $\sigma$  is measured in Siemens per meter (S/m) or by  $(\Omega \cdot \text{cm})^{-1}$  and given by

$$\sigma = 1/\rho \quad (2-2)$$

Thus it occurs for a given case, the lower the resistivity, the higher the conductivity is. Two types of electrical conduction exist; electronic (motion of free electrons in the conductive phases causes conduction) and electrolytic (the motion of ions in the pore solution causes conduction). Fresh cement pastes conduct electricity electrolytically (Non Ohmic conduction) and with addition of

conductive fibers (or filler), conduction is electronic (Ohmic). If a polymer composite (or cementitious composite) should be able to self-sense strain, used fibers must be more conducting than the matrix. Moreover the fiber diameter should be less than crack length, and fiber should be well dispersed (Chung, 2002).

Carbon fibers have been studied and used by many researchers as good conductive filler [(Sett, 2003), (Chung, 2002), (Bing et al., 2004), (Manuela & Raffaele, 2004), and (Hui et al., 2006)]. Depending of method of manufacturing, carbon fiber falls into two categories; viz. PAN (Polyacrylonitrile based) and pitch (coal tar and petroleum products based). Carbon fiber can be any one of continuous carbon fibers, short carbon fibers, short carbon filaments and carbon black.

### **2.1.2 Percolation Theory**

The resistivity of multiphase solids, with one phase conductive and others insulated, depends on the volume content of conducting solids (Sett, 2003). For very low fraction of conductive solids, the mean distance between adjacent solids is large and the resistance is limited by insulative solids. The conducting solids get closer and form linkages, when a sufficient amount of conductive solids are loaded. The critical amount of conducting solids at which materials change from insulator to conductor is referred to as percolation threshold. The essence of percolation theory is to determine how a given set of lattices, regularly or randomly positioned in some space, is interconnected.

There exists a percolation threshold in fiber-matrix (polymeric or cementitious) composites, above which fibers touch one another to form continuous electrical path ((Chung, 2002), (Sett, 2003)). Here conductivity is by contact resistance at fiber-fiber contact. On the other hand at filler contents below percolation threshold, contact resistance at fiber-matrix interface governs conductivity. The resistance of the contact spots is the leading contributor to the overall composite resistivity (Sett, 2003). The constriction resistance of a contact spot and the tunneling resistance between the conductive solids are the two factors which contribute to the contact

resistance. Tunneling is defined as the transfer of electrons which occur when two fibers are close by, even though the fibers do not physically contact each other.

In a study done by Manuela and Raffaele (2004), with a water/cement ratio of 0.45 and sand/cement ratio of 1.0, percolation threshold was found to be 0.15 % when using 6 mm carbon fiber and it gave an electrical conductivity of  $0.1 (\Omega \cdot \text{cm})^{-1}$ . Threshold value was less for long carbon fiber (6 mm) compared to short carbon fiber (3mm). Bing et al. (2004) found that electrical conductivity of cement based composite reduced from 0.0028 to 0.0015 S/cm when increasing the s/c ratio from 0 to 3 while keeping the w/c ratio at 0.45 and CF content at 0.4%. While studying voltage-current behavior of epoxy based composite, non Ohmic behavior was observed by Yang et al. (2007) when short carbon fiber volume content was less than 8%. Ohmic behavior occurred when content was increased up to 20%.

Bing et al. (2005) reported that adjacent fibers connect with each other under compression (in lower stress values) and conductivity increases (or resistance decreases). If the stress value increases, it causes crack opening and consequently fibers pull out. This leads to breakage of conductive network and an overall increase in resistivity as a result. Similar trend was reported by Sett (2003) for fiber reinforced polymer composite.

### **2.1.3 Piezoresistivity**

A material is said to be piezoresistive if resistivity of that material changes under applied stress. In contrast to the piezoelectric effect, the piezoresistive effect only causes a change in electrical resistance; it does not produce an electric potential. Piezoresistivity has been proven to be a good sensing property in the literature [(Carmona et al., 1987), (Durand and Tellier, 1996), (Vipulanandan and Sett, 2004) and (Todoroki et al., 2009)]. It can be used to self-sense stress/strain, sense damage and thermoelectric properties and monitor health of the structure and more. Development and characterization of piezoresistive smart structural materials led a new path to study on Piezoresistive Structural Sensors (PRSS).

Extensive research is being done on self-monitoring behavior and piezoresistivity of composites. Cement based composites have been studied by many researchers [(Chung, 1999), (Bing et al., 2004), (Manuela & Raffaele, 2004), (Hui et al., 2006), and (Zhang et al., 2007)] while few [(Choi & Chung, 2000), (Vipulanandan & Sett, 2004), and (Yang et al., 2007)] reported on composites like polymer concrete. These polymeric and cementitious composites serve in a wide range of applications such as aerospace, automotive, marine, and construction industries.

#### **2.1.4 Measurement**

Since electrodes should be attached in order to measure resistance, type, size, and number of electrodes (or probes) matter. Conductive cable, copper electrode and steel nets were commonly used in the literature. Most of the researchers attached the electrodes at the ends or around the perimeter while few embedded electrodes inside specimen [(Sett, 2003), (Bing et al., 2004), (Prashanth, 2010)]. Effect of number of probes on resistance values was studied by Manuela and Raffaele (2004). In 4-probe method, current flows in external probes and potential was measured in internal probes. According to the study, the 4-probe method gave smaller scatter in experimental data in contrast to the 2-probe method for which higher variation was observed. Furthermore it was reported that electrode contact area strongly influenced resistance measurements. Manuela and Raffaele (2004) studied the influence of AC/DC power supply on resistance. Hui et al. (2006) reported that shortening the probe distance has no significant effect on stress strain relationship.

Impedance spectroscopy (IS) is a powerful method of characterizing electrical properties of materials and their interfaces with electronically conducting electrodes. It was reported by Reza et al. (2003) that with AC supply, a constant value was observed for impedance at the frequency of 100 kHz which indicates pure ohm resistance (real part of impedance). Prashanth (2010) used IS to measure the contact resistance inherent in a polymeric composite using two

probe method. It was proved that contact resistance is less than 1% of the bulk resistance and therefore not significant. Mason et al. (2002) investigated the various factors governing the impedance spectra of fiber reinforced cement composites, including fiber aspect ratios, fiber volume fractions fiber orientation and fiber shape using steel and carbon fiber reinforced composites.

## **2.2 Piezoresistive Repair Materials**

### **2.2.1 Cementitious Material**

Chung (2002) reported the variation of fractional change in longitudinal resistivity and longitudinal strain with time for cement based composites reinforced by 0.72 and 0.36 vol. % short steel fiber (8  $\mu\text{m}$  diameter), 0.5 vol. % short carbon fiber (15  $\mu\text{m}$  diameter and 5mm length), and 0.5 vol. % short carbon filaments. The resistivity increased upon tension and reduced under compression. The fractional change in resistivity under tension (<0.5 MPa) varied from 0 to 30% and under compression (max 6 MPa) varied from 0 to 25%. Also 0.5 vol. % carbon fiber reinforced cement paste showed a resistivity of  $1.5 \pm 0.1 * 10^4 \Omega.\text{cm}$ .

A study was done by Manuela and Raffaele (2004) to investigate the curing effects and percolation on piezoresistivity of cementitious composite. Sand and silica fume were used in that study along with 0.15% short carbon fiber. Conductivity in the order of  $0.1 (\Omega.\text{cm})^{-1}$  were reported. In another study done by Bing et al. (2005) resistivity of a silica fume added cementitious composite decreased by 0.26% until 57% stress level.

### **2.2.2 Polymeric Composites**

Polymer is a popular alternate material to cement because of its rapid setting, high strength to density ratio, high specific stiffness, outstanding fatigue performance and ability to withstand corrosive environments (Sett, 2003 and Boger et al. 2008). Fiber-reinforced polymer

(also fiber-reinforced plastic and often referred as FRP) is a composite material made of a polymer matrix reinforced with fibers. In literature, polymer was commonly epoxy or polyester thermosetting plastic and fibers were mainly carbon based or steel based.

A study was done by Vipulanandan and Sett (2004) on piezoresistivity of polymer concrete based on workability and performance. Polyester Resin (20% by wt.), sand and conductive fillers were the constituents along with Cobalt naphthanate (CN) and methyl ethyl ketone peroxide (MEKPO) as initiator and promoter. Insulator material became a conductor with 3% conductive filler content. It was reported that though the increase in conductive fiber content improved the mechanical properties, it deteriorated the self-monitoring properties. Thus optimum conductive filler was derived as 6% by weight and used in the studies. Resistivity was less than 100  $\Omega$ .cm with 6% conductive filler loading.

### **2.2.3 Additives**

Studies have been reported in the literature on characterizing the effect of water/cement ratio (w/c), additive content and conductive filler content on piezoresistive behavior of composites. Researchers found that some additives (other than conductive solids) had worthy effect on piezoresistivity. As reported by Chung (1999), addition of a second filler (silica fume or sand), that is essentially nonconducting, decreased the resistivity of the composites only at low volume fractions (below 1% by vol. for silica fume and 0.5% for sand). The change was attributed to the improved fiber dispersion. Lim and Mohd (2008) studied the effect of filler on strength development of epoxy grout which is used as structural repair material. Epoxy resin (a thermosetting polymer) and hardener were mixed with graded sand and ground granulated blast furnace slag (GGBFS, a filler). Consistency of flow and strength were not affected when sand was replaced by slag up to 50%. It reduced the brittleness, and enhanced cohesiveness and durability.

#### **2.2.4 Fiber Dispersion and Modification**

Fiber dispersion plays an important role in piezoresistive behavior. Zhang et al. (2007) used silica fume together with methyl cellulose (defoamer) and water reducing agent (contains sodium salt of condensed naphthalene sulfonic acid) partly to help fiber dispersion. Chuang et al. (2008) used a new dispersant (hydroxyethyl cellulose) to disperse fibers using an ultrasonic wave.

Treatment of fillers proved to be a good method to improve the piezoresistivity. Chung (1999) did a study with ozone, dichromate, and silane as treatments for silica fume. Silane treated silica fumes gave substantially higher strength and modulus than as-received. With silane treated fibers, strength was 56% higher where it was 26% without treatment; making silane treatment of silica fume and fibers equally valuable. Carbon fiber oxidized with nitric acid as well as treated with a coupling agent (glutaric dialdehyde) was used by Choi et al. (2000) to check the effect on electrical and mechanical properties. Electrical conductivity of composite made using fiber treated with coupling agent showed an increase (from 0.1 to 0.4 S/cm) at 10% carbon fiber by wt. Under constant current and temperature, electrical stability is best for specimen with high strength carbon fiber and worst for high modulus carbon fiber (Yang et al. 2007).

#### **2.2.5 Environmental Effects**

One or all of curing time, temperature, and relative humidity can have influence on electrical resistivity. At one day of curing and lower sand/cement values (<0.5) cement based composite was highly conductive and with the increase of sand, conductivity diminished as reported by Manuela and Raffaele (2004). Zhang et al. (2007) observed that resistance increased with curing age linearly until 21 days (around 14 k $\Omega$ ) & nonlinearly after that. 21 days was attributed as near the ending of hydration. Bing et al. (2004) found that relative humidity influenced the conductivity of the composites in low fiber contents (<0.6 %), and it had no significant effect when CF content was increased. Manuela and Raffaele (2004) studied the effect

of hydration time on threshold value of conductivity and found no significant effect even though values decreased a little in lower fiber contents. Behavior at 28 days is attractive for resistance-based strain sensing considering the reversibility and noise (Chung 1999).

### **2.2.6 Curing Monitoring**

Abo El-Enein et al. (1995) studied the influence of silica fume on curing of concrete and electrical conductivity. Electrical conductivity of cement paste, cement mortar and concrete was measured during setting and hardening. Electrical conductivity increased to reach a peak at 1-3 hours of hydration and then decreased gradually. Increase in conductivity was attributed to increase of ionic concentration and the mobility of ions during the initial stages. At later stages of hydration, formation and later accumulation of cement hydrates resulted in decrease in conductivity. It was concluded that electrical conductivity can be used as an indicator for setting characteristics and the structural changes of hardened pastes with and without silica fume. Also it was observed that electrical conductivity increased as the water to cement ratio increased.

Choi et al. (2000) discussed about the possibility of temperature sensing through the thermistor effect. It was reported that the resistivity for CF and silica fume filled cement paste decreases upon heating (from  $4.5 \times 10^4 \Omega \cdot \text{cm}$  at  $2^\circ\text{C}$  to  $0.5 \times 10^4 \Omega \cdot \text{cm}$  at  $45^\circ\text{C}$ ) and the effect was quite reversible upon cooling (returns to  $5.3 \times 10^4 \Omega \cdot \text{cm}$  at  $2^\circ\text{C}$ ).

McCarter et al. (2005) measured the spatial distribution of electrical conductivity within the cover-zone of concrete specimens subjected to a range of natural exposure conditions using an electrode array system. They found that conductivity measurement can be used as an indicator of free ions in pore solution.

A summary of reviewed literature related to piezoresistivity are shown in Table 2-1. About 25% of studies comprised of polymeric composites and 69% used cementitious composites. As reported, 31% used pitch based carbon fibers and 38% used PAN based carbon fibers. Around 31% of the researchers used the 2-probe method. Most of the studies (~44%) were concentrated on characterizing piezoresistivity under compressive or tensile loading.

**Table 2-1: Summary of literature related to piezoresistivity**

Reference	Main parts	Conductive fiber & content	Electrical measurement	Piezoresistivity	Main study	Remarks
Boschetti-de-fierro et al. (2009)	Epoxy, resin	PAN 0.02-0.24%	Cu-Ag 2 probe at ends, Stainless steel embedment 2 probe	Unidirectional gage factors 0° ply- 416.7 90° ply- 50	Effect of arrangements of reinforcement under tensile stress	Composite with 2.5 wt. % was suitable for real time monitoring
Chuang et al. (2008)	Cement, silica fume	PAN-5mm	-	Carbon fiber dispersion	Effect of ultrasonic waves on improving the dispersion	Compressive, tensile strengths increased, flexural strength decreased
Yang et al. (2007)	Epoxy, resin	Pitch-continuous	Cu cable with Ag paint	R <sub>0</sub> range: 3.188 Ω to 13.164 Ω	Temperature sensitivity of fiber reinforced polymer concrete	Showed resistance can be used as a temperature sensor
Zhang et al. (2007)	Cement, aggregate, silica fume	PAN, 7μm 3 mm 0.2,0.5%	DC, 2 probe, steel net	40% increase at 21 days	Curing age	Studied the effect of water reducing agent
Sihai & Chung (2007)	Cement, sand, silica fume	Pitch, 15 μm 5 mm 0.3-1.5%	DC, 4 probe around specimen	-	Sand volume fraction optimization	Did Ozone treatment for CF
Hui et al. (2006)	Cement	120 nm carbon black 5-25%	DC, 4 probe, Cu net	8000 to 100 Ω.cm Gage factor 55.28	Stress-strain	Dealt effect of probe distance
Bing et al. (2005)	Cement, silica fume	Pitch, 7μm 0.8%	2 probe Cu electrode	Δρ/ρ decreased by 0.26% until 57% stress level	Compressive strength	Studied behavior under loading & unloading
Vipulanandan & Sett (2004)	Polyester resin, sand	Short carbon fiber, 6%	Conductive cable, embedded	< 100 Ω.cm at 6% CF	Tensile properties	Piezoresistive model was proposed
Manuela & Raffaele (2004)	Cement, sand, silica fume	PAN, 8μm 3,6 mm, 0.15%	AC, 2&4 probe, Cu electrode	Conductivity 0.1 (Ω.cm) <sup>-1</sup>	Hydration time, percolation, curing	Curing effect on conductivity was studied

**Table 2-2: Summary of literature related to piezoresistivity (continued)**

Reference	Main parts	Conductive fiber & content	Electrical measurement	Piezoresistivity	Main study	Remarks
Bing et al. (2004)	Cement sand	Pitch, 7 $\mu$ m	2 probe Cu-embedded	0.0028 to 0.0015 S/cm	Percolation & fiber length	Effect of humidity was studied
Chen and Lin (2004)	Diabase, limestone and marble rock samples	NaCl solution	Gelatin mixed Cu powder, 2 probe	Nonlinear piezoresistive behavior	Stress-strain-electric resistance relationship during compression	Change in resistivity was modeled by considering the behavior in 4 different sections
Reza et al. (2003)	Cement, sand, silica fume	PAN 6mm 0.2-0.6%	Cu electrode-Ag paint, 4 probe	Average sensitivity of 0.003 $\Omega$ /MPa	AC measurements at 20 Hz, 100 Hz, 10 kHz 1 MHz frequency	Resistance change reversible when loading up to 30% of the ultimate strength
Chung (2002)	cement	15 $\mu$ m CF, 0.5%	DC supply	25-30% increase	Tensile & comp strength, curing	Reported behavior while curing
Choi et al. (2000)	Phenolic resin comp	PAN, 6.8 $\mu$ m 2mm, 10%	-	Conductivity 0.1 to 0.4 S/cm	Mechanical properties	Studied oxidization and effect of coupling agent
Chung (1999)	cement	Pitch, 15 $\mu$ m 5 mm 0.2, 0.5%	-	from 0.1 to 0.4 S/cm at 10% CF by wt.	Effect on piezoresistivity by fiber treatment	Treatment of fillers improved piezoresistivity. Addition of 2 <sup>nd</sup> filler reduced resistivity
				10% at 7 days, 2% at 28 days 4.5*10 <sup>4</sup> $\Omega$ .cm	thermistor effect, curing age	Surface treatment on CF was studied
Abo El-Enein et al. (1995)	Sand cement silica fume	-	-	-	influence of silica fume on electrical conductivity	Conductivity increased to reach a peak at 1-3 hours of hydration and then decreased gradually
<b>Remarks</b>	25% polymeric 69% cement.	31% pitch 38% pan base fiber	19% reported 4-probe and 31% 2-probe. 44% Cu elect. 12% embedded	44% analyzed conductivity 19% resistivity	44% studied strength	Fiber treatment & optimization, curing conditions, and sensing abilities studied

## **2.3 Self-Sensing**

### **2.3.1 Self-Sensing Material**

Emerging applications especially related to disasters require the material to be multifunctional. These functions include structural strength, self-sensing, electromagnetic interference shielding and thermal interfacing pertain to applications (Wen and Chung, 2007). A material which can monitor itself depending on its intrinsic properties is referred to as self-sensing or self-monitoring material (Sett, 2003). With self-sensing materials, embedded or externally attached sensors are not required because of their greater sensing capability and lower cost. Self-sensing ability is essential for load monitoring, structural health monitoring and structural vibration control (Wen and Chung, 2007). However the multifunctional smart self-monitoring materials should respond to applied stresses and other changes while performing as per structural requirements.

### **2.3.2 Real Time Disaster Monitoring**

Natural disasters such as earthquakes, tornados and hurricanes impose random and extreme loads on structure which cause partial damage or collapsing of structures. Since these types of disaster can be sudden, it is important to monitor the behavior of structures which are prone to such disasters. As summarized by Kiremidjian et al. (1997), four important components are required to have a robust health monitoring system during a disaster. They are, identifying the presence of damage, location of damage in the structure, severity of damage and remaining service life.

### **2.3.3 Low Stress Monitoring**

While a structure is exposed to wind, the surface areas of it are subjected to varying pressures that are continuously changing. It is critical to monitor structures during disaster events

to study the effect of different intensity loadings. As per the provisions for wind loads on structures in ASCE 7-10, velocity pressure exerted by a 50 m/s gust on a part of a structure which is 10 m above ground is 1.28 kPa (0.186 psi). According to Saffir–Simpson Hurricane Scale which categorizes the hurricanes depending on the intensities of their sustained wind, the speed 50 m/s is the lower limit for category 3.

Since the pressure applied by hurricane winds on structures are small, the sensors should be made highly sensitive to detect minute pressures. Very limited information is available in literature on structural materials that can sense very small stresses. Prashanth and Vipulanandan (2010) studied piezoresistive structural sensors (PRSS) of different shapes and sizes that were developed to sense small stresses in different applications such as wall of a water pipe and civil infrastructures during hurricanes. Those shapes were tested under compression, tension and bending loading conditions to obtain mechanical and self-monitoring characteristics. As reported by Prashanth and Vipulanandan (2010), the smallest stresses that could be measured using a thin circular disk shaped piezoresistive structural sensor (PRSS) were 50 kPa (7.4 psi) and 38 kPa (5.4 psi) during bending and splitting tensile loading, respectively. In that study disks with different thicknesses were investigated to determine the effect of specimen thickness on the sensitivity, and it was shown that the sensitivity increased when the disk thickness was reduced.

#### **2.3.4 Piezoresistive Sensors**

As summarized in Table 2-2, polymeric and cementitious materials have been used to develop piezoresistive sensors. Also varying amount of conductive fibers and fillers has been used. The amount of conductive fillers used varied from 0.2% to 6% (Table 2-2) and piezoresistive materials with various sizes and shapes have been tested in compression, tension and bending. The maximum change in resistivity varied from 3 to 40%. Also, linear, nonlinear and incremental models have been used to model the material behavior.

**Table 2-3: Recent studies on piezoresistivity in polymer & cement composites**

Reference	Material	Conductive filler and amount	Shape/ Test	Max $\Delta\rho/\rho_0$	Piezoresistive Model	Remarks
Ku-Herrera & Aviles (2012)	Vinyl ester resin	0.3% Carbon nanotube w/w	Dumb-bell/ tension	3%	Linear relationship	Nonlinear compressive behavior
Prashanth & Vipulanandan (2010)	Resin & sand	6% carbon fiber w/w	Thin disk/ bending & splitting T	25%	Linear trend	Lowest stress of 5.4 psi was sensed
Boger et al. (2008)	Epoxy resin & glass fiber laminate	0.3% Nano carbon particles	Beam/ tension & bending	10-40%	Exponential power law	$\Delta R$ was related to dynamic modulus
Waterfall et al. (2008)	Poly-silicon	-	Folded beam/ bending	10%	Nonlinear model	Micro scale specimen
Wen and Chung, (2007)	Cement & silica fume	Short carbon fiber & Carbon black, 0.5-3.5% w/w	Cube/ compression	20%	-	EMI shielding effectiveness was analyzed
Chen et al. (2005)	Cement & silica fume	0.2-0.8% short carbon fiber v/v	Cube/ compression	20%	-	Memory effect on resistance under repetitive loading
Vipulanandan & Sett (2004)	Resin & sand	3, 6% conductive filler w/w	Dumb-bell/ tension	6%	Incremental nonlinear model	Stress & strain were related to resistivity
<b>Remarks</b>	Polymer and cement based materials have been used	0.2 % to 6% conductive fiber/filler used	Various shapes/ Compression, tension and bending tests performed	Varied from 3% to 40%	Linear, non-linear and incremental models	Have the potential for multiple applications

Piezoresistive model proposed by Vipulanandan and Sett (2004) is of interest and is given by,

$$\left(\frac{\Delta\rho}{\rho_o}\right)_i = \Pi_{ijk} \Delta\sigma_{jk} = \Pi_{ijk} C_{jkmn} \Delta\varepsilon_{mn} = M_{ijk} \Delta\varepsilon_{jk} . \quad (2-3)$$

In Eqn. 2-3,  $\frac{\Delta\rho}{\rho_o}$  is fractional change in resistivity,  $\Pi$  is piezoresistivity coefficient which relates specific change in electrical resistivity to change in stress tensor, and  $M$  is elasto-resistance tensor (known as gage factor) which signifies sensitivity of change in resistivity measurement to strain. Both piezoresistivity coefficient and gage factor were used to quantify piezosensitivity.

## 2.4 Tack coat

For cases where an existing cement concrete pavement is repaired by laying fresh asphalt concrete over it, good bonding between the asphalt and cement concrete is very critical for the transfer of forces arising from the traffic loads. Slippage cracks often appear under the shearing action of traffic due to turning of the vehicles at a curve or due to braking traction generated between the tire and the pavement. This may lead to extensive cracking, delamination, and development of pot-holes (Romanoschi and Metcalf, 2001). Due to sustained traffic loads, varying temperatures, and exposure to moisture, the interlayer bonding may weaken changing the state of adhesion at the interfaces. Even a small amount of slippage is enough to generate strains nearing full slippage cases (Sahin et al., 1987). Insufficient bond decreases pavement bearing capacity and may cause tensile stresses to be concentrated at the bottom of the wearing course. Such concentrated stresses may accelerate fatigue cracking and lead to total pavement failure (Mohammad et al., 2002). Hence the importance of proper bond between the existing under layer and the freshly laid asphalt course cannot be undermined.

Tack coats are used for bonding existing and newly laid surfaces. Normally three types of tack coat are used; asphaltic emulsions, cutback asphalts and asphalt cements. Bonding of tack coat depends on many parameters including material, application rate, temperature, surface properties. As reviewed in the report ICT-R55 by Al-Qadi et al. (2008), many studies have been performed in the past investigating the bonding properties of tack coats. Uzan et al. (1978) studied the interface adhesion properties of hot mixed asphalt (HMA) layers based on direct shear tests. Santagata et al. (1994) used a shear strength testing apparatus to evaluate the strength of tack coat interfaces. In this, displacement was measured in normal and shear direction. Tshegg et al. (1995) developed a testing method called wedge splitting tension. A fixture was developed at Virginia Tech by Donovan et al. (2000) which is based on direct shear test. Tashman et al. (2006) used a torque bond test and Pull-off test device to characterize tack coat materials.

Liu and Vipulanandan (2005) investigated the tensile bonding characteristics of epoxy coating to wet and dry concrete. One of the test methods was done according to CIGMAT CT-3 standard where coating was sandwiched between a pair of rectangular concrete blocks and then tested for bonding strength. Five failure types were identified namely; concrete failure, coating failure, bonding interface failure, bonding+concrete failure and bonding+coating failure. Illustration of these failure types are shown in appendix (A-1). Table 2-4 summarizes the studies related to tack coat.

## **2.5 Material Modification**

Admixtures such as fly ash have worthy effects on improving strength of materials (Chowdhury and Basu, 2010). Fly ash has many benefits as a partial replacement material for cement. Components of fly ash vary considerably, but all fly ash includes substantial amounts of silicon dioxide ( $\text{SiO}_2$ ) (both amorphous and crystalline) and calcium oxide ( $\text{CaO}$ ). Class F fly ash is pozzolanic in nature, and contains less than 20% lime ( $\text{CaO}$ ). As fly ash continues to hydrate

after 28 days, hydrated products modify microstructure, seal cracks and prolong the service life. These kinds of admixtures have potential for improving the piezoresistivity as well.

Basheer et al. (2002) studied the resistance of concretes containing alternative cementitious materials (ACM) to chloride penetration by using electrical resistance measurement. The studied ACMs were pulverized fuel ash, ground granulated blast furnace slag, microsilica and metakaolin. Microsilica and metakaolin react with calcium hydroxide which is released during hydration process of Portland cement. This results in improved resistance against chloride penetration from early age. On the other hand, fly ash and slag will be effective in later stages only because of their late hydration. Change in electrical resistance could be due to continued hydration, pozzolanic reaction, chloride binding or a combination of these.

**Table 2-4: Summary of studies related to tack coat**

<b>Authors</b>	<b>Year</b>	<b>Purpose of study</b>	<b>Primary test</b>	<b>Remarks</b>
Uzan et al.	1978	Study the interface adhesion properties of HMA layers	direct shear tests	
Santagata et al.	1994	Evaluate the strength of tack coat interfaces	shear strength testing apparatus	displacement was measured in normal and shear direction
Tshegg et al.	1995	Study the tack coat strength	wedge splitting tension	
Donovan et al.	2000	Evaluate the shear strength of tack coat interface	direct shear test	
Liu and Vipulanandan	2005	Study the bonding of epoxy coating to wet and dry concrete	tensile bonding test	Crossed brick specimens were used
Tashman et al.	2006	Characterize tack coat materials	torque bond test and Pull-off test device	
<b>Remarks</b>		Bonding interface, bonding strength, and tack coat materials were studied	Shear, tension, and torque tests were performed to characterize the bonding	

## **2.6 Shrinkage**

Kawashima and Shah (2011) studied the early-age autogenous and drying shrinkage behavior of cellulose fiber reinforced cementitious materials. Autogenous shrinkage is bulk shrinkage that is due to hydration exclusively and the surrounding environment will have no influence on it. Addition of 1% by mass of cement helped in controlling drying shrinkage while providing some internal curing. Sahmaran et al. (2009) studied about the internal curing of engineered cementitious composites (ECC) for prevention of early age autogenous shrinkage cracking. Used ECC was a fiber-reinforced cementitious composite which had Portland cement, fly ash, microsilica cement and poly-vinyl-alcohol fibers. Study was done to see the effects of replacement of saturated lightweight fine aggregate (volcanic pumice sand) as an internal curing agent. It was reported that up to 20% replacement of normal-weight silica sand with saturated light weight aggregate was very effective in reducing the autogenous shrinkage and drying shrinkage of ECC.

### **Summary**

Based on the detailed review of literature closely related to the objective of this research, the following can be summarized:

1. Carbon fiber reinforced repair materials are being used in wide variety of applications to attain good strength, sensing and health monitoring. Temperature sensing and curing monitoring were possible using fiber reinforced composites.
2. Carbon fiber modification and dispersion improved the piezoresistive behavior.
3. Bonding of tack coats have been studied using different test methods.
4. Fly ash modification improved the piezoresistive behavior of concrete
5. Very limited information related to low stress sensing materials is available in the literature.

## **CHAPTER 3 CHARACTERIZATION OF BULK REPAIR MATERIALS**

### **3.1 Introduction**

Based on the strength, ductility, bonding ability, setting time and workability requirements different types of materials are used for structural repair. Most common repair materials are bulk materials such as polymer based materials or cementitious repair materials. In this chapter, four different bulk repair materials are characterized. The effect of adding conductive filler on the strength and ductility of a polymeric composite and two cementitious composites were investigated.

Highway Patch material is a one component, fast setting hydraulic cement material ideal for horizontal repairs of concrete in traffic areas. Since this material is used in highway repairs, there is a potential to use it as a tack coat material after proper characterization. Initial studies on strength characteristics (compression and tension) indicated that the patch material is strong enough to be used as a tack coat. Also it gets its strength very quickly. In addition, it should have good bonding strength to be eligible for a good tack coat. Hence bonding characteristics of patch material with concrete and asphalt must be investigated. Therefore appropriate testing method is of importance to define the bonding ability of the material. In this study, bonding tests were done to characterize the bonding ability of patch to asphalt and/or concrete. Tensile and shear bonding tests were performed. Tensile and double shear bonding tests were performed to determine the failure mode and the bonding strength of the material.

## 3.2 Materials and Methods

### 3.2.1 Materials

Four different bulk repair materials; epoxy grout, cement grout, concrete and highway patch material were studied. Except for epoxy grout all the other three were cement based. Each material's constituents and typical applications are summarized in Table 3-1. Epoxy grout is a three component composite which included epoxy resin, hardener and dry mix (aggregates). Other three materials were cementitious dry mixes for which water was added to get the composite.

**Table 3-1: Type of materials studied**

<b>Material</b>	<b>Constituents</b>	<b>Typical applications</b>
Epoxy grout	Epoxy resin, hardener, dry mix	Foundation rebuild, Vibration damping, Installation of anchors & dowels
Cement Grout	Dry mix, water	Grouting of anchors and dowels, support of tanks and vessels
Concrete	Dry mix, water	Rapid repair of load bearing walls, marine & hydraulic structures repair
Patch	Dry mix, water	Highway & bridges airport runway, dowel bar retrofit, cold weather repair

Particle size distributions of all four dry mixes are shown in Figure 3-1. Dry mix of epoxy grout was relatively coarser while cement grout had higher percentage of fine aggregates (90% of the aggregate was <0.6 mm in size). Table 3-2 summarizes the coefficient of uniformity ( $C_u$ ) and coefficient of curvature ( $C_c$ ) of the dry mixes obtained using the particle size distribution. Epoxy grout dry mix and concrete dry mix were relatively well graded.

**Table 3-2: Particle size distribution of dry mixes**

Dry mix	$C_u$	$C_c$	Remarks
Epoxy grout	4.4	0.45	Relatively coarser, well graded
Cement Grout	2	0.82	Had more fines
Concrete	4.7	0.67	Relatively well graded
Patch material	1	2.8	Not well graded

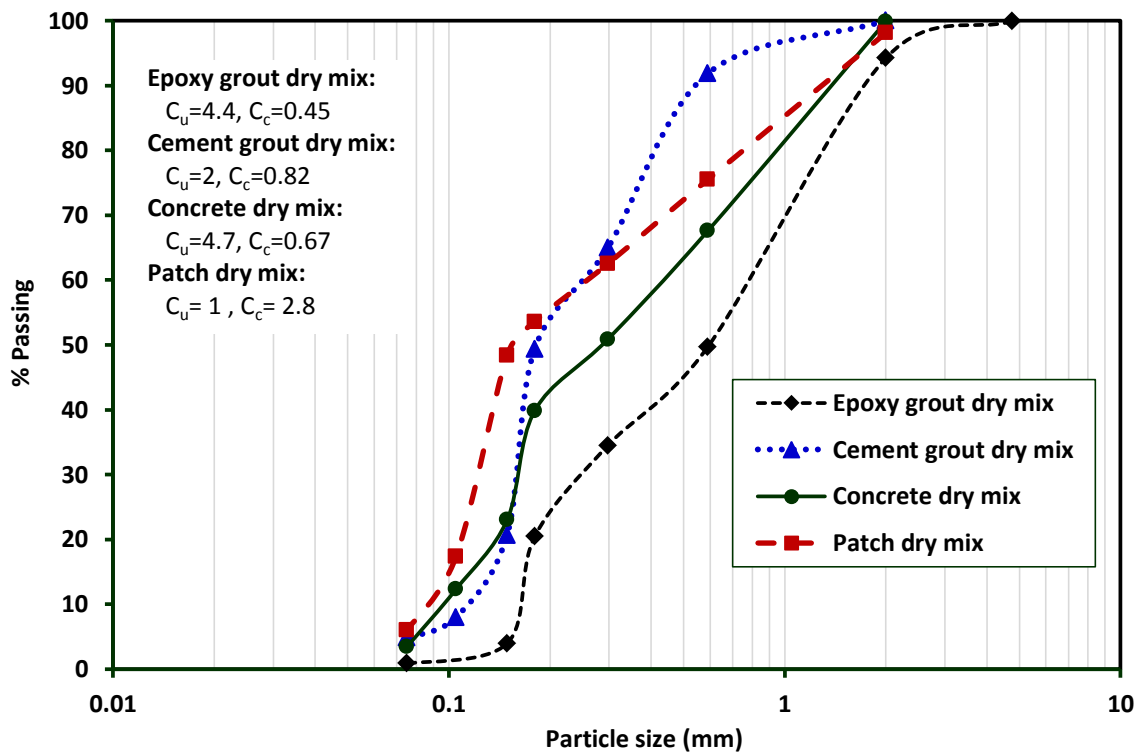


**Figure 3-1: Particle size distribution of the dry mixes of used composites**

For bonding studies, ordinary Portland cement (type I/II) and a commercially available asphalt binder PG 64-22 was used. A commercially available class-C fly ash was used in order to modify the concrete material. A Polyacrylonitrile (PAN) based Carbon fiber was added as conductive filler to the composites. Both short fibers (6 mm in length) and modified fibers were used. Modification was done to the short fibers by mechanically dispersing it.

### **3.2.2 Mixing and Curing Conditions**

Specimens were prepared according to CIGMAT PC 1-02 (2002) standards while adhering to product specifications on mix proportions. Either drill and paddle type mixer or a Hobart type mixer was used to prepare the specimens. For the epoxy grout composite, hardener and resin were mixed initially for 90 seconds using a drill and paddle type mixer and dry mix was added afterwards and mixed for another 2 minutes. Resin and hardener accounted for 12% of the total mix. Other three composites were mixed using a Hobart type mixer. Water was added to the aggregate and mixing was done (for about 2 min) until a consistent mix was obtained. The amount of water used in cement grout was 20.8% (by wt. of aggregate) whereas 12.5% of water was used for concrete and patch composites. For testing the compressive strength, cylindrical specimens with a diameter of 1.5 in were prepared using Teflon molds. Specimens were demolded after one day and cured at room conditions (75<sup>0</sup> F and 65% RH) until the time of testing.

### **3.2.3 Compression test (ASTM C39)**

Uniaxial compression tests were performed on the cylindrical specimens until failure using the Tinius Olsen testing machine. An experimental setup for a compression testing along with resistance measurement (which is associated to and discussed in Chapter 4) is shown in Figure 3-2. Commercially available 10 mm resistance strain gages were used for strain measurement. Sulfur capping was done to get smoother ends.

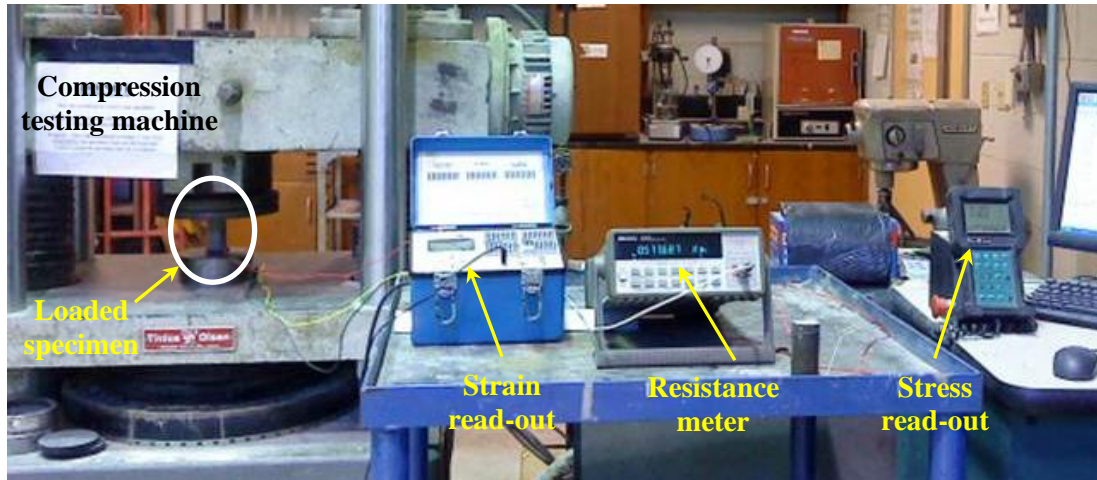


**Figure 3-2: Experimental set up for uniaxial compression testing**

### **3.2.4 Tensile Bonding Strength Test (CIGMAT CT-3, modified ASTM C321)**

Sandwiched specimens were prepared for studying the strength according to CIGMAT CT-3 standard. Different specimens were prepared by using concrete bricks and bricks made of patch. Concrete bricks (average unit weight of 144 pcf) were prepared in CIGMAT laboratory using ordinary Portland cement (type I/II). Likewise, bricks were prepared using patch material also. The bonding material was either paste made of patch or asphalt binder.

Procedure used to prepare the bonding test specimens is as follows:

- Step1: Bricks were made using normal concrete or patch material in advance and allowed to cure under room temperature.
- Step2: The surface was cleaned with wire brush to roughen the surface. Tests were performed on smooth and rough surfaces.
- Step3: Bricks were marked to ensure that the crossed bricks were placed in the middle and at right angles to each other.
- Step4: In case of asphalt as a tack coat, asphalt was heated up to about 200°C. If patch was the tack coat, it was prepared per manufacturer's specification.

Step5: The asphalt or patch was applied over the area on one of the bricks (concrete or patch) that was marked. The thickness of the tack coat was measured after preparing the specimens.

Step6: The second brick was placed on mortar and the oriented correctly.

Step7: The specimens were allowed to cure at room condition (23 °C and 60% humidity) till the time of test.

A typical specimen prepared for tensile bonding is shown in Figure 3-3, a. In this specimen, the bonding layer consisted of two patch layers and one asphalt layer in the middle all of which were sandwiched between two concrete bricks (concrete-patch-asphalt-patch-concrete from top to bottom). Specimens were tested by subjecting to tensile loading as shown in the experimental setup in Figures 3-4 and 3-5. One brick was held by stationary jaws while the other brick was pushed by moving jaws creating a tensile force on the bonding.

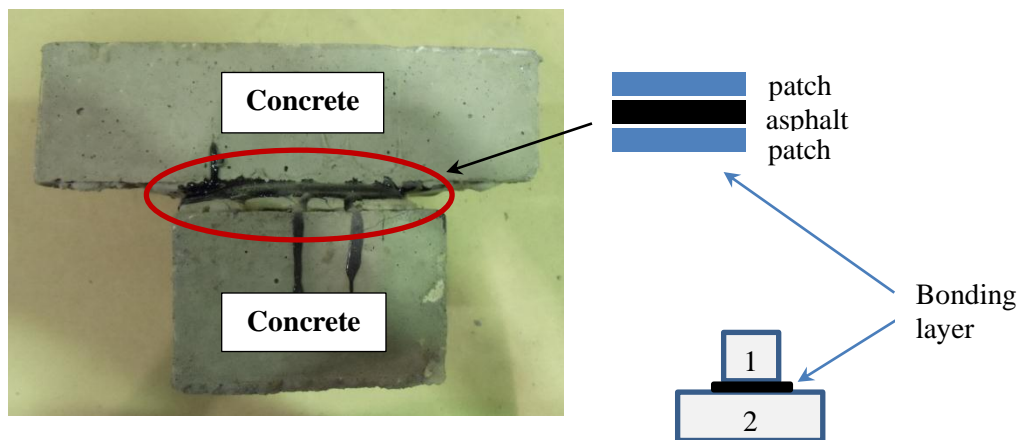


**Figure 3-3: One type of tested crossed brick specimen**



**Figure 3-4: Experimental setup of tensile bonding strength test**

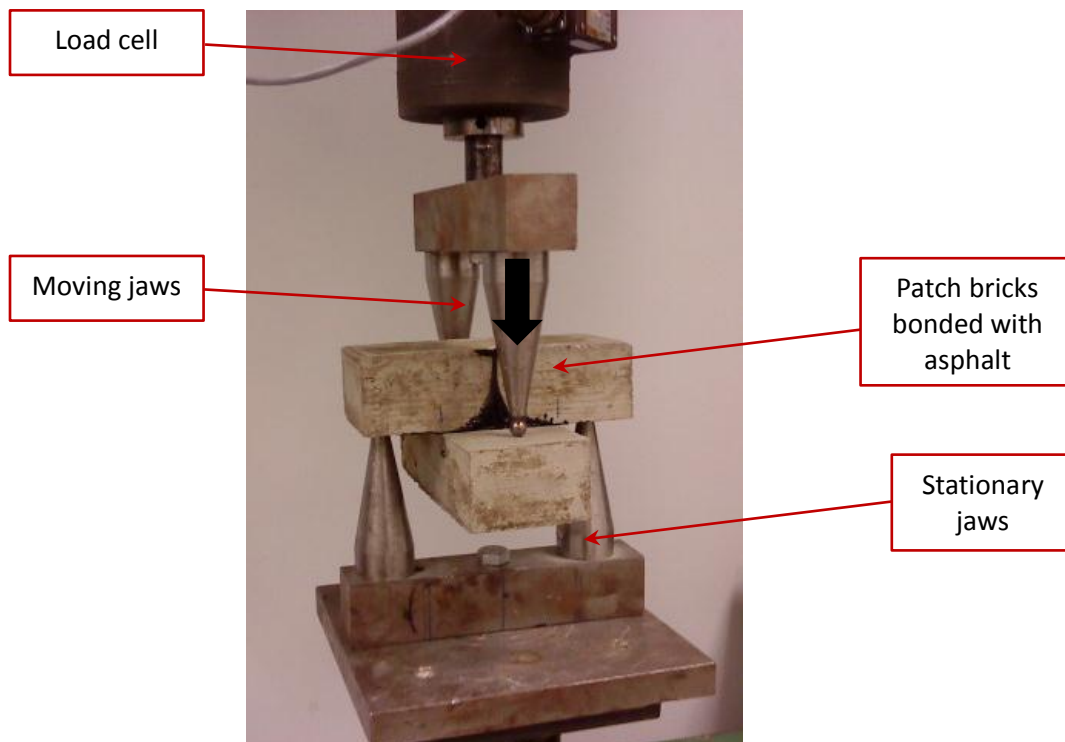


**Figure 3-5: Specimen under tensile loading**

### 3.2.5 Double Shear Bonding Strength Test (CIGMAT AC 3-08)

Specimens for double shear bonding tests were prepared according to CIGMAT AC 3-08 standard by bonding three bricks with the bonding material in between as seen in Figure 3-10. In this case, the brick was made of concrete and bonding material was patched. The procedure of preparing the specimen is similar to that of tensile bonding specimen except for the number of bricks and the number of bonds.

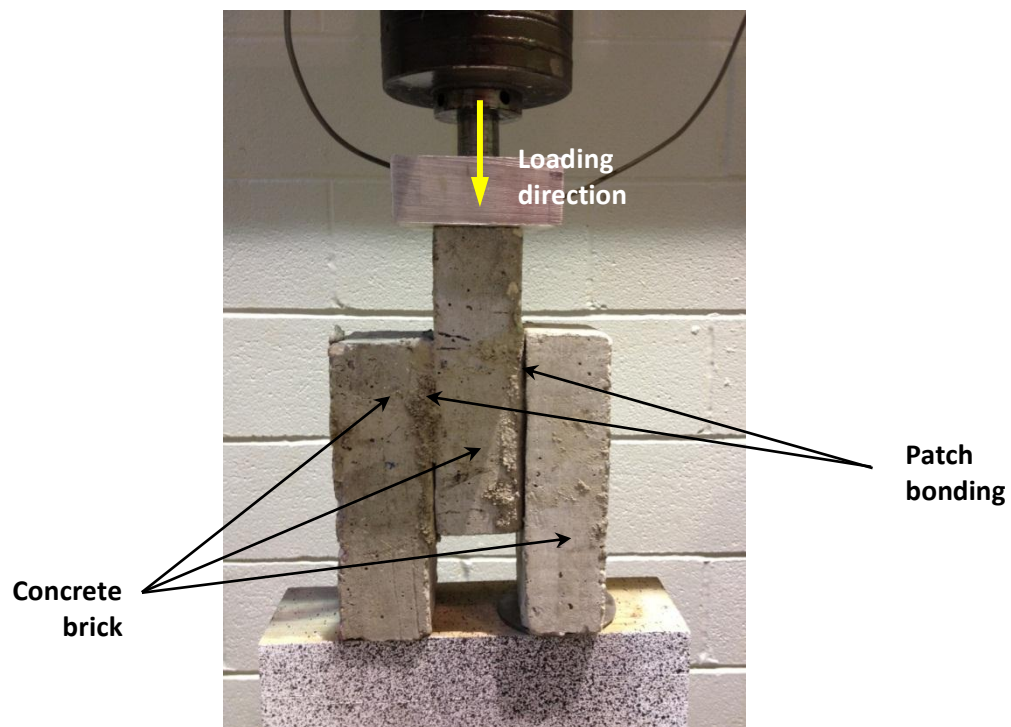


Figure 3-6: Specimen under double shear loading

## 3.3 Stress-Strain Characterization

### 3.3.1 Epoxy Grout

Figure 3-3 shows the effect of addition of fiber on the compressive stress-strain behavior of epoxy grout. Two different conductive filler proportions, 4% short fiber and 0.6% modified fiber, were used. Strength was affected by adding the conductive filler. When 0.6% modified

fiber was used, strength was reduced by 15% from the control (specimen without fiber). But it is evident that the ductility and toughness of the specimen with modified fiber was increased. The strain energy at failure for the epoxy grout was  $2.108 \text{ kJm}^{-3}$ . With the addition of short and modified fibers the strain energy at failure was  $1.784$  and  $2.563 \text{ kJm}^{-3}$  respectively.

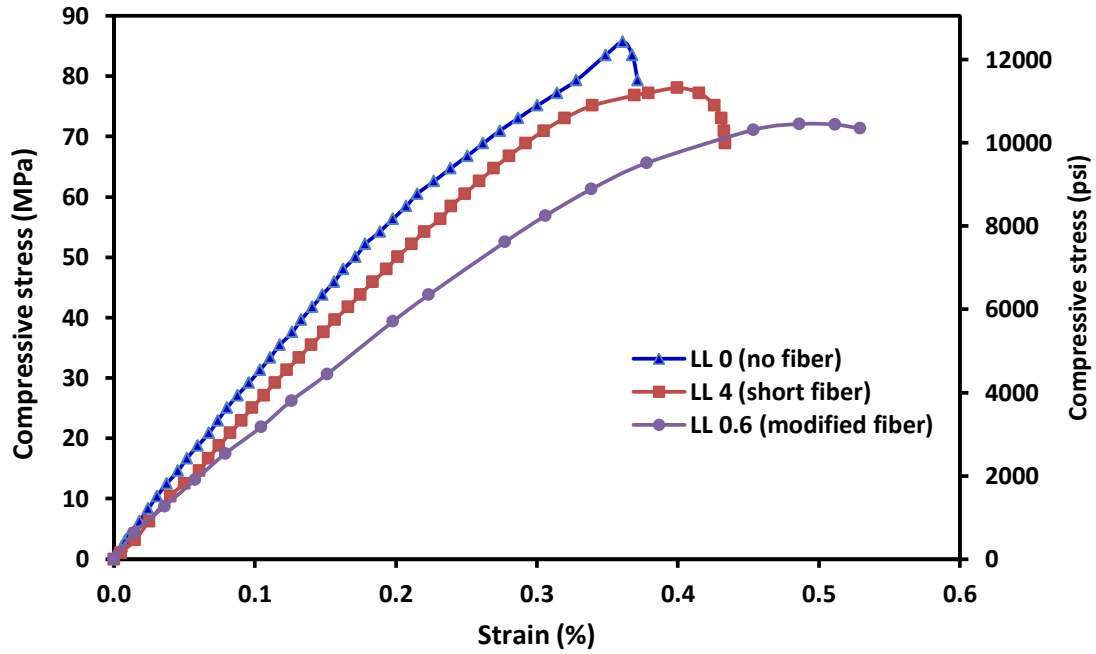


**Figure 3-7: Effect of fiber on stress-strain behavior of epoxy grout**

Compressive stress-strain behavior of six epoxy grout specimens which had 0.6% (w/w) modified fiber is shown in Figure 3-8. Tests were done after 28 days of curing. Specimens had compressive strength in the range of 60-72 MPa. Compressive moduli of specimens were in the range of 13-20 GPa.

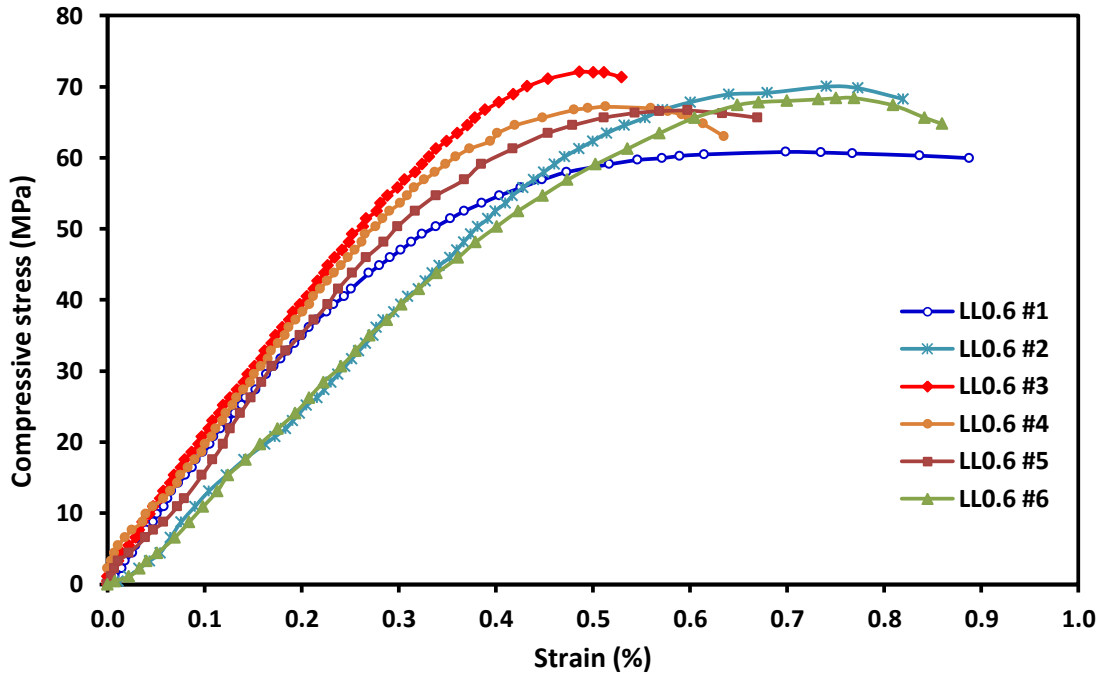


Figure 3-8: Stress-strain behavior of fiber reinforced epoxy grout

### 3.3.2 Cement Grout

#### 3.3.2.1 Effect of fiber on stress-Strain behavior

Effect of modified fiber on the compressive stress-strain behavior of 28 day cement grout is shown in Figure 3-9. Two fiber contents with 0.1% and 0.15% (by wt.) were tested. There weren't significant differences observed in the strength by adding fiber. However addition of fiber increased the ductility and toughness significantly. Failure strain was doubled by the addition of fiber.

Compressive stress-stain behavior of five cement grout specimens with 0.1% (w/w) modified fiber is shown in Figure 3-10. Tests were done after 14 days of curing. Specimens had compressive strength in the range of 28.3-36.5 MPa. Compressive moduli of specimens were in the range of 7-11.7 GPa.

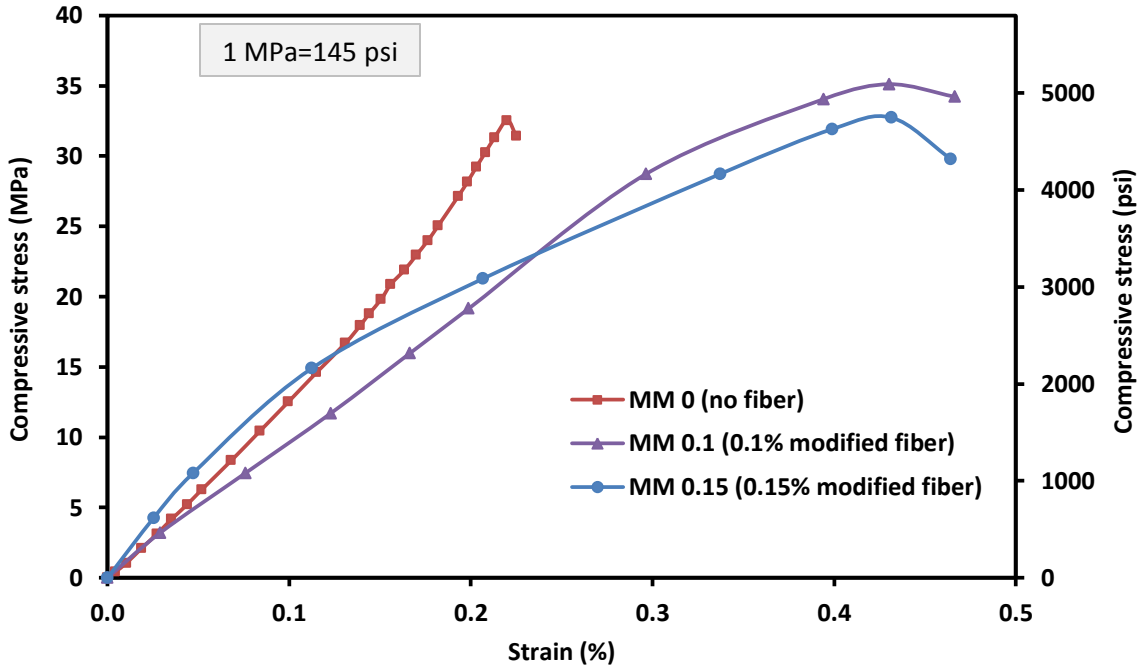


Figure 3-9: Effect of fiber on stress-strain behavior of cement grout

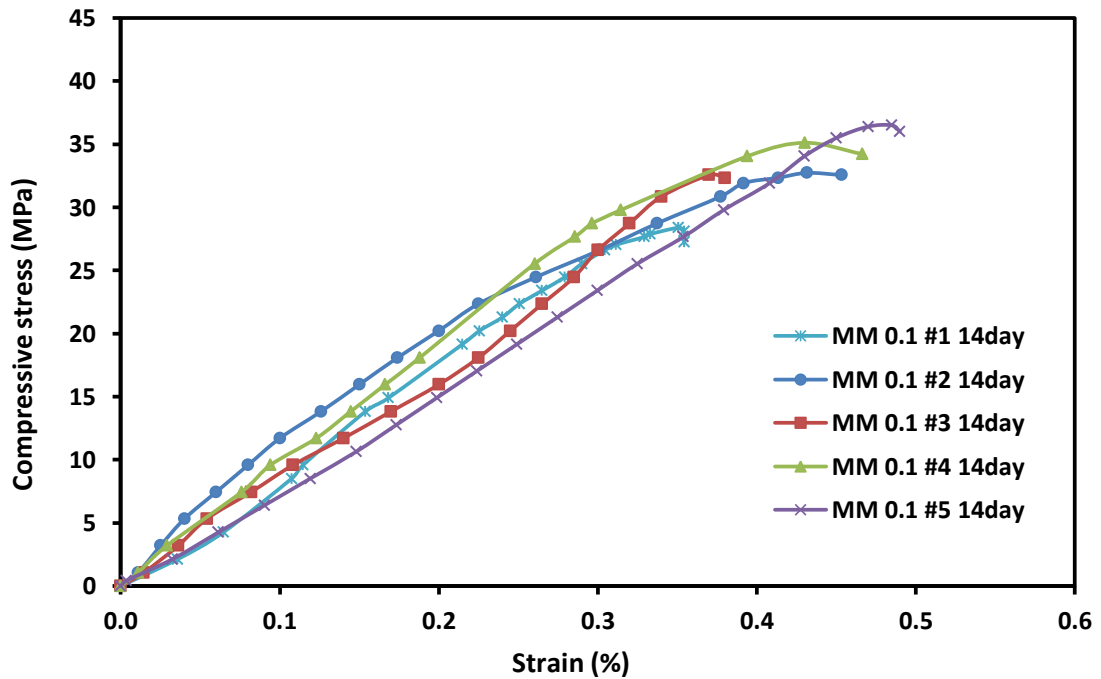


Figure 3-10: Stress-strain behavior of fiber reinforced cement grout

### 3.3.2.2 Effect of curing conditions on Stress-Strain behavior

Cement grout specimens (with 1.5” diameter) were prepared with 0.1% (by wt.) fiber loading to study the effect of curing. After seven days of curing at room temperature (25°C), specimens were subjected to five different curing conditions (two specimens for each) as summarized in Table 3-3. All the specimens were put into different curing conditions for a period of 17 days except the specimen #2 which was continuously cured at room conditions.

**Table 3-3: Different curing conditions applied for cement grout specimens**

<b>Specimen no</b>	<b>Medium of curing</b>	<b>Temperature (°C)</b>	<b>Simulated environment</b>
#2	Air	25	Normal condition
#4	Water	25	Wetting
#6	Air	55	Heating
#7	Air	5	Thawing temperature
#10	Air	-15	Freezing temperature

The compressive stress-strain relationships for the specimens after subjected to different curing conditions are shown in Figure 3-11. Unit weight of corresponding specimens used for the study varied from 118 to 132 pcf. It was noted that water cured specimen showed higher strength while heat cured specimen had lesser strength. However, Young’s modulus of all the specimens were found to be similar. Cement grout is a multiphase material with inert aggregates held together by the hydrated cement paste. When it is exposed to temperatures, changes in mechanical properties were observed. Because of changes in the moisture condition of the grout constituents and the resulting deterioration of the cement paste-aggregate bond the load-carrying capacity, and the ductility is affected.

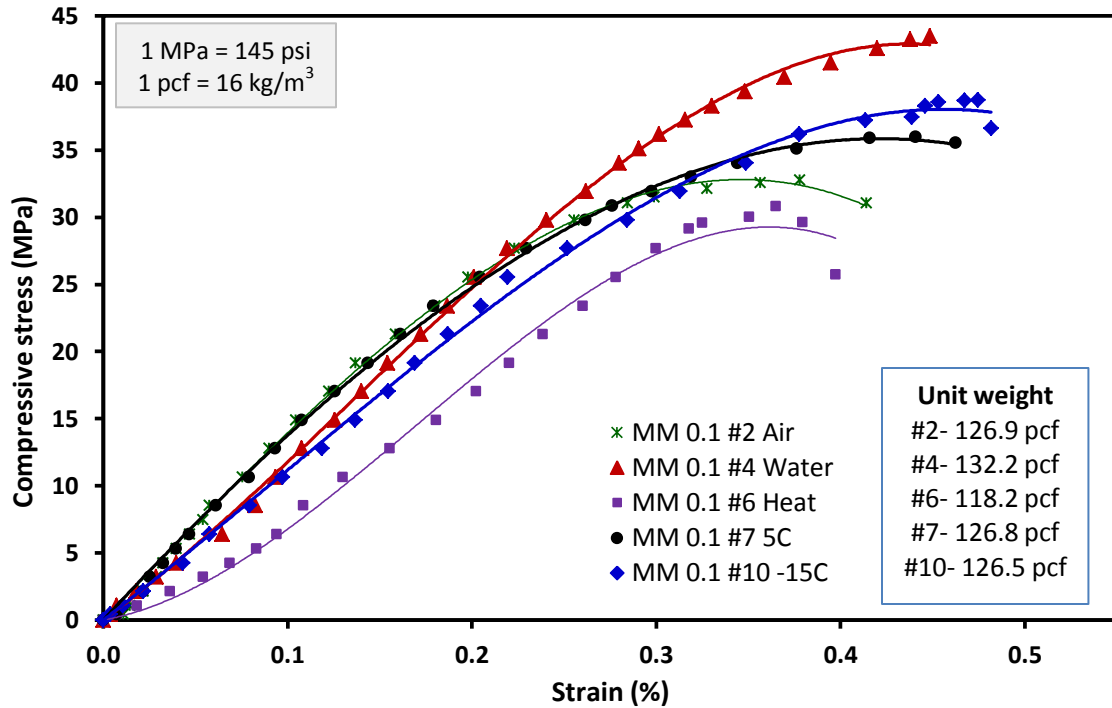


**Figure 3-11: Stress-Strain relationship of cement grout specimens at different curing conditions**

### 3.3.3 Concrete

Effect of material modification and fiber addition on the compressive stress-strain behavior of concrete air cured for 28 days in room temperature (25°C) is compared in Figure 3-12. The control specimen (no modification) had strength of 42.8 MPa. Addition of 0.5% fiber improved the failure strain of the concrete material. The failure strain increased from 0.15% to 0.20%. Replacing the concrete material with 1/3 fly ash (class C) reduced the strength of the concrete but did not affect the failure strain.

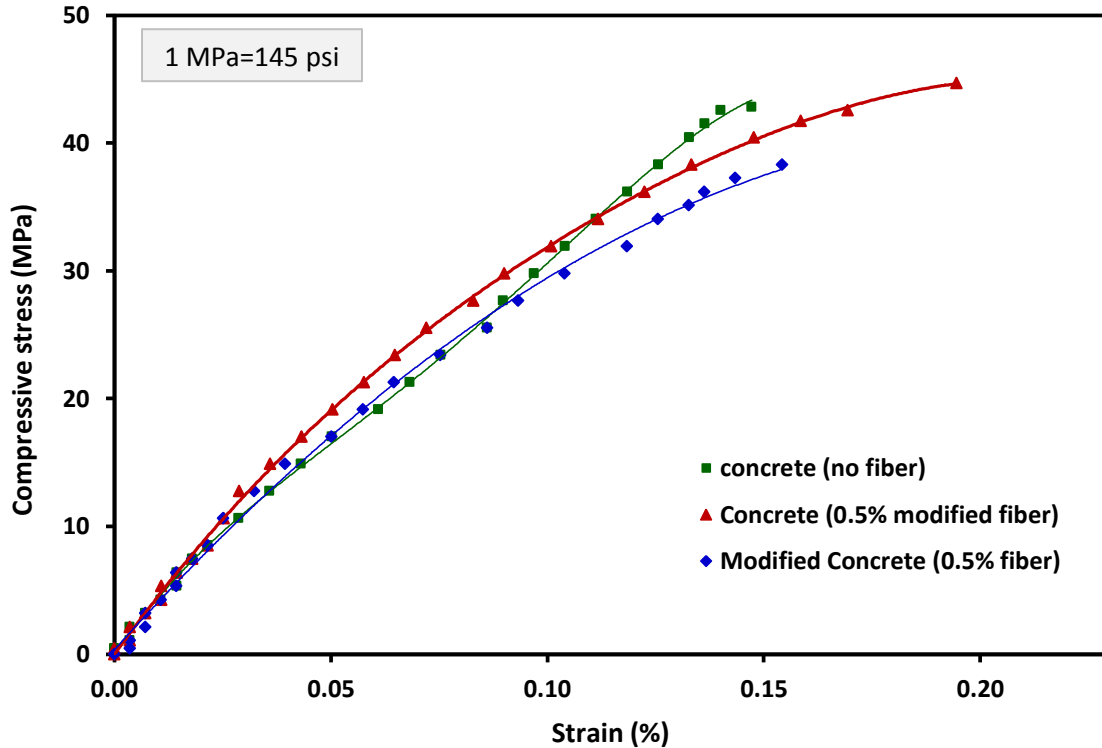


**Figure 3-12: Stress-Strain behavior of concrete due to material modification and fiber addition**

### 3.3.4 Patch Material

The compressive strength of the patch composite with curing time was studied. Cylinders of size 2 in diameter and 4 in height were prepared according to ASTM C31 and the testing was done according to ASTM C39. Tests were performed on specimens after curing them for 45 minutes, 1.5 hour, 3.5 hour, 1 day and 3 days. Likewise splitting tensile test was done on one 2 in. diameter and 4 in. height cylindrical specimen after one day of curing to determine the indirect tensile strength as per ASTM C496. One day splitting tensile strength of patch material was 262 psi (1.8 MPa).

Compressive stress-strain relationships for patch material at different curing times are shown in Figure 3-13, and the strength and unit weights of specimens with curing time are summarized in Table 3-4. The average unit weight of the patch specimens was 131.3 pcf (2103

kg/m<sup>3</sup>). The specimen cured for 45 minutes had a compressive strength of over 1200 psi (8.3 MPa). The compressive strength of patch composite cured for 45 minutes doubled after 3.5 hours of curing. It was observed that the specimen at very early age (up to 90 minutes) had higher strains to failure. Also, specimen cured for one day, attained almost 90% of the 3rd day strength. It was observed that specimen cured for 3.5 hours almost reached the elastic modulus of the 3day specimen. Figure 3-14 shows the strength development of patch with curing time.

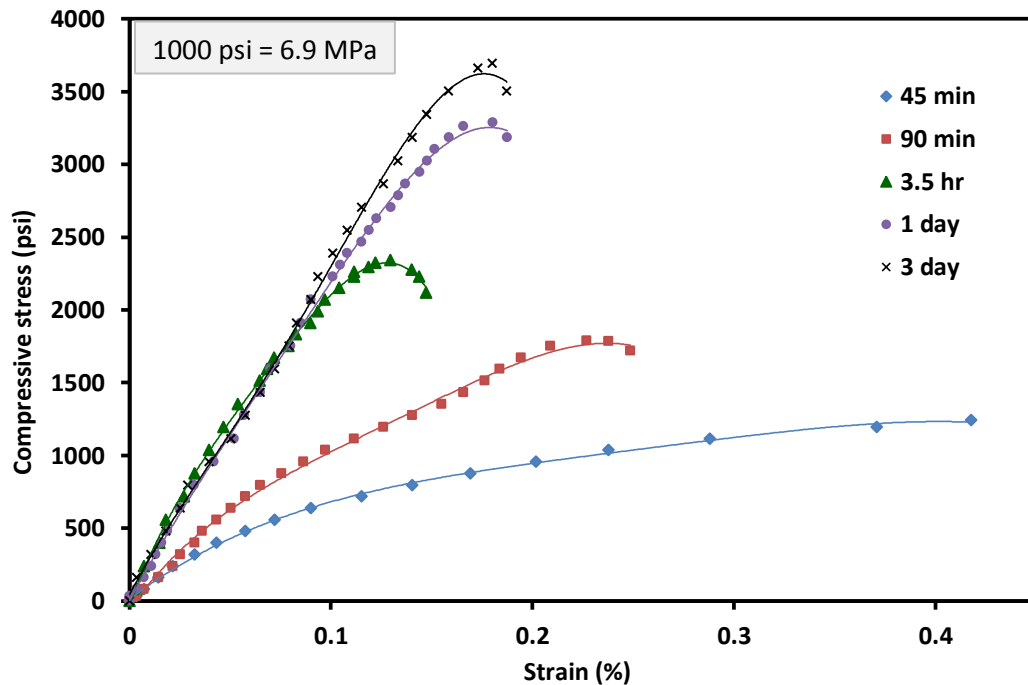
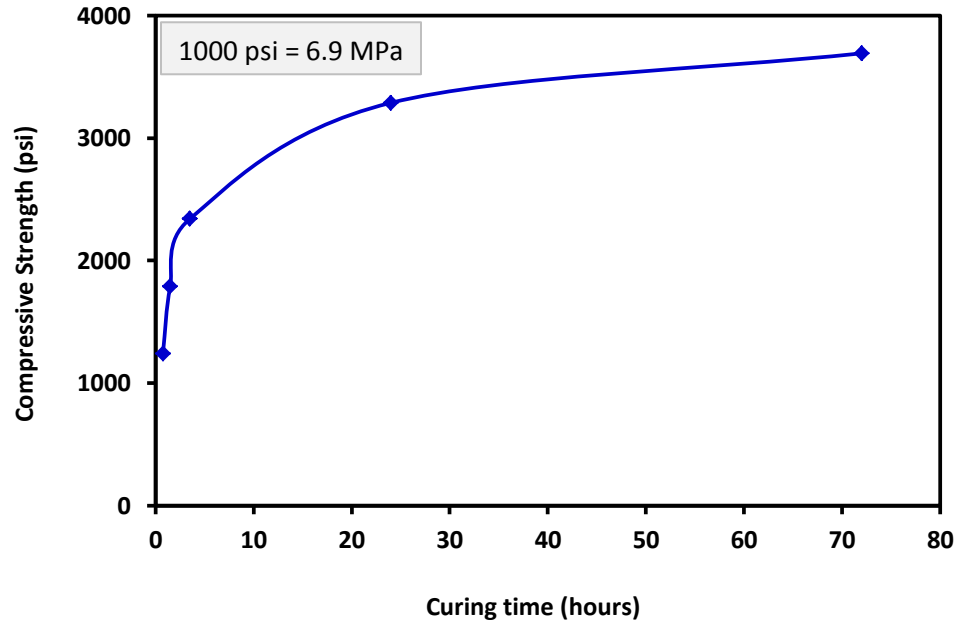


Figure 3-13: Variation of Stress Strain relationship for patch material with curing time

Table 3-4: Summary of Compressive strength of patch material with curing time

Age	Strength (psi) (1 psi = 6.9 kPa)	Unit weight (pcf) (1 pcf = 16 kg/m <sup>3</sup> )
45 min	1240	133.4
1.5 hour	1788	131.1
3.5 hour	2340	131.7
1 day	3288	130.9
3 day	3692	131.6



**Figure 3-14: Compressive strength development of patch material**

### **3.4 Bonding characterization**

#### **3.4.1 Initial Characterization**

Tensile bonding test was performed in two series. In the first series the potential of the patch material as a tack coat was investigated. In the second series more detailed investigations were undertaken. The results for the first series are summarized in Table 3-5. In this series, surfaces of the concrete bricks were cleaned before applying the patch or asphalt. The test results are compared in Figure 3-15.

In the Concrete-Patch-Concrete specimens the average bonding strength between concrete (rough) and patch was about 100 psi and the failure was by bonding (Type-3). For Concrete-Asphalt-Concrete specimens, the failure was by bonding failure (Type-3) with an average bonding strength of 20 psi. The average bonding strength of patch to roughened concrete was about 5 times higher than the asphalt tack coat. In the case of Patch -Asphalt- Patch, the failure was in the asphalt (Type-2) and the average strength was 34 psi. Hence patch had better bonding strength to asphalt than concrete (20 psi).

**Table 3-5: Tensile bonding test results for first series**

No	Brick1	Brick2	Bonding material	Strength (psi)	Remarks on failure (After Liu and Vipulanandan, 2005)
1	Concrete	Concrete	Patch	108	Bonding failure (Type-3)
	Concrete	Concrete	Patch	93	Bonding failure (Type-3)
2	Concrete	Concrete	Asphalt	16	Bonding failure (Type-3)
	Concrete	Concrete	Asphalt	24	Bonding failure (Type-3)
3	Patch	Patch	Asphalt	34.1	Asphalt failure (Type-2)
	Patch	Patch	Asphalt	34.4	Asphalt failure (Type-2)

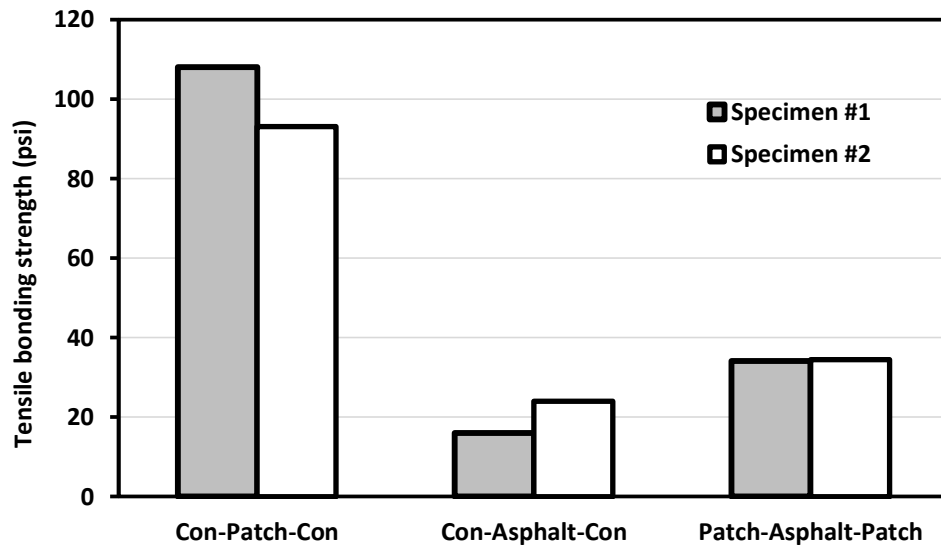


**Figure 3-15: Comparison of Tensile bonding strength of series 1 specimens**

### 3.4.2 Tensile Bonding Strength

Total of 43 bonded specimens were prepared for this second series of tests. Specimens were prepared using either smooth surfaces or rough surfaces of the concrete bricks. Types of specimens prepared in this series are summarized in Table 3-6.

**Table 3-6: List of specimens for series 2**

<b>Case</b>	<b>Brick1, Brick2</b>	<b>Bonding layer</b>	<b>Type of test</b>	<b>No. of spec</b>
1	Concrete, Concrete	Patch	Bonding strength development (1hr, 2hr, 4hr) - non cleaned	3
			2 different Thickness of layer, Smooth & non cleaned surface	5
			2 different Thickness of layer, Rough & cleaned surface	4
2	Concrete, Concrete	Asphalt	Bonding strength development (1hr, 4hr) - Smooth, rough	3
			2 different Thickness of layer, Smooth & non cleaned surface	6
			2 different Thickness of layer, Rough & cleaned surface	2
3	Patch, Patch	Asphalt	Bonding strength development (1hr, 4hr) - smooth, rough	4
			2 different Thickness of layer, Smooth & cleaned surface	4
			2 different Thickness of layer, Rough & cleaned surface	4
4	Concrete, Concrete	Patch + Asphalt + Patch	2 different Thickness of layer, Smooth & non cleaned surface	2
			2 different Thickness of layer, Smooth & cleaned surface	3
			2 different Thickness of layer, Rough & cleaned surface	3
Total # of crossed brick specimens				<b>43</b>

**3.4.2.1 Concrete-Patch-Concrete specimens**

The test results are summarized in Table 3-7. The specimens were prepared with smooth (not cleaned) and roughened concrete surfaces. The bonding strength of specimens with smooth (not cleaned) surface (concrete) had only about half the bonding strength (46 psi after one day curing) compared to specimens which were prepared using cleaned concrete (rough) surface (91.9 psi after one day of curing). This could be due to the excess cement on the concrete surface which could have prevented the penetration of patch into the concrete substrate.

Furthermore, considering bonding strength at 1, 2 and 4 hours, it can be stated that specimens achieve the bonding strength after 1hour. Comparison of 1day tensile bonding strength is shown in Figure 3-16. Two different thicknesses were used in this study. However, no clear

trend was observed. Therefore it can be concluded that thickness of bonding layer had little influence on the bonding strength, because the mode (type) of failure.

**Table 3-7: Test results for Concrete-Patch-Concrete specimens (all Type-3 Failure)**

Surface		Age	Average thickness (in)		Strength (psi)	Remarks
Rough	Cleaned	1day	Thick	0.28	92.3	Average 1day strength for rough surface bond was 91.9 psi (neglected 77 psi)
				0.30	77.1	
			Thin	0.15	91.3	
				0.14	92.1	
Smooth	Non-cleaned		Thick	0.27	48.2	Average strength for smooth surface bond is 46 psi
				0.31	44	
			Thin	0.16	38	
				0.14	43.7	
		0.16		56		
		1hr	Thin	0.16	47.5	Strong bonding was reached at 1 hour
		2hr		0.15	47.2	
		4hr		0.16	44.4	
Rough surface bonds had twice the strength of smooth surface bonds. Thickness had little influence in bonding						

All the specimens failed by de-bonding between concrete and patch (Type-3). Average bonding strength of specimens having rough concrete surface was 91.9 psi and was comparable to the results obtained in series 1 test (100 psi).

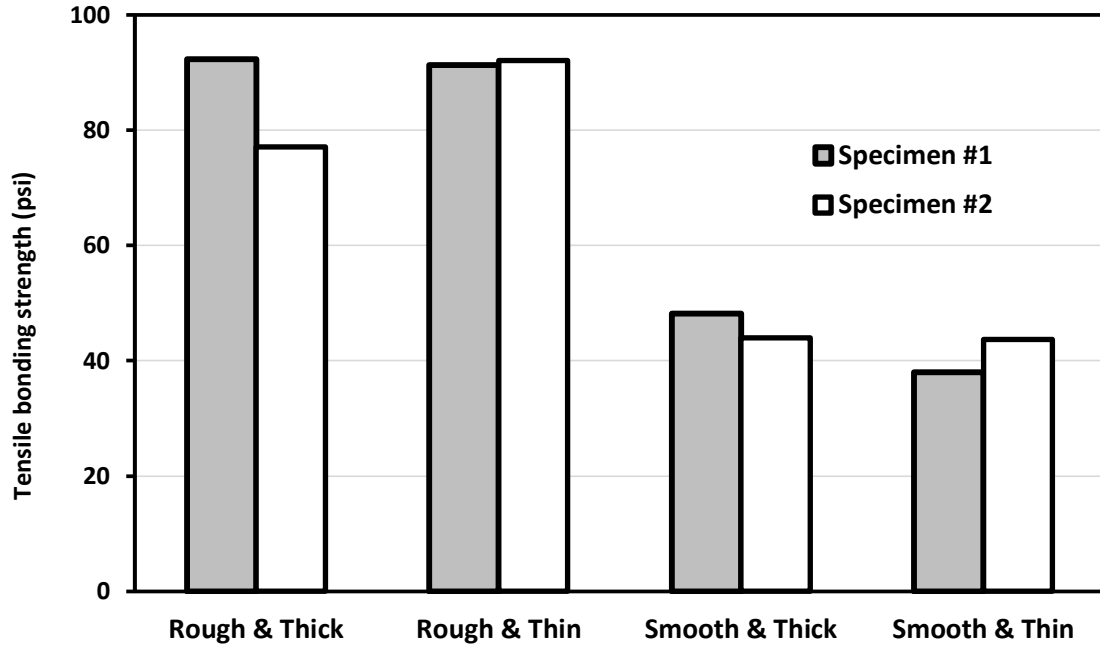


**Figure 3-16: One day tensile bonding strength of Concrete-Patch-Concrete specimens**

### 3.4.2.2 Concrete-Asphalt-Concrete specimens

Test results are summarized in Table 3-8. It was observed that asphalt bonding failure was predominant. In two out of 11 specimens, both bonding and asphalt failure (Type-5) was observed. One day tensile bonding strengths of Concrete-Asphalt-Concrete specimens are compared in Figure 3-17. It was observed that neither the thickness nor surface texture had any effect on the bonding strength of asphalt tack coat to concrete. The bonding strength of asphalt was affected by curing time, average strength of 7.2 psi after one hour (Type-5), and the average bonding strength was 16 psi after four hours (Type-3).

**Table 3-8: Test results for Concrete-Asphalt-Concrete specimens**

Surface		Age	Average thickness (in)		Strength (psi)	Failure	Remarks	
Rough	Cleaned	1day	Thick	0.09	14.7	Bonding (Type-3)	Average 1day strength was 17.9 psi	
				0.09	8.6			
Smooth	Non-cleaned		Thin	0.055	21.1	Asphalt+bonding (Type-5)		
				0.045	16.1	Bonding (Type-3)		
				0.045	17.8			
			Thick	0.09	15.4			
				0.1	20.2			
				0.095	20.1			
Smooth	Cleaned		1hr	Thin	0.045	7.2		Asphalt+bonding (Type-5)
Rough					4hr	0.05		24.3
		0.05	7.8					
Both Type 3 (82%) and Type 5 (18%) failures were observed								

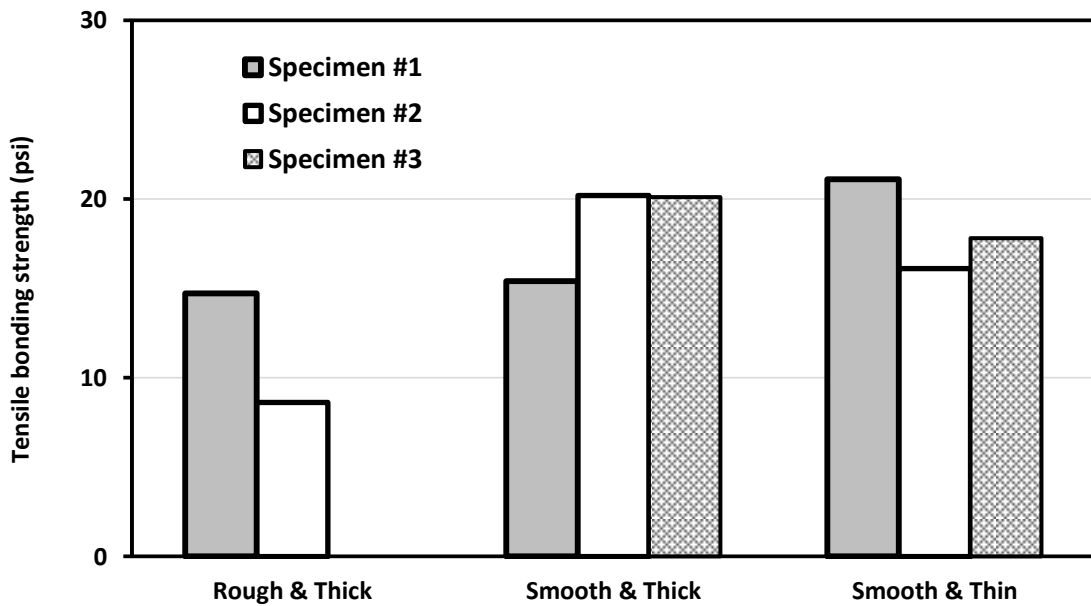


**Figure 3-17: One day tensile bonding strength of Concrete-Asphalt-Concrete specimens**

### 3.4.2.3 Patch-Asphalt-Patch

The test results are summarized in Table 3-9. Figure 3-18 compares the one day tensile bonding strength of Patch-Asphalt-Patch specimens. It was noticed that the specimens with thin asphalt layer performed better (26.6 psi) than the thick layer (24.2 psi) when the patch surface was relatively rough. No such trend was observed with smooth patch bonding surface (28 psi). All specimens failed as asphalt stretched (Type-2), hence the bonding strength was influenced by the asphalt curing. The bonding strength was 13.9 psi after 1 hour and 16.8 psi after 4 hours. The average asphalt strength after one day curing was 24.4 psi (new batch) compared to the asphalt strength of 20 psi in series 1.

**Table 3-9: Test results for Patch-Asphalt-Patch specimens (All Type-2 Failure)**

Surface	Age	Average thickness (in)		Strength (psi)	Average strength
Smooth	1 day	Thick	0.095	34.6	28 psi
			0.1	21.3	
		Thin	0.05	31.5	28.6 psi
			0.045	25.7	
Rough	1 day	Thick	0.1	15.7	14.2 psi
			0.09	12.6	
		Thin	0.05	22.8	26.6 psi
			0.055	30.4	
Smooth	1 hr	Thin	0.045	15.8	13.9 psi
Rough			0.045	11.9	
Smooth	4 hr		0.055	21.3	16.8 psi
Rough			0.05	12.3	
All specimens failed by asphalt failing (Type-2). Average 1 day bonding strength is 24.4 psi.					

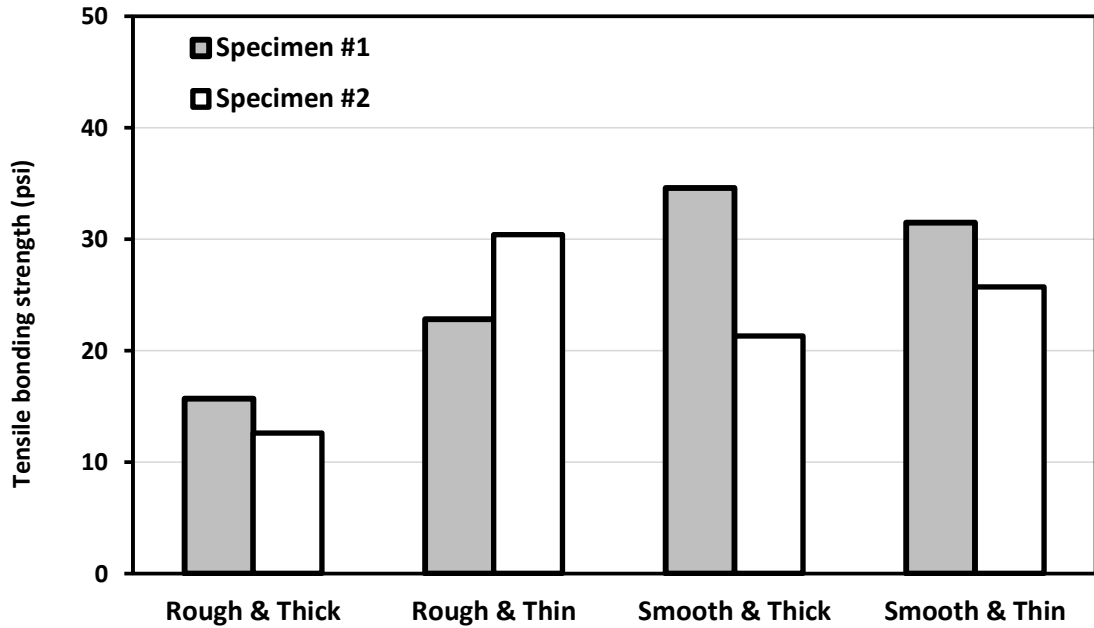


**Figure 3-18: One day tensile bonding strength of Patch-Asphalt-Patch specimens**

#### **3.4.2.4 Concrete-(Patch+Asphalt+Patch)-Concrete**

The test results are summarized in Table 3-10 and average tensile bonding strengths are compared in Figure 3-19. It was observed that when the specimen was made of concrete bricks with a smooth (not cleaned) surface, concrete-patch bonding failed (Type-3) with an average bonding strength of 35 psi. On the other hand, when the surface was cleaned, the bonding between patch and concrete was better and asphalt failure was observed, with average failure strength of 32.8 psi.

**Table 3-10: Test results for Concrete-(Patch+Asphalt+Patch)-Concrete specimens**

Surface		Average asphalt thickness (in)		Strength (psi)	Failure
Smooth	Cleaned	Thin	0.045	32.1	Asphalt failure (Type-2)
			0.055	31.6	
Thick		0.1	39.2		
Rough		Thick	0.09	36.2	
		Thin	0.04	31.8	
			0.055	25.6	
Smooth	Non-cleaned	Thin	0.05	31.7	Concrete-Patch bonding (Type-3)
			0.045	38	
Specimens with thick asphalt layer performed marginally better. Average 1 day bonding strength of cleaned surface bonding is 32.8 psi					

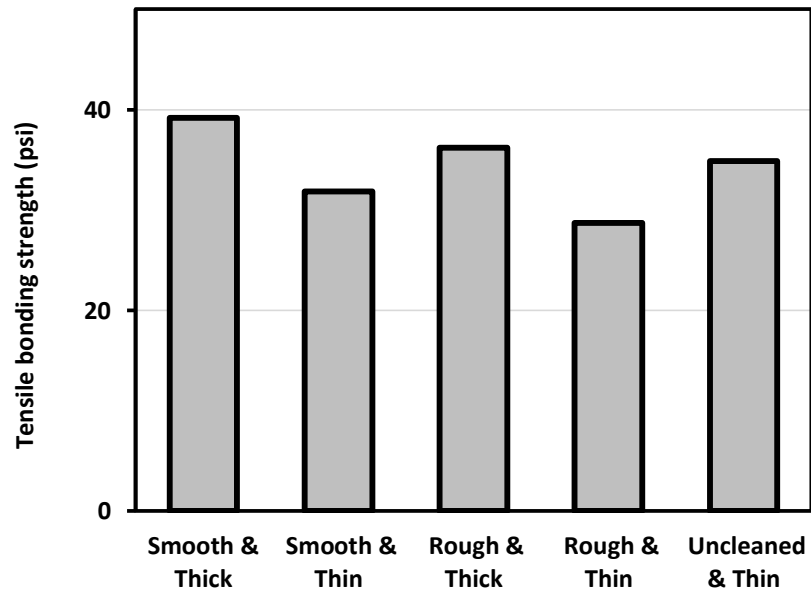


**Figure 3-19: Tensile bonding strength of Concrete-Patch+Asphalt+Patch-Concrete specimens**

### 3.4.2.5 Bonding strength

Average one day tensile bonding strength of series-2 specimens are compared in Figure 3-20 and summarized in Table 3-11. Also the common types of failures observed during this study are shown in Table 3-12. It was clearly observed that patch had better bonding with concrete (91.9 psi) than with asphalt tack coat (24.4 psi). Also patch-asphalt bonding was better than concrete-asphaltic binder bonding, because the asphalt failed instead of bond.

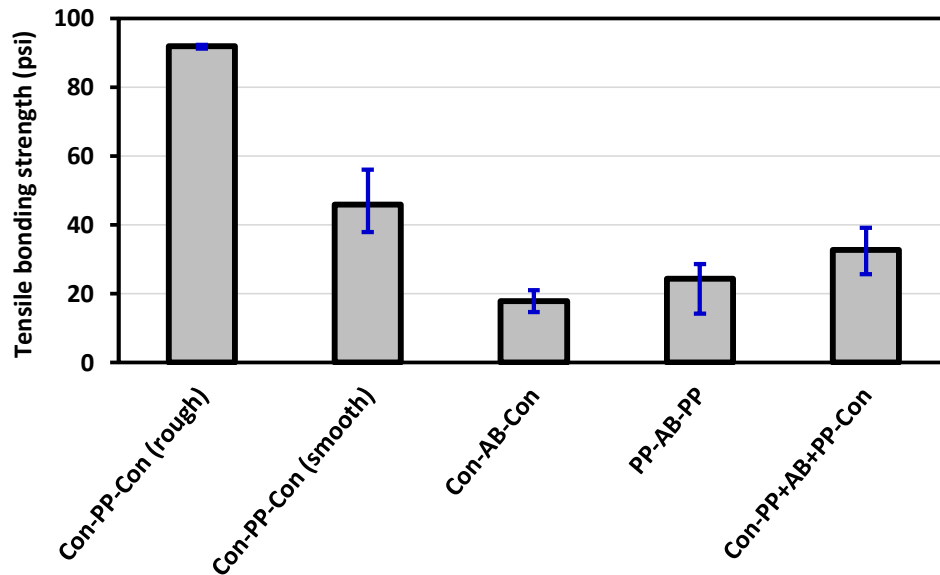


Figure 3-20: Average 1day tensile bonding strength of series-2 bonding specimens

Table 3-11: Summary of testing program and results for 2nd series studies of patch

Case	Brick1	Brick2	Bonding material	Strength (psi)	Predominant failure (After Liu and Vipulanandan, 2005)
1	Concrete	Concrete	Patch	91.9	Bonding failure (Type-III)
2	Concrete	Concrete	Asphalt	17.9	Bonding failure (Type-III)
3	Patch	Patch	Asphalt	24.4	Asphalt failure (Type-II)
4	Concrete	Concrete	Patch+Asphalt+ Patch	32.8	Asphalt failure (Type-II)

**Table 3-12: Types of failures observed in tensile bonding test**

<p><b>(a) Asphalt + Bonding failure (Type5)</b></p>  <p>Concrete - Asphalt - Concrete (smooth)</p>	<p><b>(b) Asphalt failure (Type2)</b></p>  <p>Patch - Asphalt - Patch</p>
<p><b>(c) Concrete - Patch bonding failure (Type3)</b></p>  <p>Concrete - (Patch+Asphalt+Patch) - Concrete (smooth)</p>	<p><b>(d) Asphalt failure (Type2)</b></p>  <p>Concrete - (Patch+Asphalt+Patch) - Concrete (Rough)</p>
<p><b>(e) Concrete - Patch bonding failure (Type3)</b></p>  <p>Concrete - Patch - Concrete (smooth)</p>	<p><b>(f) Concrete - Patch bonding failure (Type3)</b></p>  <p>Concrete - Patch - Concrete (Rough)</p>

### **3.4.2.6 Remarks**

The patch bonding strength was affected by the smooth and rough conditions of the concrete surface. Tensile bonding strength of patch material to roughened concrete (91.9 psi) surface was more than four times that of asphaltic tack coat (17.9 psi). By comparing case no. 2 and 3, patch had better bonding to asphaltic binder than concrete. Considering case no. 2 and 4, patch material enhanced the bonding between the asphaltic tack coat and concrete.

Patch had better bonding strength to concrete than asphalt tack coat (PG 64-22). The patch bonding strength was affected by the smooth and rough conditions of the concrete surface. The average bonding strength for patch to rough concrete was 91.9 psi as compared to the asphaltic tack coat which was 17.9 psi.

Patch demonstrated rapid gain in strength during the first 3.5 hours of curing. Asphalt can be applied on to patch tack coat in one hour because of rapid gain in compressive and bonding strength of the patch. Also this patch material enhanced the bonding between the asphaltic tack coat and concrete.

### **3.4.3 Shear Bonding Strength**

Double shear bonding strength test was done on a specimen that comprised of concrete bricks bonded with patch paste. Ultimate load till failure was obtained and the double shear bonding strength was calculated by dividing the load by bonded area (two bonding surfaces). Double shear bonding strength of patch material was 21.6 psi. Compared to the corresponding tensile bonding strength (91.9 psi for rough surface and 46 psi for smooth surface) of concrete and patch, shear strength is low. This indicates that shear is more critical in concrete-patch bonding. The specimen failed after de-bonding occurred at one bonding surface and the failure was identified as Type-3. Failed specimen is shown in Figure 3-21.

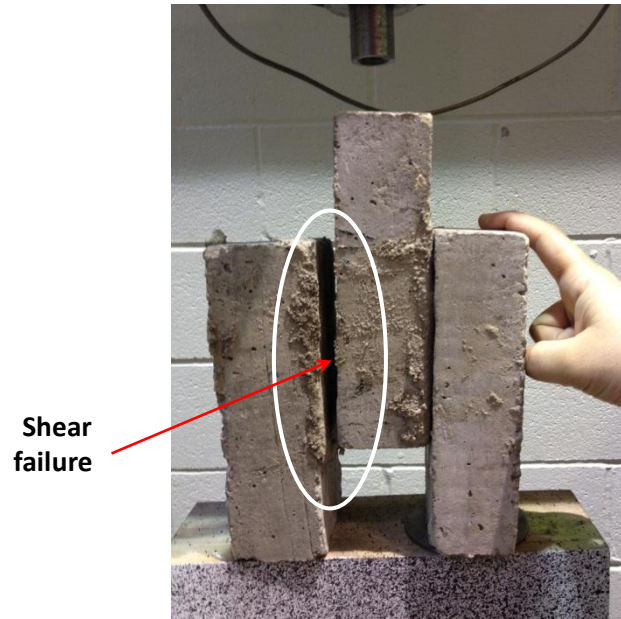


**Figure 3-21: Failed specimen after subjecting to double shear**

### **Summary**

The behavior of epoxy grout, cement grout, structural concrete and highway patch materials with and without modification were characterized. Based on the experimental study following conclusions are advanced:

1. Strength of epoxy grout was reduced by 15% by the addition of carbon fiber while minor differences were observed in the strength of fiber reinforced cement grout.
2. Ductility and toughness of the epoxy grout specimen with modified fiber was increased. The strain energy at failure for the epoxy grout was  $2.108 \text{ kJm}^{-3}$ . With the addition of modified fibers the strain energy increased to  $2.563 \text{ kJm}^{-3}$ .
3. Failure strain of cement grout doubled over by the addition of 0.1% fiber.
4. Water cured cement grout specimen showed higher strength than air cured specimen while heat cured specimen had smaller strength. However Young's modulus of the specimens were found to be similar.

5. Study proved the quick setting and early strength gain capabilities of patch material. Around 90% of the compressive strength was attained after 1 day. Specimen cured for 3.5 hours almost reached the elastic modulus of the 3day specimen.
6. From the tensile bonding strength tests, patch had better bonding with concrete (91.9 psi) than with asphalt tack coat (24.4 psi). Also patch-asphalt bonding was better than concrete-asphaltic binder bonding. Double shear bonding strength of patch material was 21.6 psi which is lower than tensile bonding strength.
7. Patch material enhanced the bonding between the asphaltic tack coat and concrete. Asphalt can be applied on to patch tack coat in one hour because of rapid gain in compressive and bonding strength of the patch.

## **CHAPTER 4      SELF MONITORING BEHAVIOR OF BULK REPAIR MATERIALS**

A material which can monitor itself depending on its intrinsic properties is referred to as self-sensing or self-monitoring material. Self-sensing ability is essential for load monitoring and structural health monitoring. In such cases the smart material should respond to applied stresses and other changes while performing as per structural requirements. In this chapter, piezoresistivity of polymeric and cementitious materials was investigated as the sensing property. Mainly compressive piezoresistive behavior was considered while tensile and flexural response was also studied. Performances due to shape effects, different service conditions, and material modification were discussed.

### **4.1 Materials and Methods**

#### **4.1.1 Materials**

Epoxy grout, cement grout and concrete materials discussed in chapter 3 were investigated for piezoresistive behavior. A commercially available PAN based short carbon fibers (6.3 mm in length) with a tensile strength of 3800 MPa, tensile modulus of 228 GPa and density of 1810 kg/m<sup>3</sup> were used in order to develop piezoresistivity. Class-C fly ash was used as a modification to concrete material.

#### **4.1.2 Modification and Optimization of Fiber**

Short carbon fiber was modified by mechanically dispersing it. It allowed reducing the amount of fiber added in composites while maintaining the piezoresistive behavior. For example, in epoxy grout composites the amount of fiber needed to attain percolation was reduced from 3% (by wt. of composite) to 0.5% which is 6 times lower. Likewise in the cement grout, only 0.1%

(by wt. of dry mix) of modified fiber was required whereas 1% short carbon fiber was needed to have similar performance.

### **4.1.3 Specimen preparation**

Cylinders with diameter of 1.5 in. were prepared for compressive piezoresistivity testing. For tensile piezoresistive testing, dump-bell shaped specimen was made. For flexural testing, beams of size 12\*2\*2 inches were prepared. Material mixing procedure is described in chapter 3.

Conductive cables were embedded in the specimen while casting. Two-probe method was chosen and cables were spaced at 1.5 to 2.5 inches. Depth of embedment of conductive part was 1 in. Preliminary Impedance Spectroscopy (IS) study done on an epoxy grout specimen showed that the contact resistance was around 1% of the bulk resistance. Therefore two-probe method is good enough for the intended applications. Also it is easy to install and cheap compared to the methods used by researchers in the literature.

### **4.1.4 Compression Test**

As shown in Figure 4-1, specimens were subjected to uniaxial compressive loading and resistivity behavior was monitored. Tinius Olsen hydraulic testing machine was used for loading. Hewlett Packard 34420A NanoVolt/Micro Ohm meter having a least count of 1  $\mu\Omega$  was used for electrical resistance measurement. Plain paper was used as an insulator to separate possible contacts with machine. In addition, a clip-gage extensometer was used to measure the strain.

### **4.1.5 Tensile Test**

Experimental set up for a tensile piezoresistive testing is shown in Figure 4-2. As shown in the figure, dump-bell shaped specimen was fixed at the bottom and a tensile force was applied from the top.

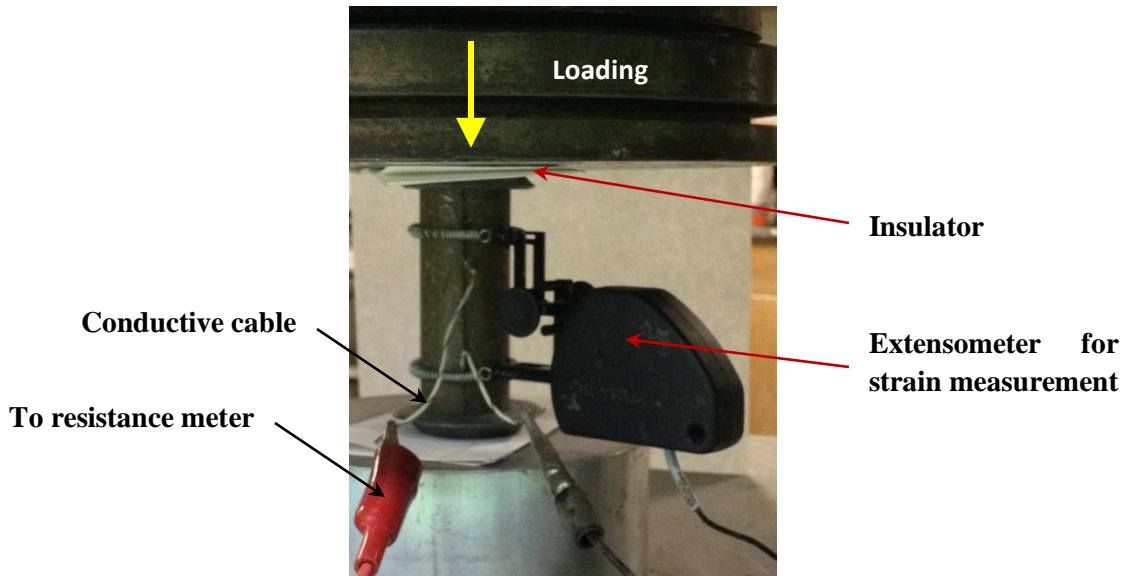


**Figure 4-1: Experimental setup for compressive piezoresistive testing**

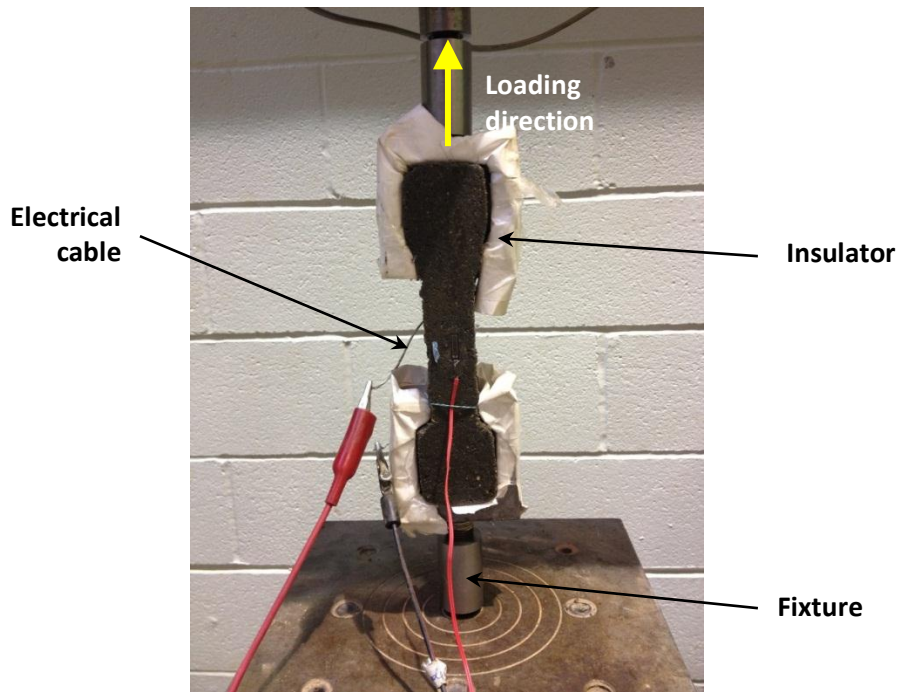


**Figure 4-2: Experimental setup for compressive piezoresistive testing**

## 4.1.6 Flexural Test

### 4.1.6.1 Beam

A beam made of MM was tested under four point bending loading to characterize the piezoresistive behavior under flexural stress. The beam was supported and loaded as shown in Figure 9, and resistivity was measured between different pair of electrical cables. MM block was tested for piezoresistivity under 3 point loading in Tinius Olsen testing machine. Experimental setup is shown in Figure 8.

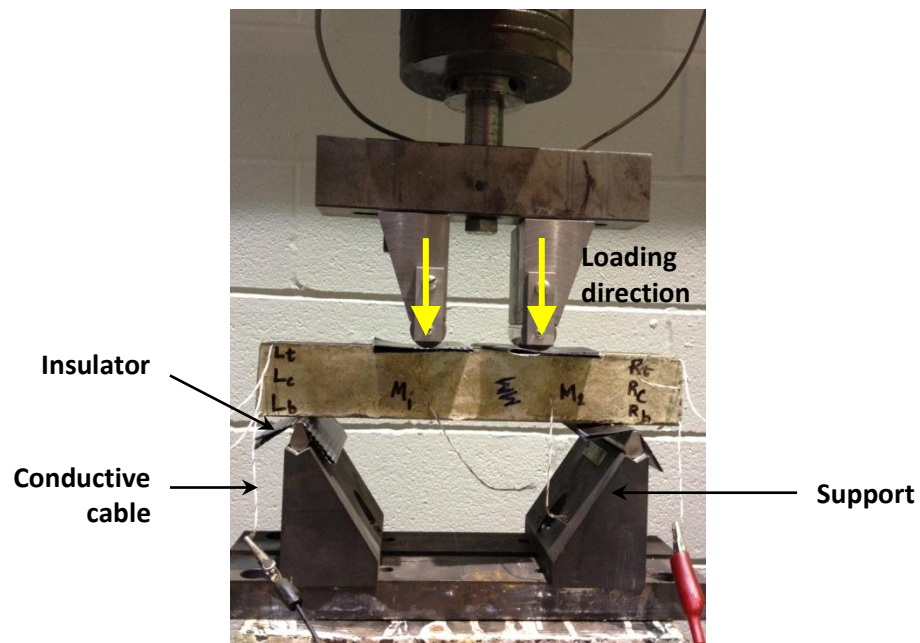
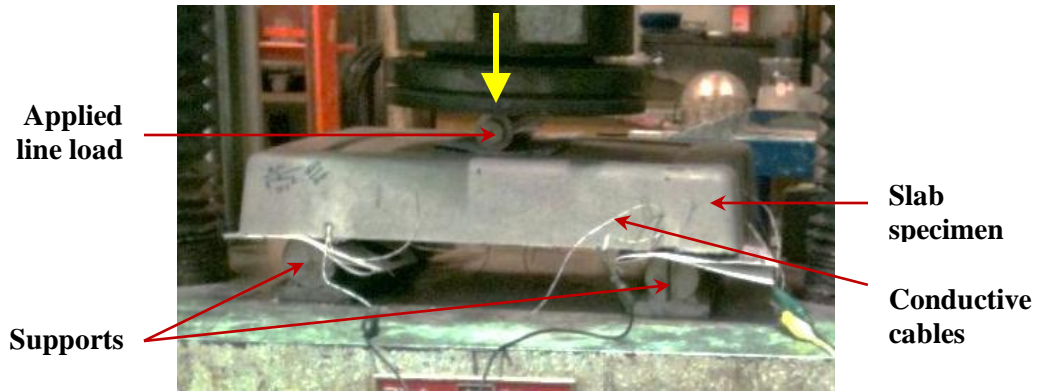


Figure 4-3: Experimental setup for flexural piezoresistive test

### 4.1.6.2 Slab

To study the scale effect in cement grout specimens, a slab having dimension of 44.5 cm\*36.2 cm\*7.6 cm was casted using 0.1% fiber loading. Compressive line loading was applied to the slab while supported on two lines. This resembles the three point bending test for beams. Figure 4-4 shows the loading setup. Embedded conductive cables were used to measure resistance.



**Figure 4-4: Testing Cement grout slab under 3 point bending loading**

#### 4.1.6.3 Thin Disk

A thin disk made of epoxy grout was tested under bending loading. It had a thickness of 0.18 in. and a diameter of 3 in. The disk was supported along its perimeter and compressive point load was applied on the disk as shown in Figure 4-5. Simultaneously electrical resistance was measured.

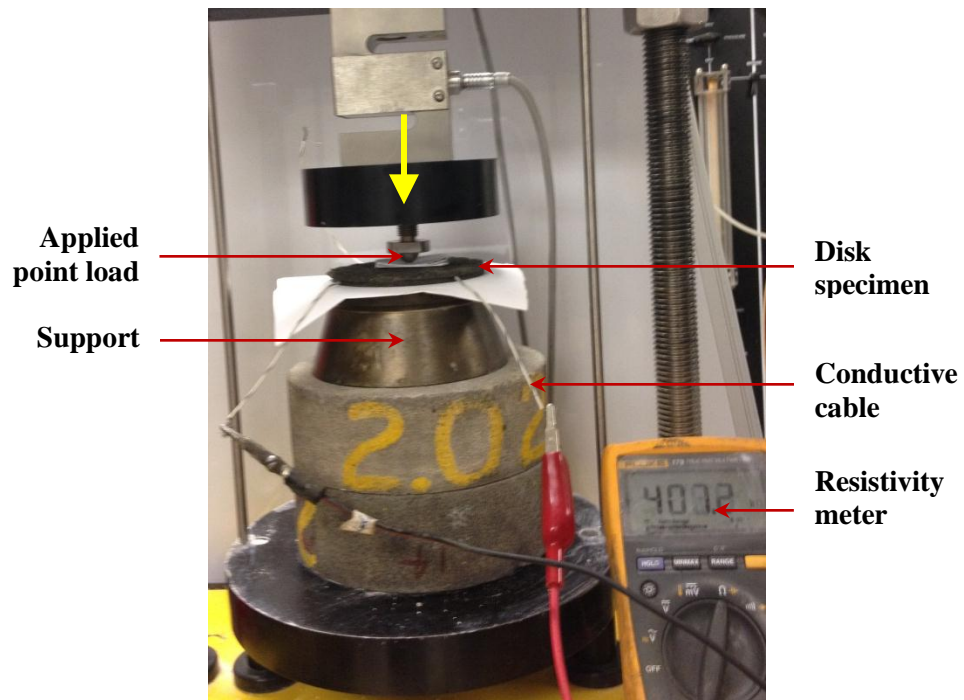


**Figure 4-5: Experimental setup for testing thin disk under bending**

## 4.2 Piezoresistive behavior

Piezoresistive characterization of epoxy grout and cement grout under different loading is dealt in the following sub section.

### 4.2.1 Compression

#### 4.2.1.1 Epoxy Grout

Piezoresistive behavior of epoxy grout with carbon fiber is shown in Figure 4-6. It should be noted that epoxy grout without the addition of carbon fiber is an insulator. In Figure 4-6, one specimen had 4% short fiber where the other one had 0.6% modified fiber. It was observed that modification of fiber not only enabled the reduction in usage of fiber but also improved the piezoresistive behavior. At the stress level of 30 MPa, specimen with short fiber showed about 0.3% of change whereas the resistivity of other specimen changed by more than 7%. At failure, specimen with modified fiber showed a change of more than 54% while the specimen with short fiber showed a change of 20%.

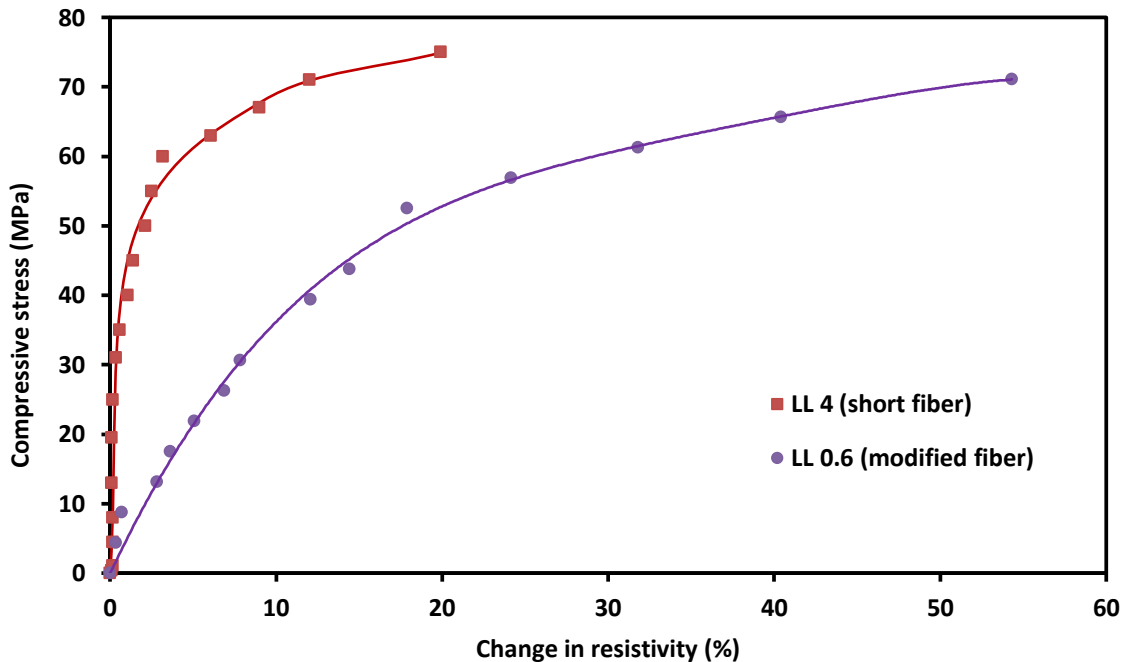
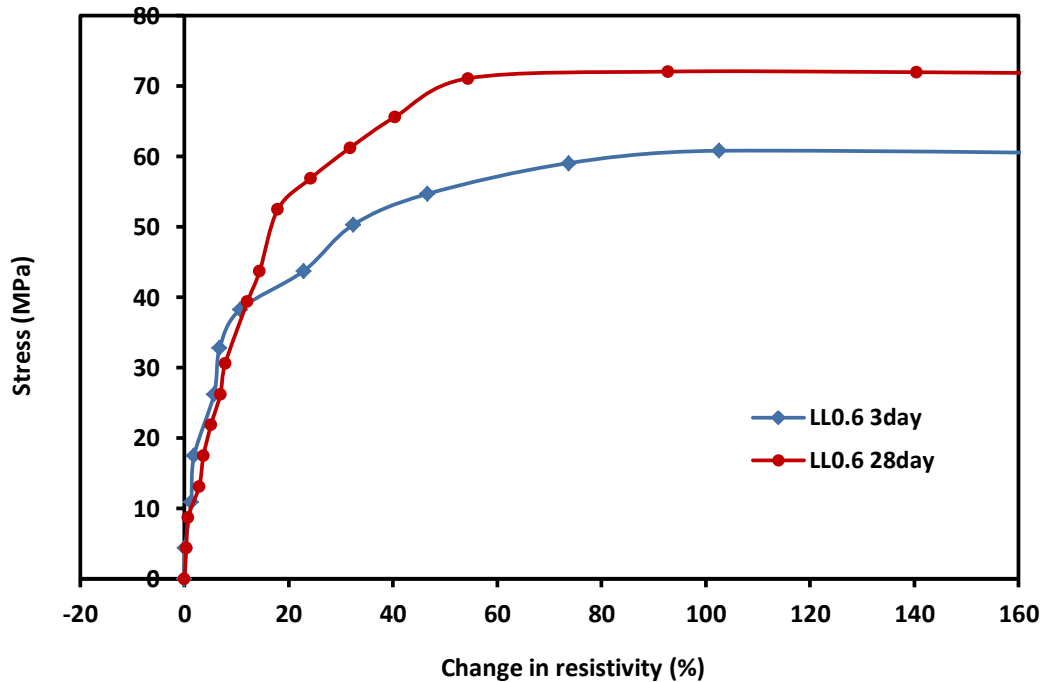


Figure 4-6: Effect of fiber modification on Stress-Resistivity relationship for epoxy grout

Effect of curing on piezoresistive behavior of epoxy grout specimen is shown in Figure 4-7. One specimen was cured for 28 days while the other one was cured for three days. As shown in Figure 4-7 piezoresistive behavior for both specimens were identical. This showed that piezoresistive behavior is not changed with curing age even though the strength improved by 20% from 3<sup>rd</sup> day to 28<sup>th</sup> day.



**Figure 4-7: Piezoresistive behavior of epoxy grout at different curing ages**

A comparison of resistivity vs. strain for the same stress levels on the specimen is done in Figure 4-8. It is clear that resistivity is a better indicator than strain. At 30 MPa, resistivity showed a change of 2% while the corresponding change in strain was 0.2%.

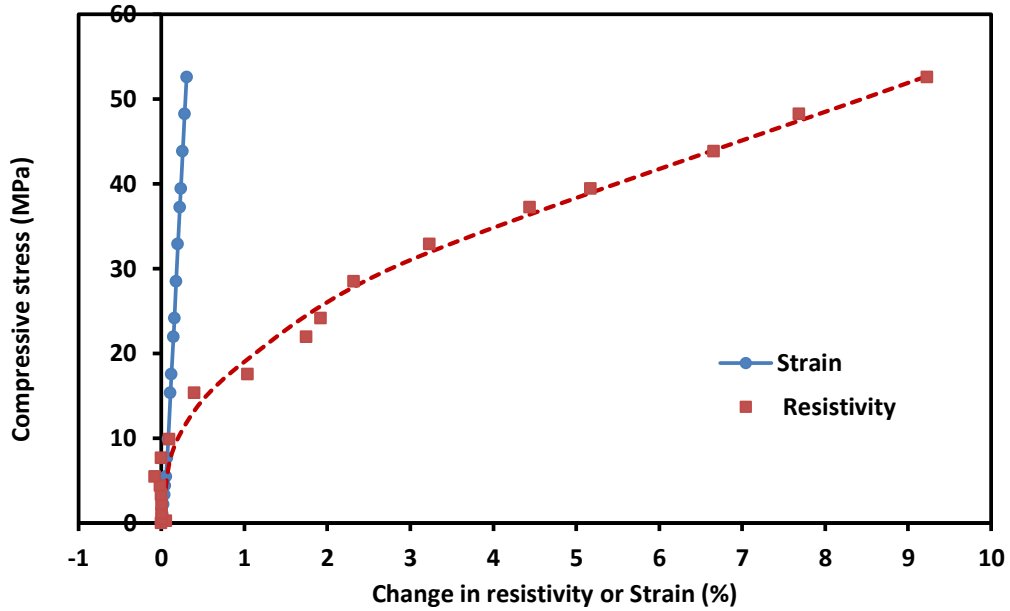


**Figure 4-8: Comparison of resistivity and strain for epoxy grout**

Piezoresistive behavior of six epoxy grout specimens with 0.6% (w/w) modified fiber reinforcement is compared in Figure 4-9. Specimens were cured for 28 days. The stress of each specimen was normalized with respect to its compressive strength. At 40% of strength, specimens showed a change of 3-10% in resistivity. Likewise at 60% strength level, 7-30% change was observed. Just prior to failure, 80-180% change in resistivity was monitored.

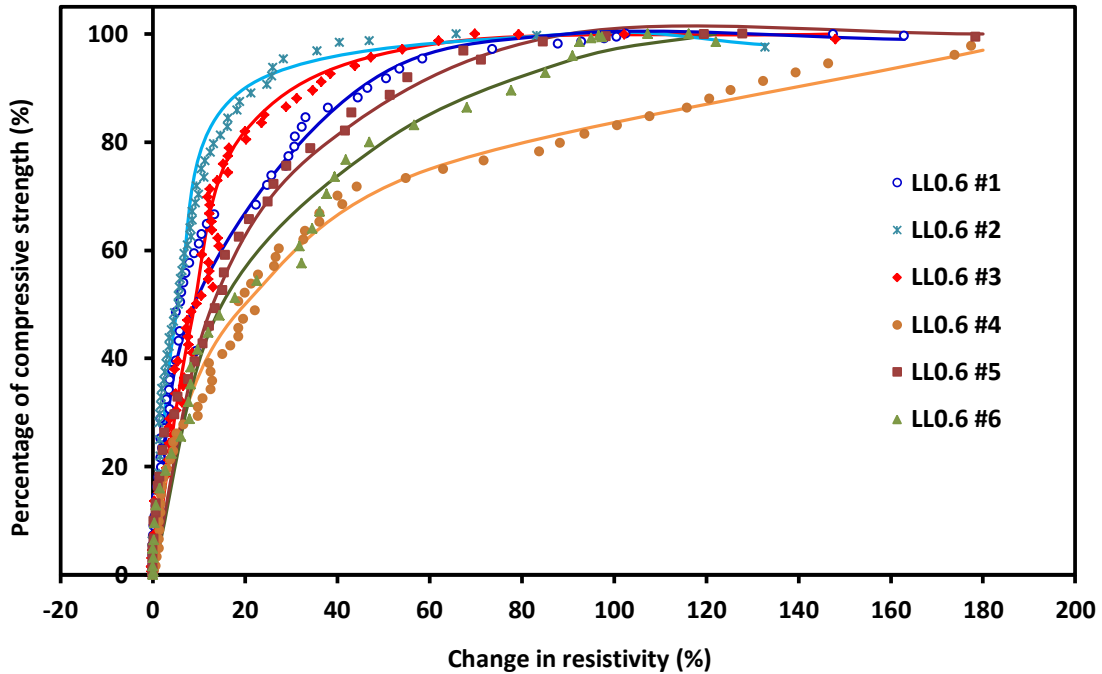


**Figure 4-9: Stress-Resistivity relationship of epoxy grout**

#### 4.2.1.2 Cement Grout

Figure 4-10 shows the effect of fiber on the piezoresistive behavior of cement grout. Specimen without fiber didn't have piezoresistivity at all. Specimens with modified fiber in the amounts of 0.1% and 0.15% both showed good piezoresistive behavior. At half the strength of cement grout, resistivity showed a change of about 6% which is 40 times more than the change in strain. This makes piezoresistivity a good self-sensing property of the material. Piezoresistive behavior of five cement grout specimens is compared in Figure 4-11. Specimens had 0.1% (w/w) modified fiber. Tests were done after 14 days of curing. At 20 MPa specimens showed more than 2% change in resistivity. Prior to failure, more than 25% change in resistivity was observed.

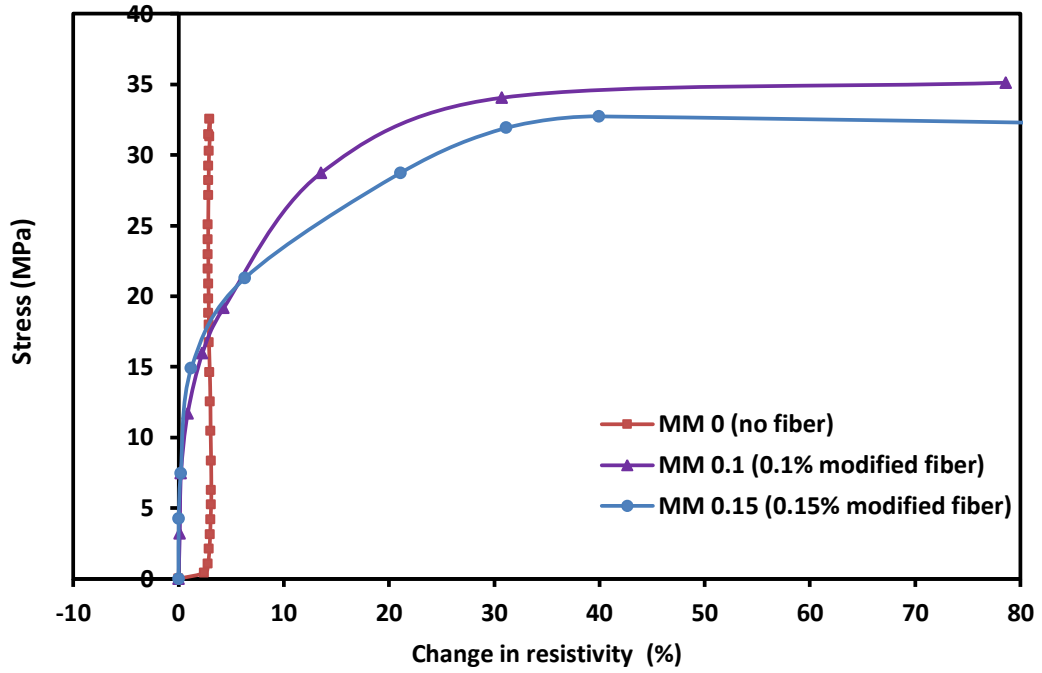


Figure 4-10: Effect of fiber on stress-resistivity relationship of cement grout

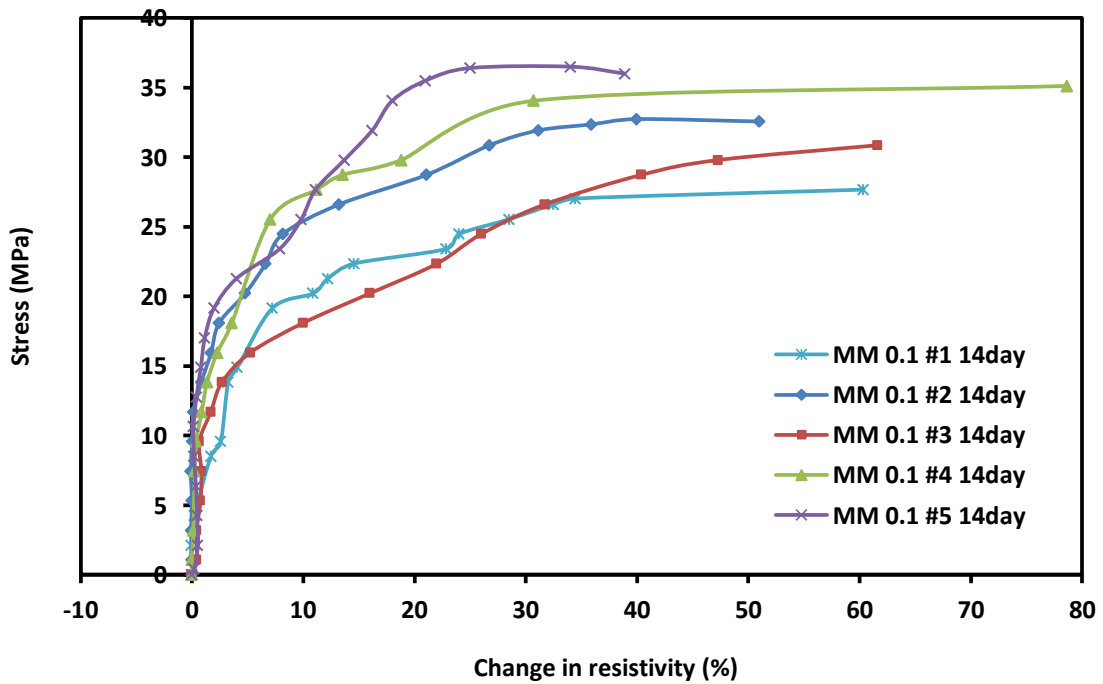


Figure 4-11: Stress-resistivity relationship of cement grout

#### 4.2.1.3 Comparison of repair materials

Piezoresistive behavior of four bulk repair materials, epoxy grout, cement grout, concrete and patch, is compared in Figure 4-12 and Figure 4-13. Amount of modified fiber reinforcement was 0.6%, 0.1%, 0.5% and 0.5% (w/w) respectively. Figure 4-12 shows the stress-resistivity behavior while change in resistivity with percentage of strength is compared in Figure 4-13. As shown in Figure 4-13, resistivity of grout materials increased with stress while concrete and patch material showed decreasing trend. Epoxy grout showed more sensitivity than the other materials. At half the strength, epoxy grout showed about 10% change in resistivity. Corresponding value was 3%, 3% and 5% for cement grout, concrete and patch. Prior to failure, change in resistivity was 92%, 78%, 13% and 18% respectively.

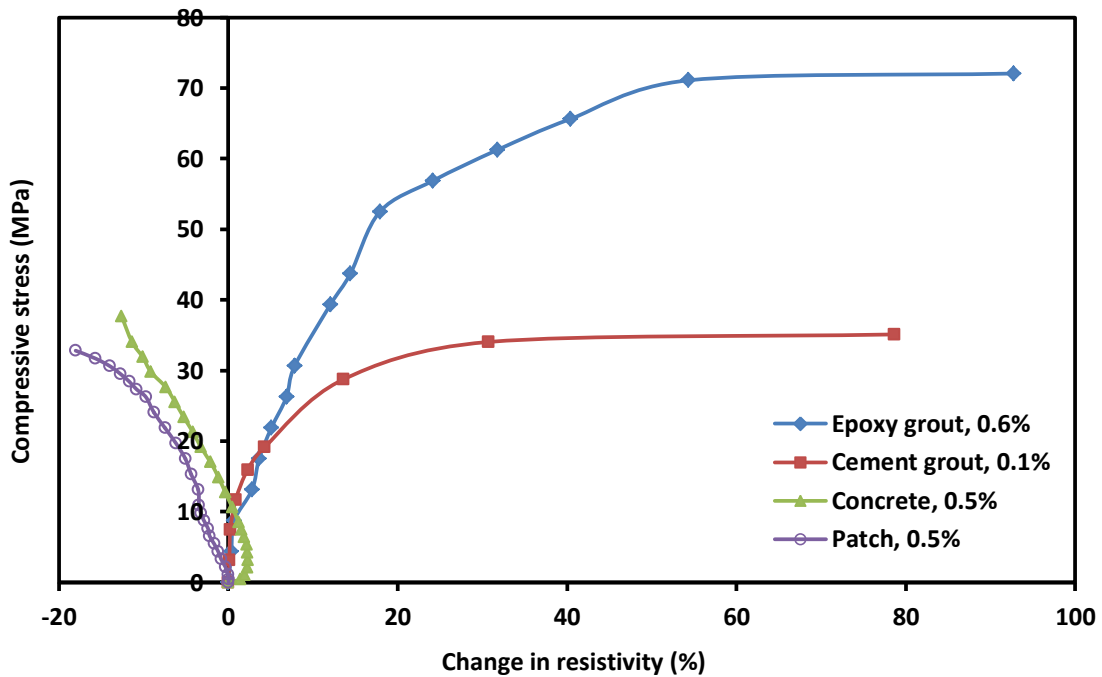


Figure 4-12: Comparison of stress-resistivity relationship of repair materials

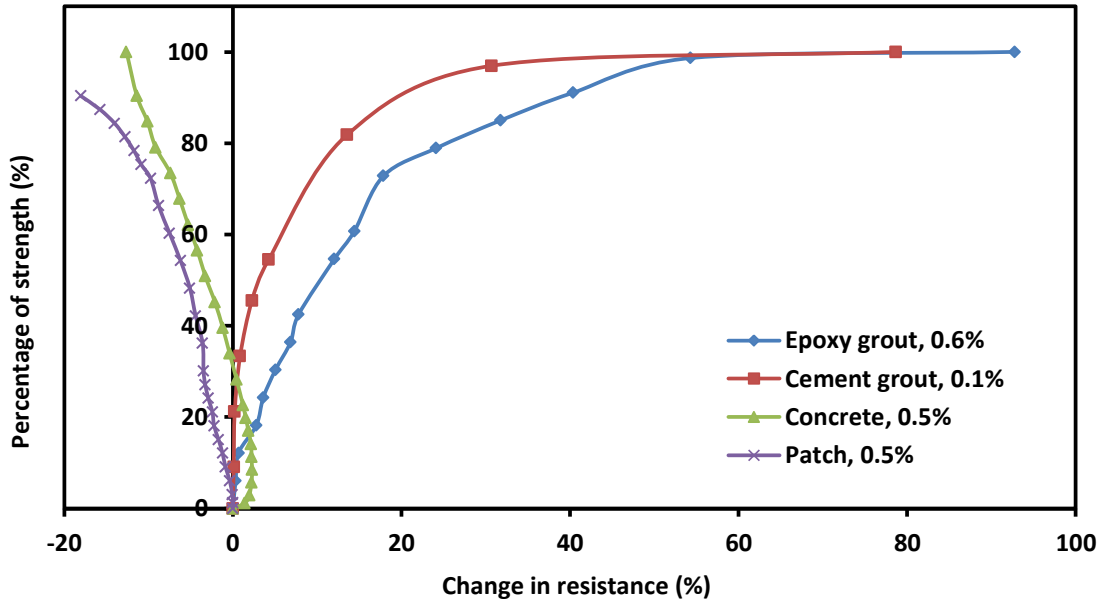


Figure 4-13: Piezoresistive behavior of repair materials with percentage of strength

#### 4.2.2 Tension

Piezoresistive behavior of 1% fiber added epoxy grout specimen under tensile loading is shown in Figure 4-14. As shown in the figure, epoxy grout had piezoresistivity. Behavior under tension was similar to that of compressive behavior.

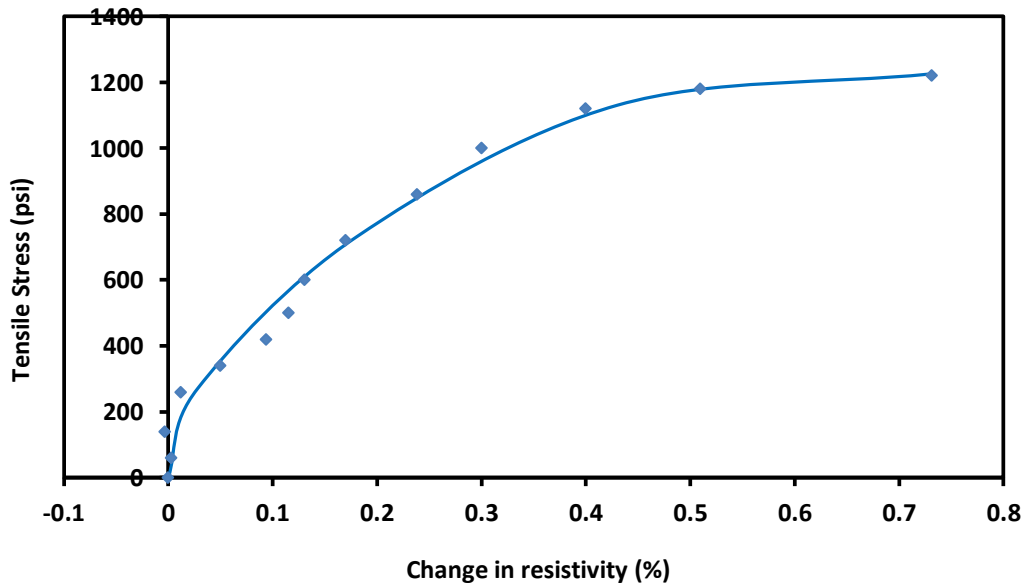


Figure 4-14: Stress-Resistivity relationship of epoxy grout under tension

### 4.2.3 Flexure

Beam made of cement grout (with 0.1% fiber) was tested under four point bending. Figure 4-16 shows the resistivity-stress behavior measured between two different pair of conductive cables in the beam. For the first one ( $L_bR_b$ ), resistance was measured between cables at the bottom in left and right sides. This represents the tension side of the beam under bending loading. The locations are indicated in the schematic as seen in Figure 4-15. Second location ( $M_1M_2$ ) was in the middle. As seen in Figure 4-16, in both cases piezoresistive behavior was observed. Unlike the cases for tension or compression, resistivity sensed even at small stress levels.

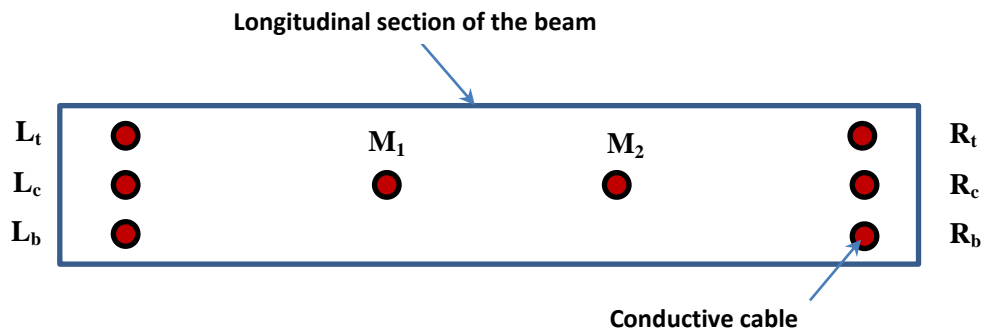


Figure 4-15: Schematic of location of conductive cables in the beam

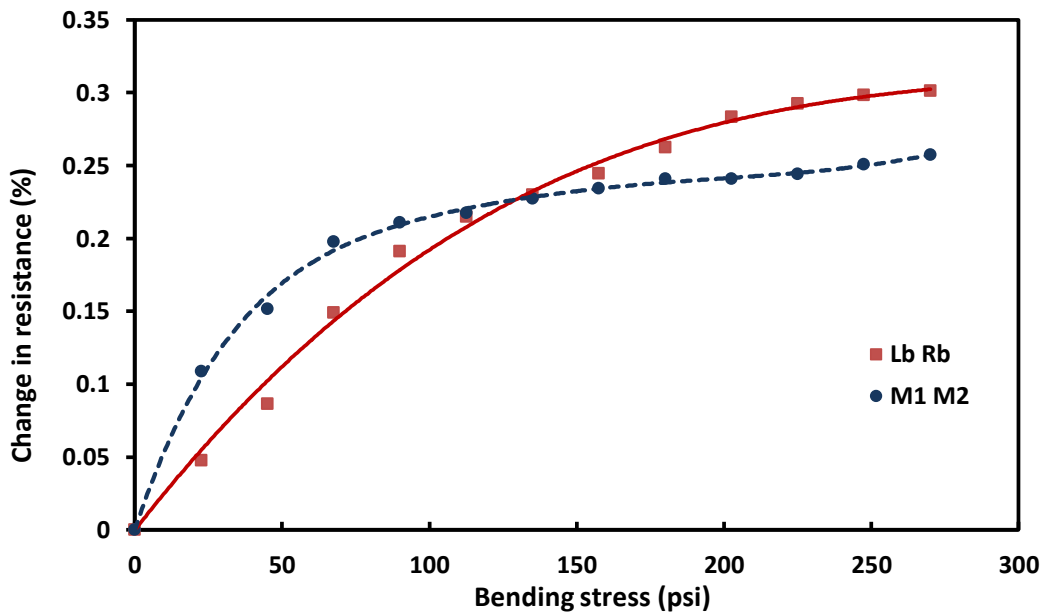
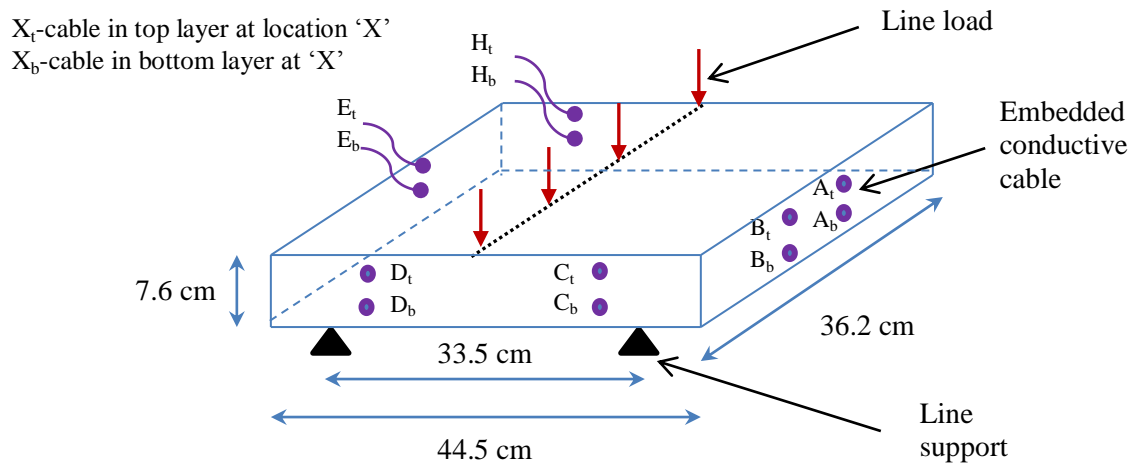


Figure 4-16: Piezoresistive behavior under flexural loading

### 4.3 Shape Effect on Piezoresistivity

#### 4.3.1 Slab

In the cement grout slab, conductive cables were embedded longitudinally at different spacing in two layers. Figure 4-17 shows the schematic diagram of the cement grout slab. Conductive cables are denoted as  $X_t$  and  $X_b$  which stand for cables at top and bottom layer respectively. For example,  $C_t$  and  $C_b$  means cables in top and bottom layers at location 'C.' The schematic of the slab and location of supports and loading are shown in Figure 4-17. Four different pairs of cables were selected and resistance was measured under the bending loading. Out of those four pairs, two ( $A_b$ - $B_b$  and  $C_t$ - $D_t$ ) were in longitudinal direction with the spacing of 10 cm and 30 cm respectively. Here  $A_b$ - $B_b$  means that resistance was measured between bottom layer cables at locations 'A' and 'B'. The other two pairs of cables ( $E_t$ - $E_b$  and  $H_t$ - $H_b$ ) were selected (with spacing of 3 cm between top and bottom layers) in a way that resistance along depth was taken into consideration.



**Figure 4-17: Schematic diagram of the casted cement grout slab**

Figure 4-18 shows the variation of resistance with the applied line load. It was observed that resistance between longitudinal cables showed an increasing pattern with load. This is acceptable as tests on cylinders also had a similar trend. However, the trend was not clear in the case of measurement across depth. The smaller changes across the depth can be attributed to the lower stress level experienced across depth.

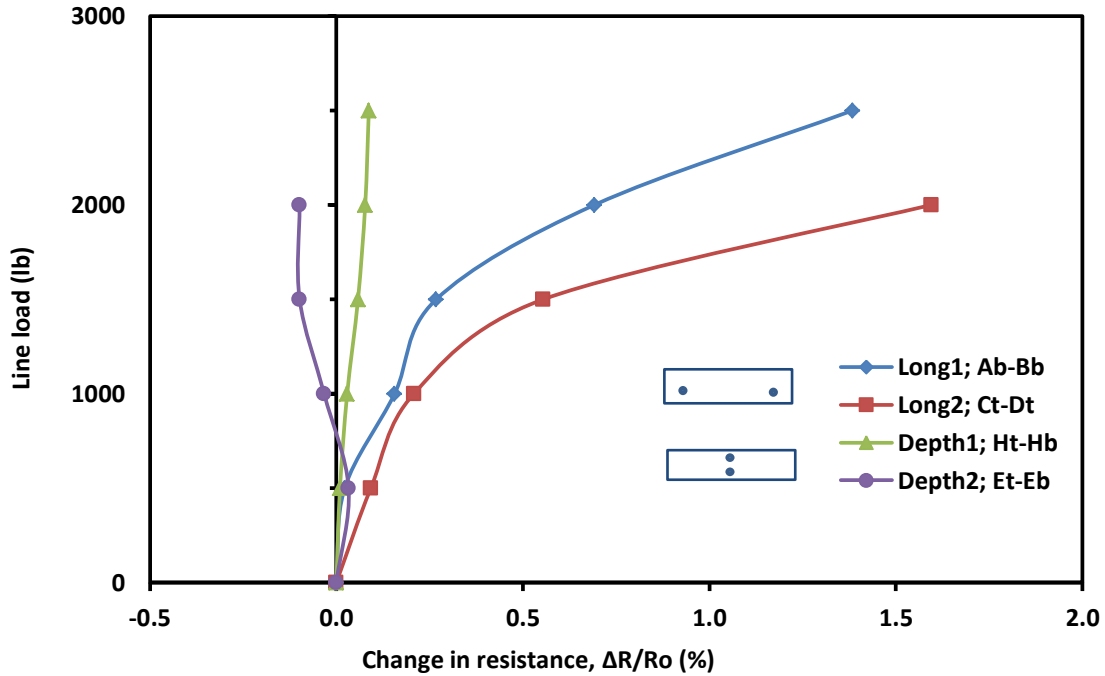
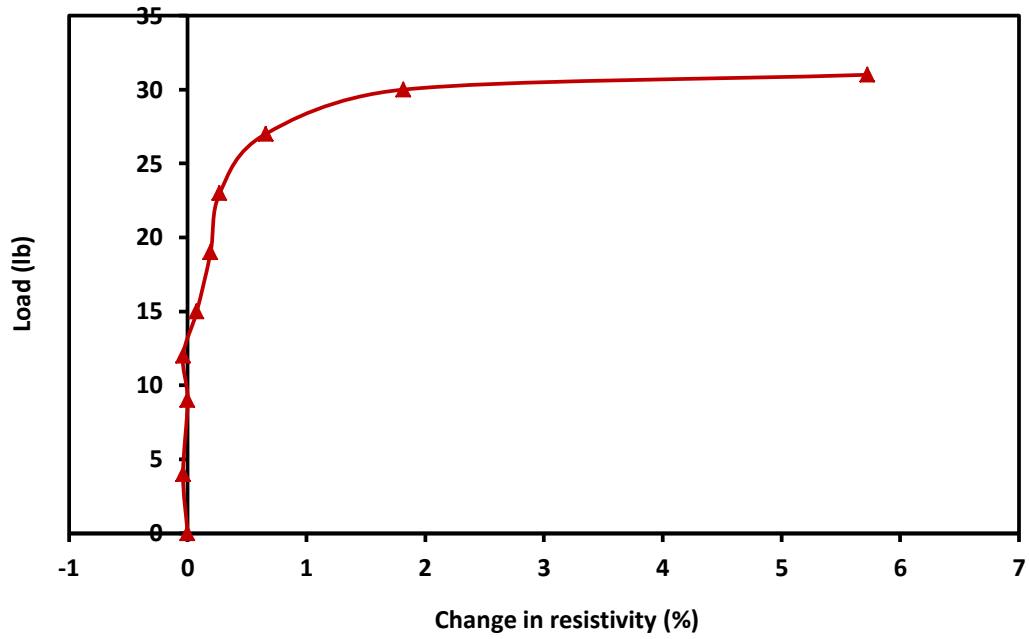


Figure 4-18: Load-resistivity relationship in cement grout slab under bending loading

### 4.3.2 Thin Disk

Figure 4-19 shows the stress-resistivity behavior of thin disk made of epoxy grout. The disk showed piezoresistive behavior and at around 30 lb, a 6% change in resistivity was monitored.



**Figure 4-19: Stress-Resistivity relationship for thin disk under bending**

## **4.4 Service Conditions**

### **4.4.1 Flowability**

When fiber was used with cement grout, flowability was affected little bit. To study the extent of the effect, flow table studies were carried out according to ASTM C 230. Procedure for flow test is shown Figure 4-20.

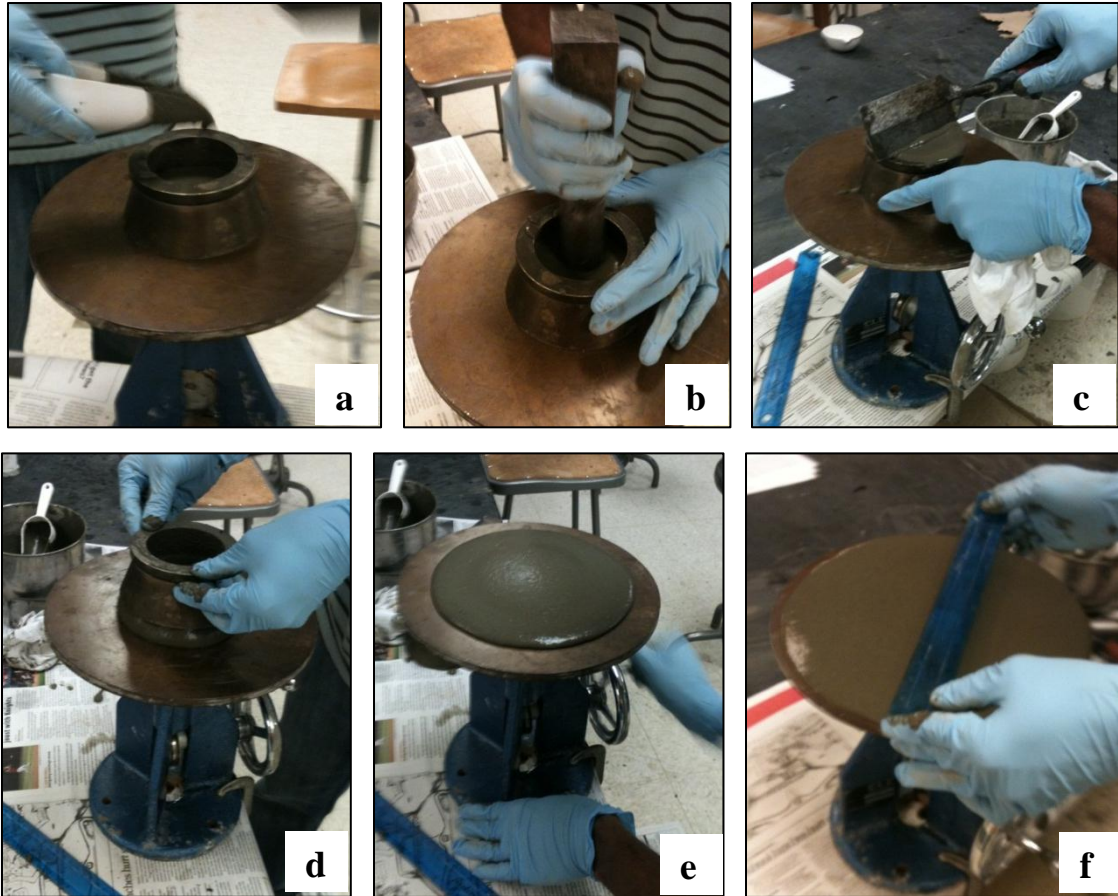


**Figure 4-20: Flow test for fiber reinforced cement grout using flow table** (a) filling mold in thirds (b) compacting (c) leveling on top (d) lifting mold (e) raising and dropping table top by rotating cam (f) measuring the flow diameter

**Table 4-1: Flow measurement for fiber loaded cement grout**

Fiber loading (w/w %)	Flow diameter (cm)	Remarks
0	25.5	-
0.1	24	With 2 more rotations, 25 cm was achieved, when preparing specimen no much difference was observed in workability.
0.15	23	With 2 more rotations, 24.5 cm was achieved; workability was affected a little bit.
0.2	22.5	-

Table 4-1 shows the average flow diameter with fiber loading. It should be noted that up to 0.15% loading, flowability was not affected much. But loading of more than 0.15% decreases the flowability; however it showed good piezoresistive relationship.

#### 4.4.2 Temperature cycling

##### 4.4.2.1 Epoxy Grout

Effect of different curing conditions on the piezoresistive behavior of epoxy grout material was studied. Ten specimens (with 1.45” diameter) were prepared with 0.6% (by wt.) fiber loading to study the effect of curing. After one day of curing in room temperature (25°C), specimens were subjected to five different curing conditions for 29 days as indicated in Table 4-2.

**Table 4-2: Different curing conditions applied for epoxy grout specimens**

<b>Specimen no</b>	<b>Medium of curing</b>	<b>Temperature (°C)</b>	<b>Simulated environment</b>
#1, #4	Air	25	Normal condition
#2, #3	Water	25	Wetting
#6, #7	Air	55	Heating
#8, #9	Air	5	Thawing temperature
#10, #11	Air	-15	Freezing temperature

Mass and electrical resistance of specimens were monitored. Variation of electrical resistance and mass are summarized in Table 4-3 and Table 4-4 respectively. After 29 days of monitoring, specimens were tested for piezoresistivity.

**Table 4-3: Variation of initial resistance of epoxy grout at various curing conditions**

No of days	Measured resistance (kilo Ohms)									
	Air cured at 25°C		Water cured at 25°C		Air cured at 55°C		Air cured at 5°C		Air cured at -15°C	
	#1	#4	#2	#3	#6	#7	#8	#9	#10	#11
0	0.545	12.28	2.204	5.899	2.055	1.192	9.96	1.587	1.468	10.52
1	0.531	10.73	2.235	5.63	1.952	1.144	9.25	1.567	1.438	9.71
4	0.512	9.9	2.67	7.19	4.17	2.88	8.29	1.503	1.295	8.67
7	0.502	9.49	2.79	7.38	3.35	2.157	7.86	1.496	1.285	7.39
11	0.502	9.41	2.947	7.27	3.219	2.271	7.74	1.495	1.161	7.29
29	0.486	8.96	2.91	7.29	3.135	2.025	7.87	1.482	1.165	7.29

**Table 4-4: Variation of mass of epoxy grout at various curing conditions**

No of days	Mass of the specimen (grams)									
	Air cured at 25°C		Water cured at 25°C		Air cured at 55°C		Air cured at 5°C		Air cured at -15°C	
	#1	#4	#2	#3	#6	#7	#8	#9	#10	#11
0	226.4	227.6	234.8	231.2	224.6	219.3	239.8	226.8	220.4	223.1
7	226.3	227.6	234.8	231.5	225.5	219.2	239.8	226.7	220.4	223.4
11	226.3	227.5	234.7	231.6	225.6	219.2	239.8	226.7	220.4	223.4
17	226.2	227.6	234.7	231.6	225.7	219.2	239.4	226.6	220.4	223.4
29	226.1	227.3	234.5	230.8	224.4	218.9	239.1	226.7	220.5	223.4

As the measurements in Table 4-3 indicate, there was not significant change in mass. In most cases, the percentage change in mass was below 0.1 %. For specimens which were air cured at 25°C, it was observed that initial resistance of specimen was dropping with curing age. However the trend showed that after 28 days initial resistance levels off. In the case of water curing, initial resistance increased by about 30% and levels off after 10 days. When the specimens were subjected to elevated temperature, a sudden increase of more than 100% in resistance was monitored at the fourth day. In thawing temperature (5°C), resistance decreased by about 5%. In freezing temperature, resistance of specimens showed a decrease of about 30% before leveling off.

It can be noted that specimens cured either in water or under elevated temperature showed an increase in initial resistance. On the other hand, the specimens which were air cured at room temperature, freezing temperature or thawing temperature showed decrease in initial resistance. But in all cases, resistance values stabilized after about 10 days. Also the lower the resistivity of the specimen, the lower the change it had in initial resistance.

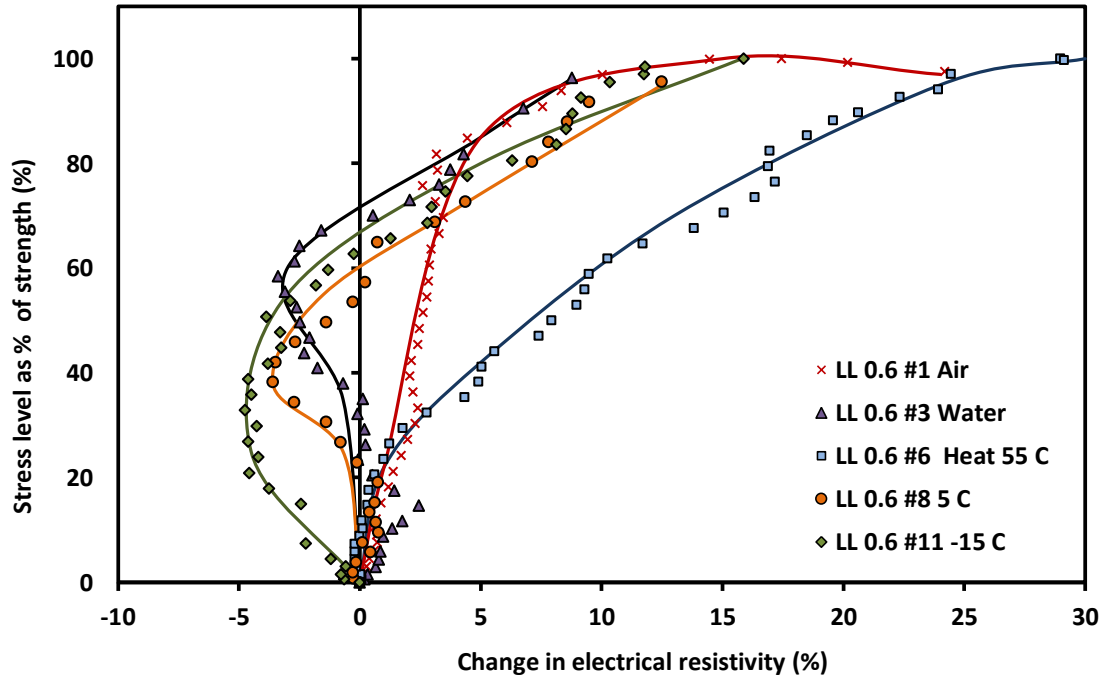


**Figure 4-21: Stress-Resistivity behavior of epoxy grout specimens after subjected to different curing conditions**

Figure 4-21 shows the stress-resistivity relationship of the specimens after subjected to different curing conditions. All the specimens showed piezoresistive behavior. Specimen which was air cured at freezing temperature showed higher sensitivity at small stress levels. After 70% of the strength was achieved, all the specimens except the heat cured one had comparable behavior. Heat cured specimen had more sensitivity at higher stress levels. Different piezoresistive behaviors show that curing condition has an effect on piezoresistivity for epoxy grout. However the material sustained the piezoresistive behavior.

#### 4.4.2.2 Cement Grout

As in the case of epoxy grout, 10 specimens were prepared and subjected to different curing conditions. Specimens #1 and #2 were kept at same temperature and condition. All other specimens were put into different curing conditions for a period of 17 days. Variation of electrical resistance and mass are summarized in Table 4-5 and Table 4-6 respectively. It should be noted that day 0 in the table corresponds to 7 days after preparing specimen at which new curing conditions were applied. After 17 days of monitoring, specimens were checked for piezoresistivity.

**Table 4-5: Variation of initial resistance of cement grout at various curing conditions**

No of days	Measured resistance (Ohms)									
	Air cured at 25°C		Water cured at 25°C		Air cured at 55°C		Air cured at 5°C		Air cured at -15°C	
	#1	#2	#3	#4	#5	#6	#7	#8	#9	#10
0	341	367	283.7	221.9	239.7	263.2	291.8	257.6	246	363
4	346.9	362.5	-	-	253.5	284.9	294	270.6	248.3	378.4
7	336.1	359.4	336.3	270.6	240.8	286.8	294	269.4	248.6	379.2
11	323	362.5	339.5	274.5	253.1	298.3	289.9	268.1	248.4	378.4
17	340.8	362.2	341.9	277.7	259.7	299.4	296.3	269.4	248.7	379.5

**Table 4-6: Variation of mass of cement grout at various curing conditions**

No of days	Mass of the specimen (grams)									
	Air cured at 25°C		Water cured at 25°C		Air cured at 55°C		Air cured at 5°C		Air cured at -15°C	
	#1	#2	#3	#4	#5	#6	#7	#8	#9	#10
0	212.5	250	215.5	214.9	202.3	214.8	205.3	215.2	200.4	255.6
4	211.9	249.2	-	-	191.8	203.3	205.5	215.4	200.6	255.8
7	211.7	248.9	222.1	221.1	190.2	201.7	205.7	215.4	200.7	255.9
11	210.7	247	223	221.4	189.7	201.1	205.8	215.5	200.4	255.4
17	212.5	250	215.5	214.9	202.3	214.8	205.3	215.2	200.4	255.6

In the case of water curing, as shown in Figure 4-22, both resistance and mass showed an increasing trend initially and leveled off after about eight days. It was observed that resistance increased by about 20%. The corresponding change in mass was about 3.5% as water was absorbed by the cement grout specimens.

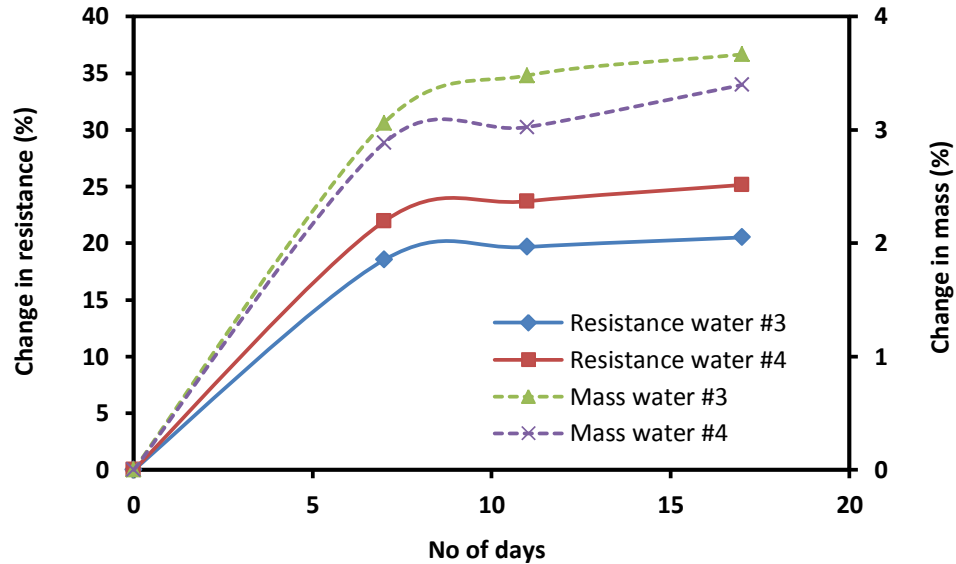


Figure 4-22: Variation of resistance and mass of cement grout specimens after water cured

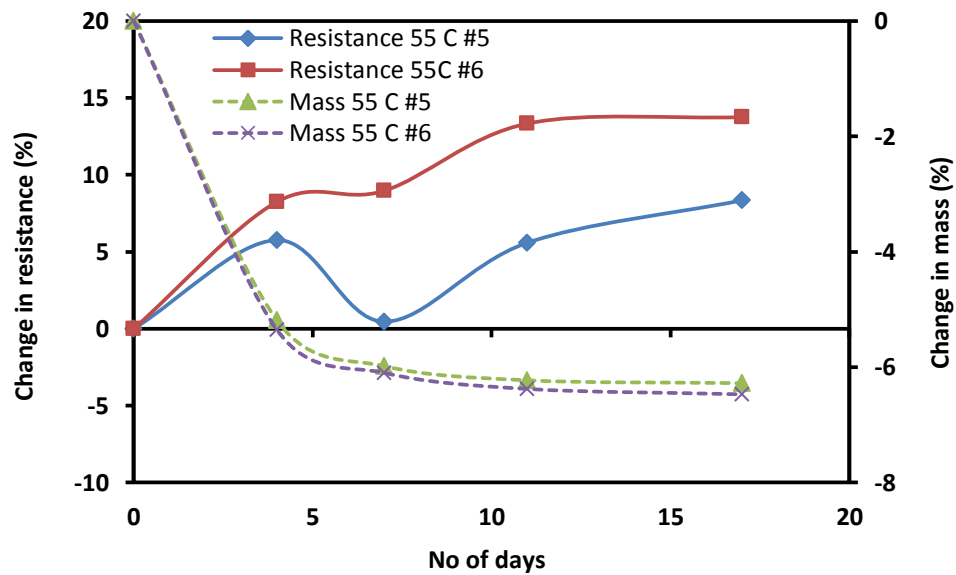
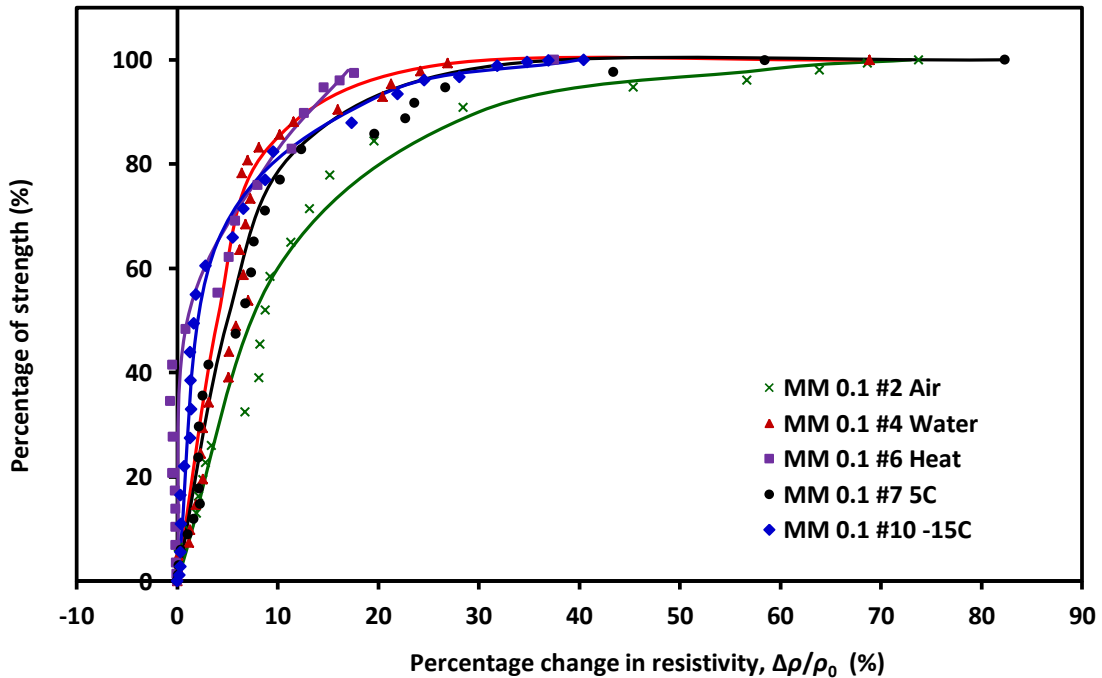


Figure 4-23: Variation of resistance and mass of cement grout specimens after heat cured

As shown in Figure 4-23, when the specimens were subjected to elevated temperature, an increase of 14% in resistance was monitored as the mass decreased by 6% because of loss of water. At thawing temperature (5°C), resistance showed a slight increase while no notable changes were observed for mass. In freezing temperature, resistance of specimens showed an increase of about 4% while the mass didn't change notably.

Figure 4-24 shows the variation in piezoresistive behavior of cement grout after subjected to different curing conditions. Stresses are normalized with respect to strength of each specimen. When comparing piezoresistive behavior of other specimens to the one which was air cured, heat cured specimen showed less sensitivity. However all the specimens more or less preserved the piezoresistive behavior. As a comparison, at a working stress of 50% of strength, specimens showed a change of more than 2% in resistivity which is about 10 times of conventional strain gage reading. Also when the stress level goes beyond 90% of the strength, resistivity changes by over 10% suddenly which is a good warning in order to prevent failure.



**Figure 4-24: Stress-Resistivity behavior of cement grout specimens after subjected to different curing conditions**

### 4.4.3 Curing Conditions

#### 4.4.3.1 Cement grout

From the moment a specimen is prepared, hydration occurs and microstructure changes. It is important to know when the material sets. It will be valuable if the internal electrical resistance can sense the changes occurring during curing time. Figure 4-25 shows the variation of electrical resistance and internal temperature of cement grout (with 0.1 % fiber) specimen from the time of casting. It was observed that both temperature and resistance showed a peak around the same time which suggests hydration activities. Also similar pattern was monitored for both parameters. Resistance leveled off approximately after 10 hours which proposes that specimen started setting. It is obvious that resistance can be relied upon for monitoring curing of cement grout, especially to decide whether the cast specimen is set enough in order to remove the formwork.

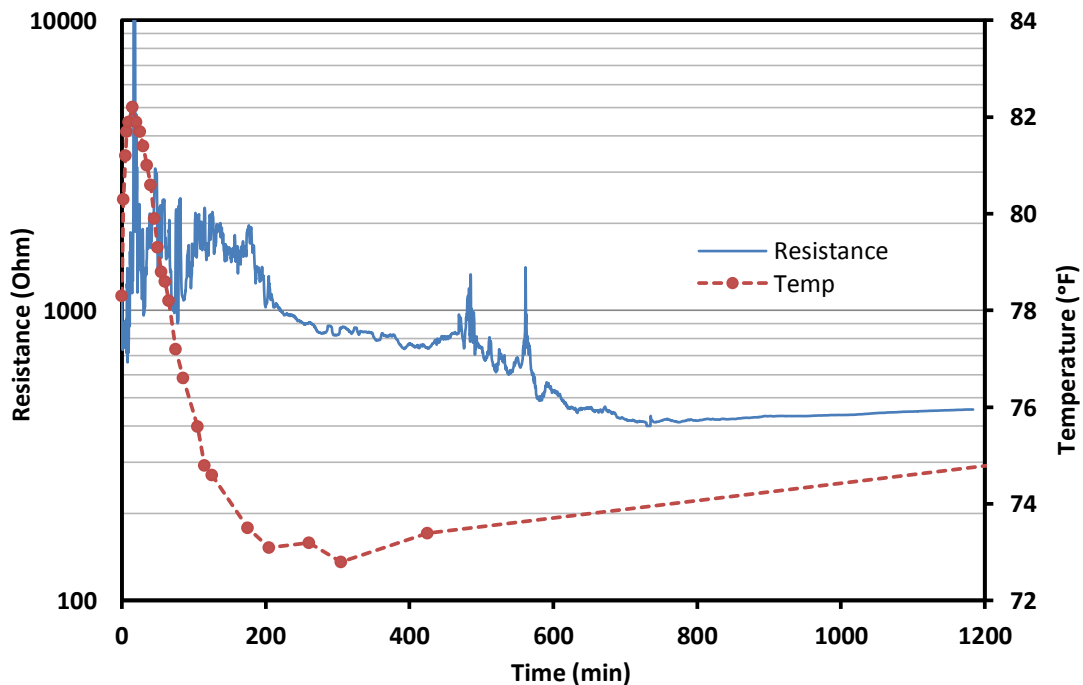


Figure 4-25: Curing monitoring from time of casting for cement grout

#### 4.4.3.2 Patch Material

In Figure 4-26, variation of resistance, internal temperature and Vicat needle penetration of patch material specimen are shown. A penetration of 25 mm is regarded as the initial setting time. As indicated by Vicat needle penetration, the initial setting time was around 30 minutes. But it is seen that resistance showed a peak just prior to that. It suggests some change in material level, and it could be the start time of the setting. Meanwhile, the temperature peak was observed just after the final setting time

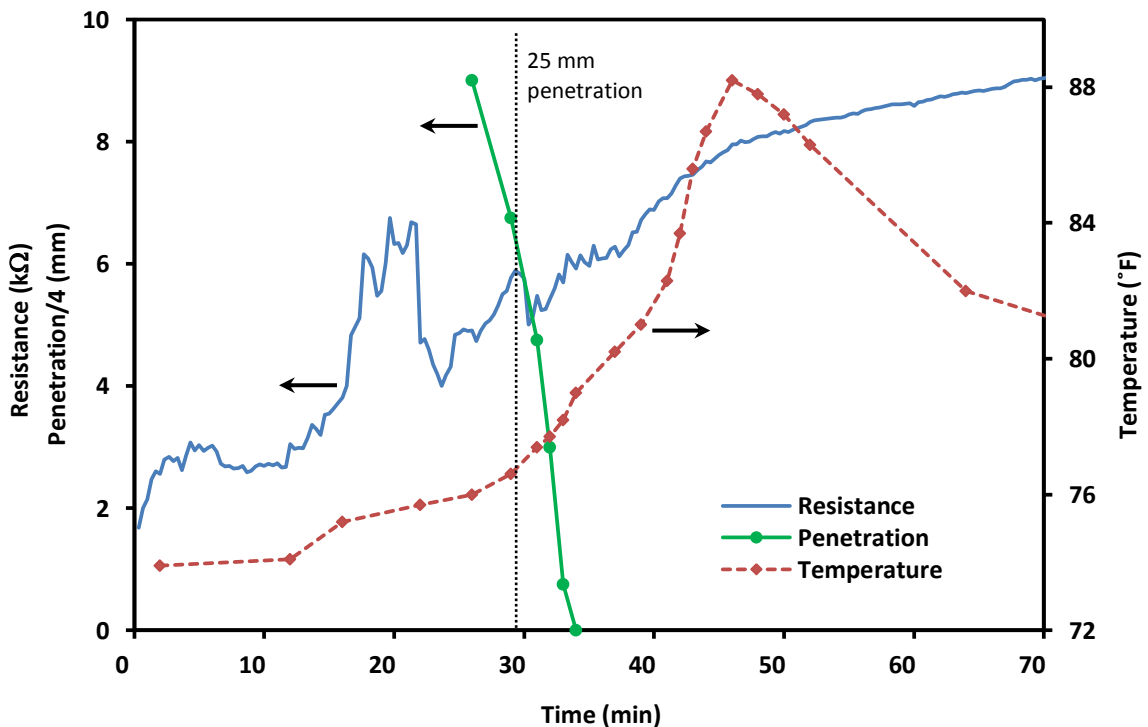


Figure 4-26: Monitoring curing of patch material

#### 4.4.4 Creep

Creep is of interest in long term perspective considering the fatigue life of materials. But creep cannot always be measured in the field. If creep can be correlated with piezoresistivity, it is worthwhile. A study was undertaken to quantify the creep using laboratory oedometer. In

particular, relationship between electrical resistivity and creep is of great attention. Figure 4-27 shows the experimental setup in an oedometer.

A cylindrical carbon fiber reinforced polymer concrete specimen was made for the testing. Two probes were embedded while casting. Compressive stress on the specimen was increased from 1.4 MPa to 7.0 MPa in stages in the increments of 1.4 MPa. It should be noted that 7.0 MPa is about 10% of the strength of the composite. Stress in each stage was sustained for 24 hours. Creep and resistance were monitored. Figure 4-28 shows the relationship between creep strain and fractional change in resistance with time. Few things are apparent from the plot. Creep strain increased with increasing stress. A variation was seen between creep strain and electrical resistance. Except noises while loading, a reduction in resistance was observed while creep rate was steady. This is explainable as when subjected to compressive stress, electrical resistance decreases in lower stress values as conduction path is formed.

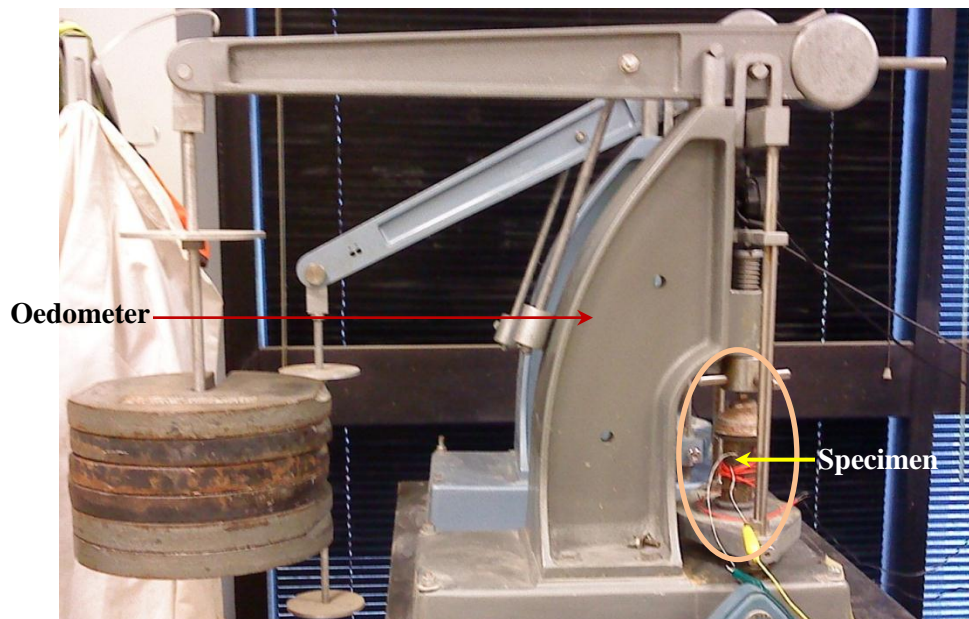


**Figure 4-27: Experimental setup for creep testing along with resistance measurement**

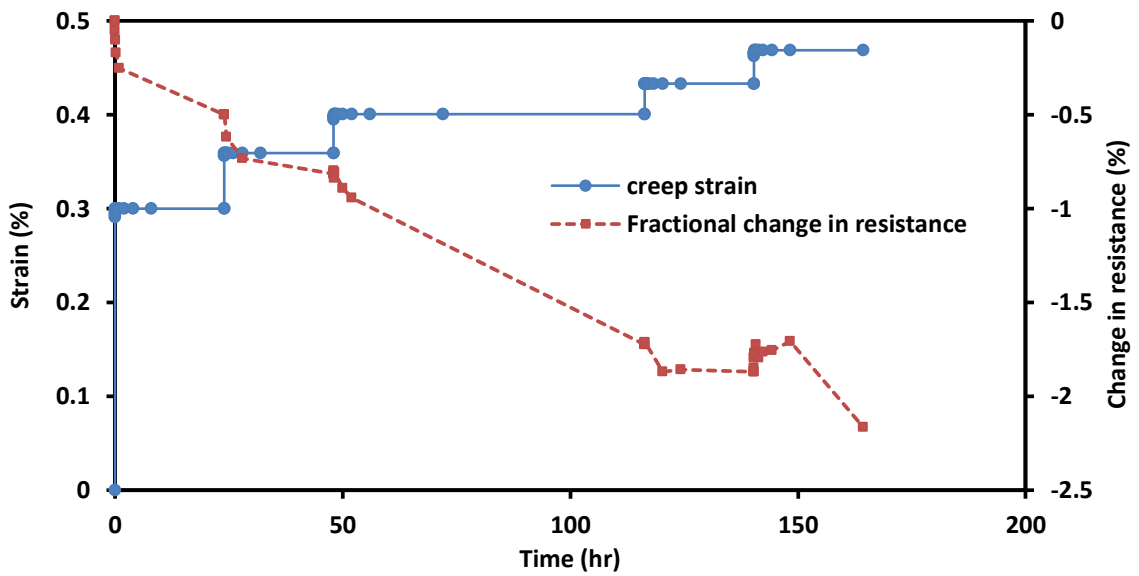


Figure 4-28: Relationship between creep strain and change in resistance with time

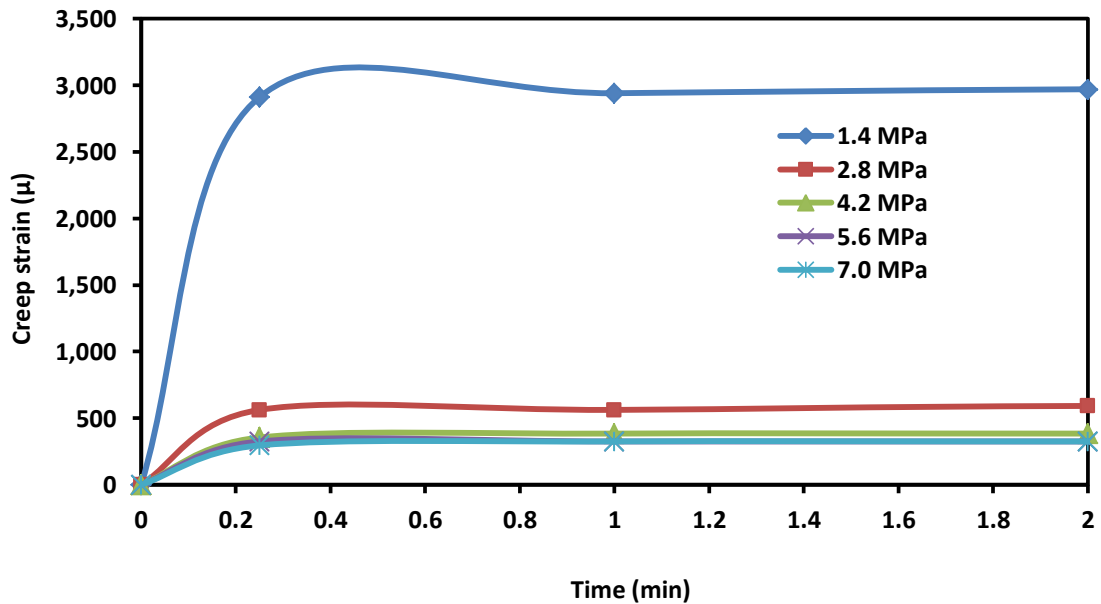
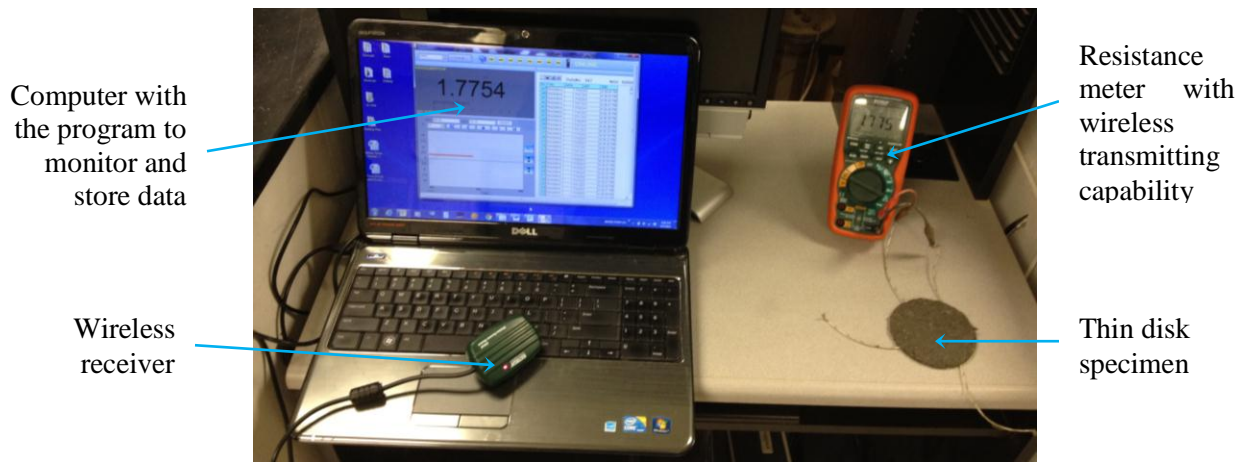


Figure 4-29: Creep strain in each stage of loading

It is clear from Figure 4-29 that creep reached to a steady value with in a short period of loading. This steadiness is referred to as secondary creep. Furthermore it is depicted that change in creep strain decreased with increasing stress level.

#### 4.4.5 Real Time Wireless Monitoring

Possibility of using a resistance meter which can transmit the reading wirelessly was studied. This is important since real time monitoring of structure may require automated continuous monitoring. The meter should be able to read the resistance at prescribed intervals while capturing the whole behavior. A test was performed on a cement grout specimen to see how accurate the wireless transmission is. For that, a commercially available resistance meter with wireless transmission capability was used along with the Ohm meter. Experimental setup for a real time wireless monitoring of a typical specimen is shown in Figure 4-30.



**Figure 4-30: Experimental setup for real time wireless monitoring**

From Figure 4-31 it can be said that wireless transmission was accurate and it captured the changes in the specimen very well. Most importantly, it was able to capture the moment of cracking and the failure very well. As shown in Figure 4-32, a sudden increase in resistance was captured when the first noise of crack was heard. Also more than 100% change in resistance was recorded just before failure. This shows how valuable the continuous monitoring of resistance could be in order to monitor the health of the structure.

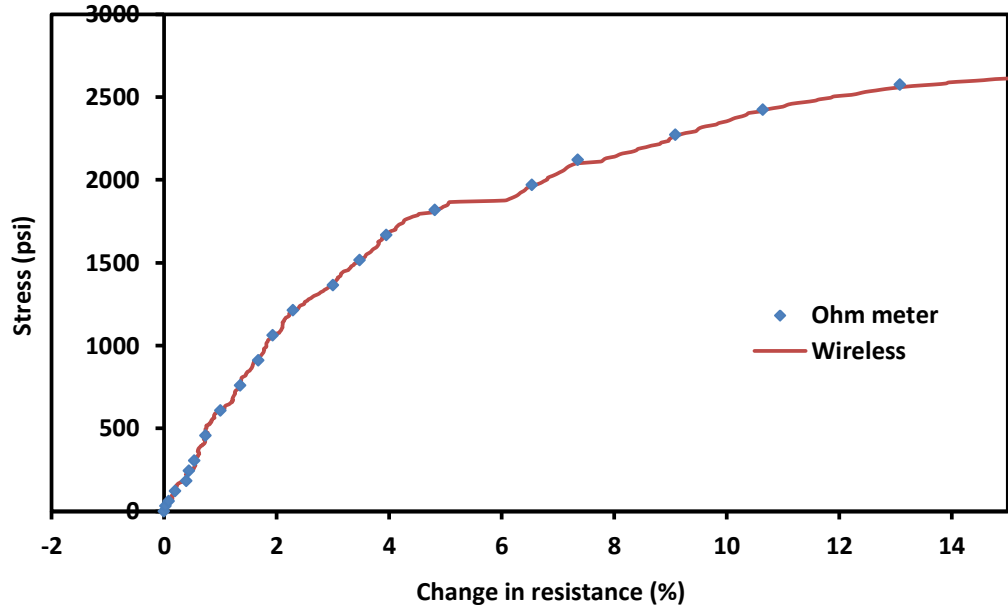


Figure 4-31: Piezoresistive behavior of cement grout specimen monitored using wireless method

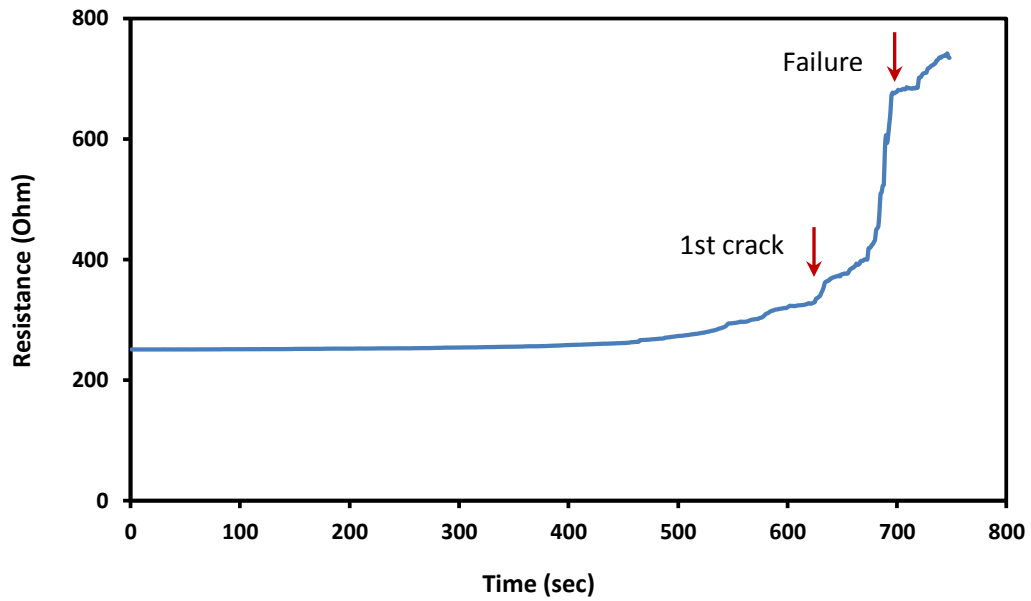
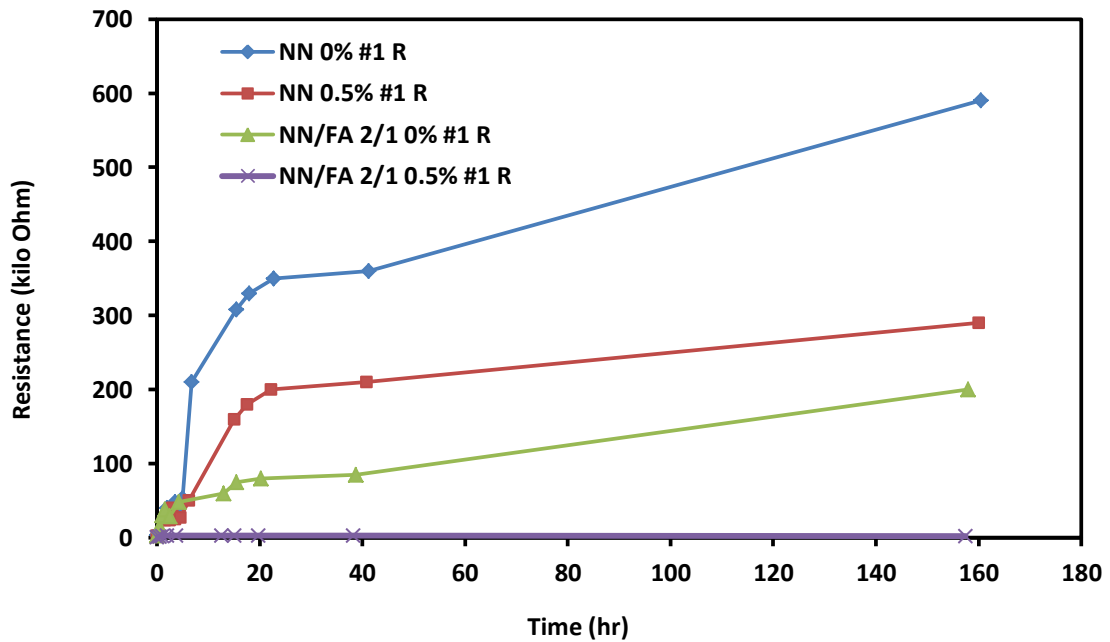


Figure 4-32: Real time health monitoring of cement grout specimen

## 4.5 Material Modification

### 4.5.1 Effect of Fly Ash

Effect of modification of material on piezoresistive behavior of concrete material was studied. For that replacement of part of dry mix by fly ash was done. From Figure 4-33, it was very evident that fly ash and carbon fiber have an advantageous effect on initial resistance. With addition of fly ash, initial resistance was brought down by 4 times. When fiber was added, the initial resistance was about 2 kilo Ohms which is a tremendous change. Also the initial resistance was very stable when both fly ash and carbon fiber were added.



**Figure 4-33: Effect of Fly Ash and fiber on initial resistance of concrete**

Figure 4-34 shows the piezoresistive behavior of concrete with and without fly ash modification. One specimen (NN 0.5%) had 100% concrete dry mix and 0.5% fiber w/w was added. The other two specimens (NN/FA 2-1 0.5%) had concrete dry mix and fly ash (both class C and class F respectively) in the ratio of 2:1 w/w and 0.5 % fiber w/w as well. It was observed that the specimens with fly ash showed good piezoresistive behavior and had a clear trend.

Comparing the behavior of specimens with class C and class F fly ash, class C fly ash showed more sensitivity with a continuously increasing trend. It was found that addition of about 1% fiber w/w is required to improve the piezoresistive behavior in pure concrete mixes. Considering all this it can be said that addition of class C fly ash with at least 0.5% fiber w/w is efficient and cost effective.

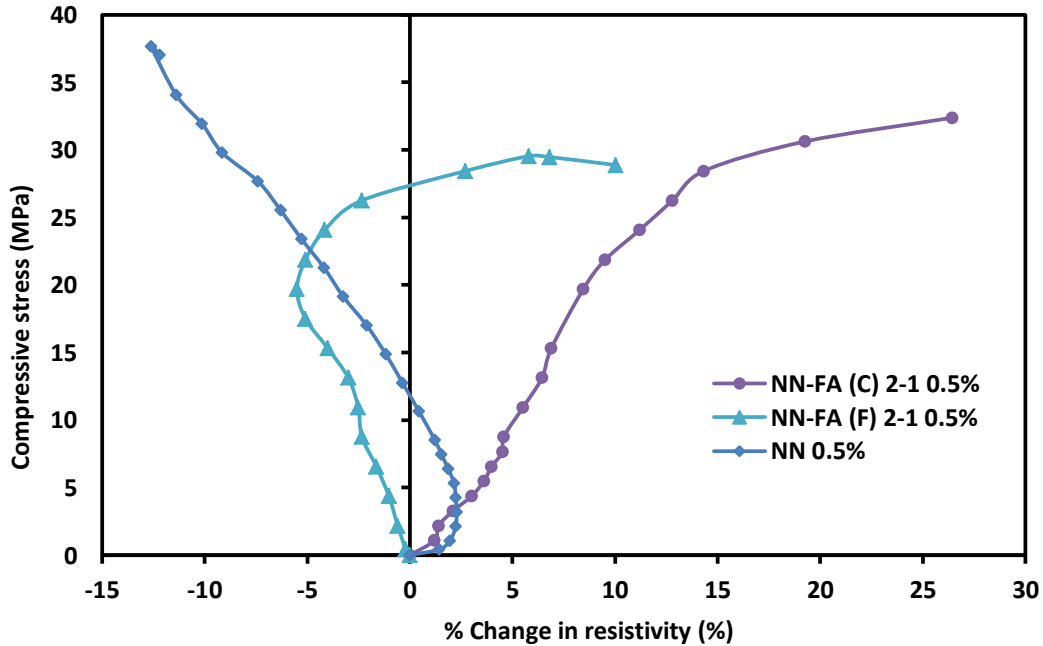


Figure 4-34: Piezoresistive behavior of concrete with and without fly ash

## 4.6 Low Stress Monitoring

### 4.6.1 Cantilever Model Design

A finite element analysis was used to investigate the effect of various shapes in magnifying the stress to measure the changes in resistivity. This is important since the applied stresses (example wind stresses during a hurricane) are very small compared to the strength of the material. For this study, cantilever beam configuration was selected. In order to magnify the stresses in the piezoresistive material, cantilever beam with varying cross sections was

investigated. The cross section of the beam was reduced in steps from the clamped end and hence referred to as 'stepped beam'. Based on initial study and ease of construction, the cantilever beam with three different sections was selected for detailed analyses. The schematic diagram of the stepped beam is shown in Figure 4-36. Three different depths were selected which were 35, 20 and 8 mm. The length and width of the beam are 240 mm (9.5 in) and 52 mm (2 in) respectively. The maximum depth of the beam selected was 35 mm.

Over 700 elements were used with 1512 nodes in the 3D static analysis in ANSYS. Assuming the material to be linear elastic the stepped beam was clamped at one end (section of 35mm\*52mm) and a uniformly distributed load was applied at various distances from the clamped end. Figure 4-34 shows a typical stress distribution on the compression side of the stepped beam and solid beam under the applied stress of 1.414 kPa (0.2 psi) applied 190 mm from the clamped end. It can be seen that, for the stepped beam, a stress concentration is developed close to the location where the cross sections change while other parts of the specimen are carrying relatively lower stresses. The maximum stress developed in this case was around 600 kPa which yielded a magnification of 425. Considering the solid beam, it developed a maximum stress of around 77 kPa near the clamp. Comparing the maximum stress developed in both beams, magnification produced by the stepped beam was around 8 times that of the solid beam.

#### **4.6.2 Results and Discussion**

In order to verify the findings from FEM analysis and to study the shape effect on piezoresistivity, a stepped beam was made using epoxy grout. Monitoring wires were embedded in selected locations denoted in the schematic diagram shown in Figure 4-36 while casting. Specimens were demolded after one day and cured at 75°F. Density of the stepped beam was 2166 kg/m<sup>3</sup>. To investigate the uniformity of the specimen, ultrasonic pulse (P) wave velocity method was used. Travel time of wave was measured (up to an accuracy of 0.1 μs) across the

width at four different sections and across the length. Average pulse velocity was 3650 m/s (11977 ft/s) and all the measurements were within 2% which indicated that the cantilever beam had uniform properties.

#### **4.6.2.1 Experimental Results**

A comparison of piezoresistive response at different locations in the stepped beam with increasing loading is shown in Figure 4-37. The locations plotted represent unique parts of the beam where G-H is the thinnest part of the beam. The location F-G represents a section with changing cross section. Both of these locations had piezoresistive response for small stress levels (Figure 4-37). However the change in F-G was greater than that of G-H which was mainly due to the greater level of stress experienced at this location (Figure 4-35).

#### **4.6.2.2 Experimental Verification**

The measured resistivity of the stepped cantilever beam (at F-G) is compared to the pure compressive piezoresistive model (is discussed in Chapter 6) in Figure 4-38. The response under bending was nonlinear while the prediction was nearly linear in the stress range considered. The difference can be attributed to the type of loading and shape of the beam. At applied stress of 1 kPa the stepped beam and compressive cylinder responses were 0.5% and 0.1%, about 5 times higher. Similarly at applied stress of 7 kPa the stepped beam and cylindrical responses were 0.8% and 0.4%, 2 times higher. Hence the stepped cantilever beam was much more sensitive than the cylindrical specimen in compression.

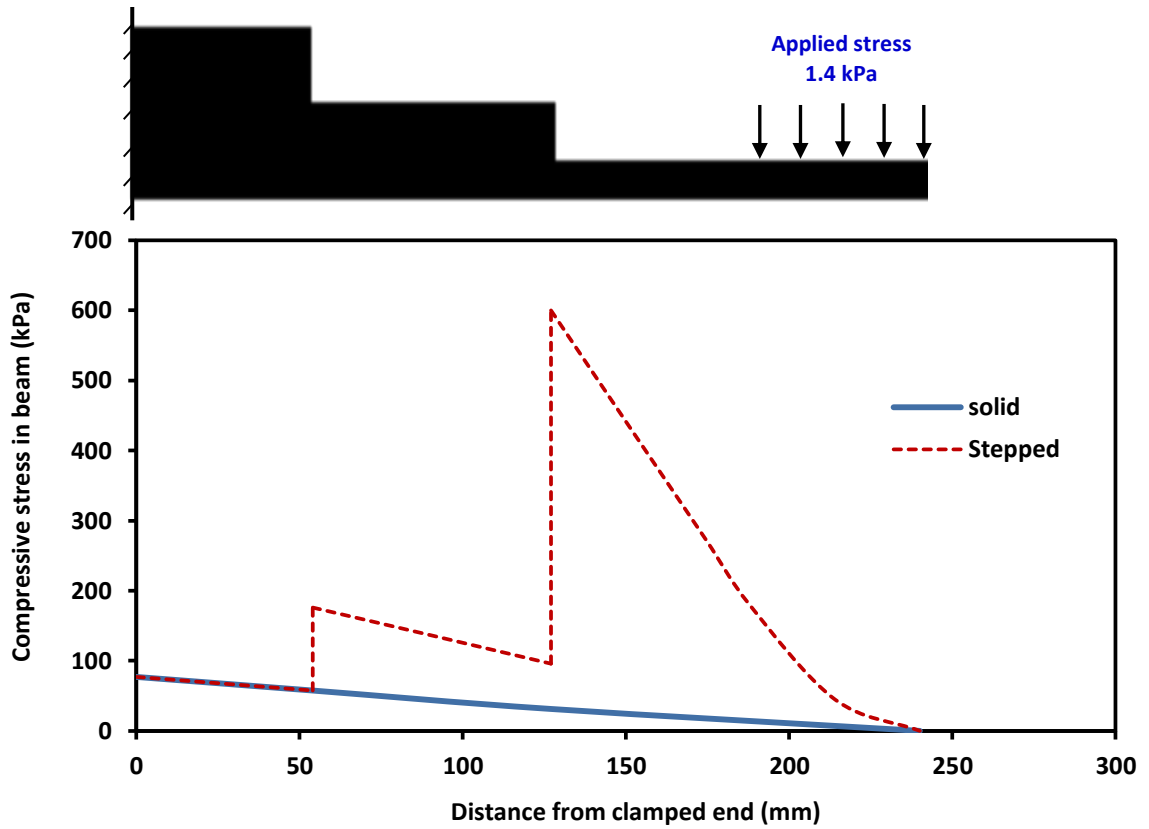


Figure 4-35: Stress distribution along the compression sides of stepped beam and solid beam

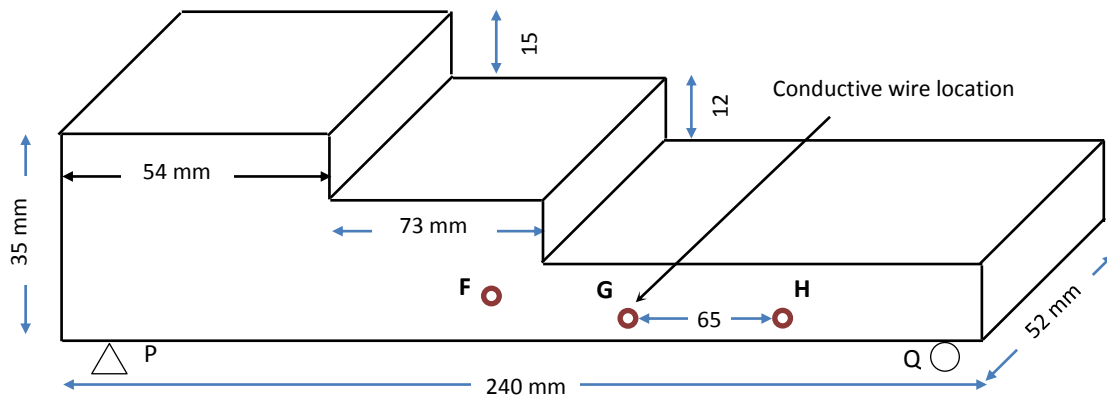


Figure 4-36: Schematic diagram of the stepped beam

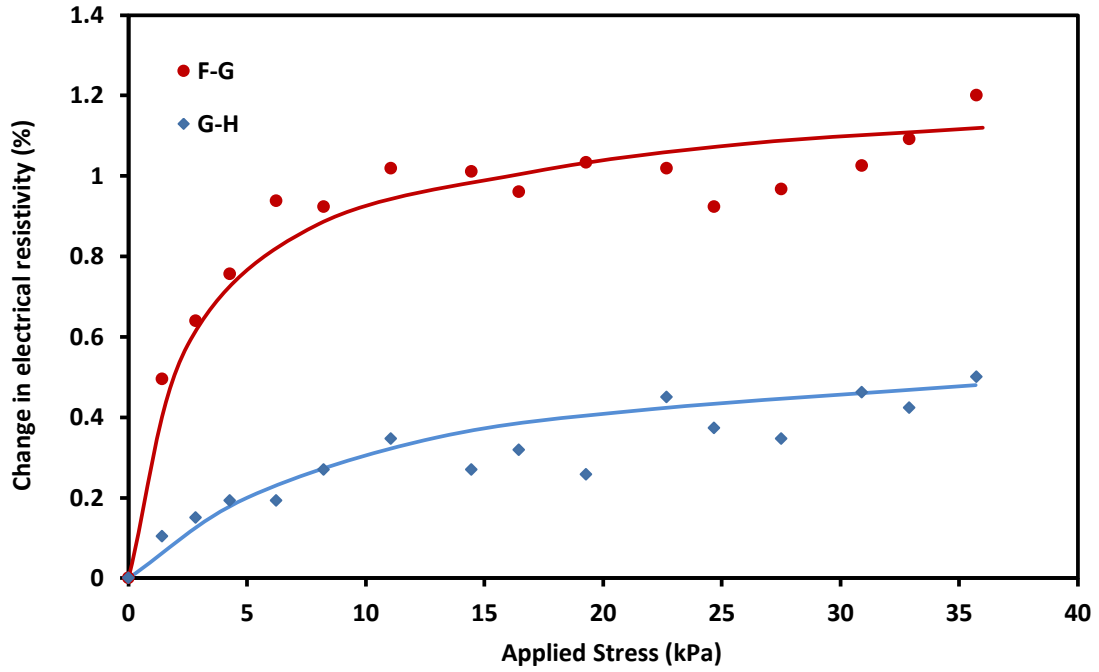


Figure 4-37: Comparison of piezoresistive response at different locations of stepped beam

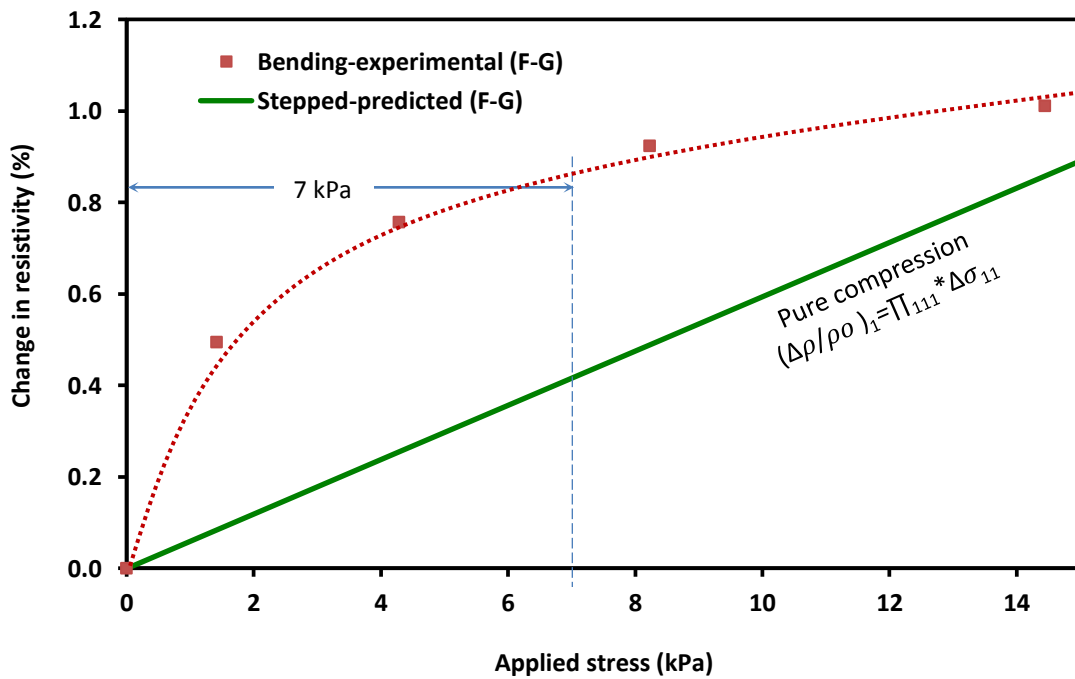


Figure 4-38: Comparison of resistivity in bending with pure compression

Based on the experimental study and modeling the observed multifunctional behavior of the piezoresistive polymer composite the following conclusion can be drawn. Cantilever stepped beam configuration was effective in detecting pressure of 1.4 kPa (0.2 psi) using the multifunctional polymer composite. The cantilever beam internal stresses were magnified by 425 times the applied so that the change in resistivity in the beam was measurable.

## 4.7 Piezoresistive Structural Sensors (PRSS)

### 4.7.1 Hollow Cylindrical Sensor

It is interesting to study the possibility of using a material to make small piezoresistive sensor which can be buried in required locations of a structure. Epoxy grout, which has already been proven to be a self-sensing material, was used to investigate the possibility of making small sensors. Hollow shapes are promising since they will ensure good bonding inside the host material. The dimensions of the tested specimen are shown in the schematic diagram in Figure 4-39.

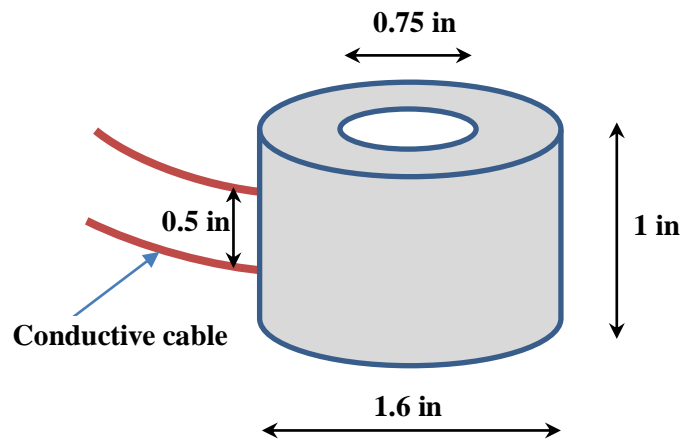


**Figure 4-39: Schematic diagram of hollow cylindrical sensor**

The hollow cylindrical sensor was subjected to uniaxial compressive load while electrical resistance between the cables was measured. Piezoresistive behavior of the sensor is shown in

Figure 4-40 and Figure 4-41 along with the behavior of a typical LL solid cylindrical specimen. Hollow cylindrical specimen had lower strength than solid specimen. It is clear that hollow cylindrical sensor was piezoresistive. Initially, at lower stress level, the resistivity decreases and then increases. After about 75% of the strength is achieved, electrical resistance increased very rapidly. As shown in Figure 4-41, when comparing the behavior of hollow cylinder to solid cylinder at the same load level, hollow specimen was sensitive at lower load levels. For example, up to 2000 lb, solid specimen was not as sensitive as hollow one.

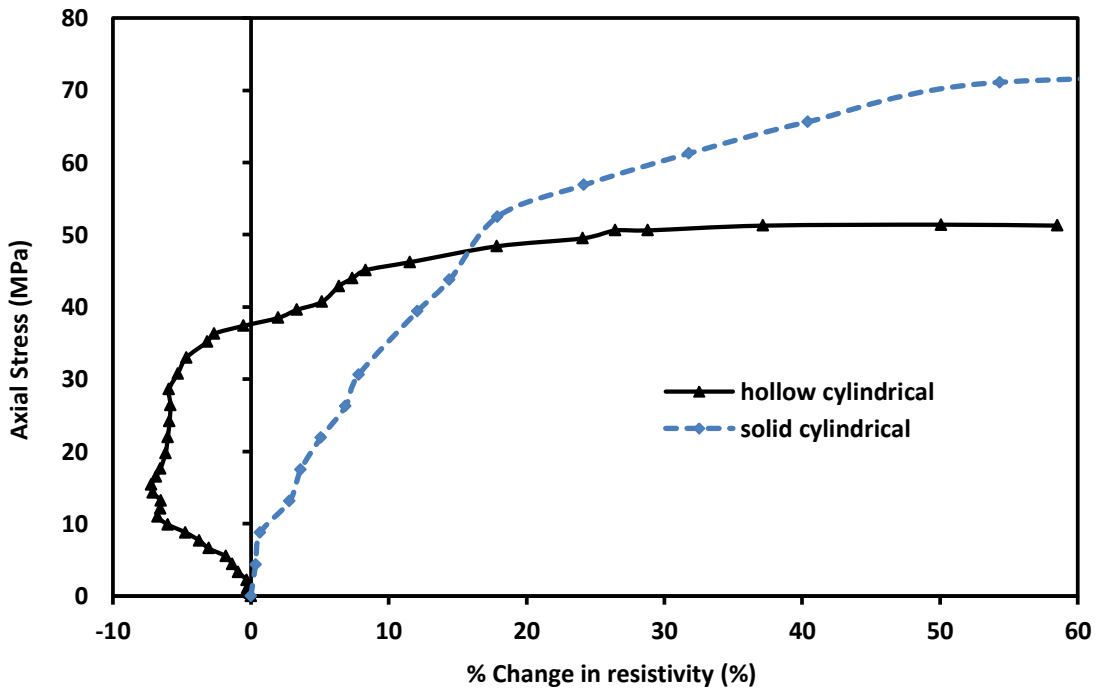
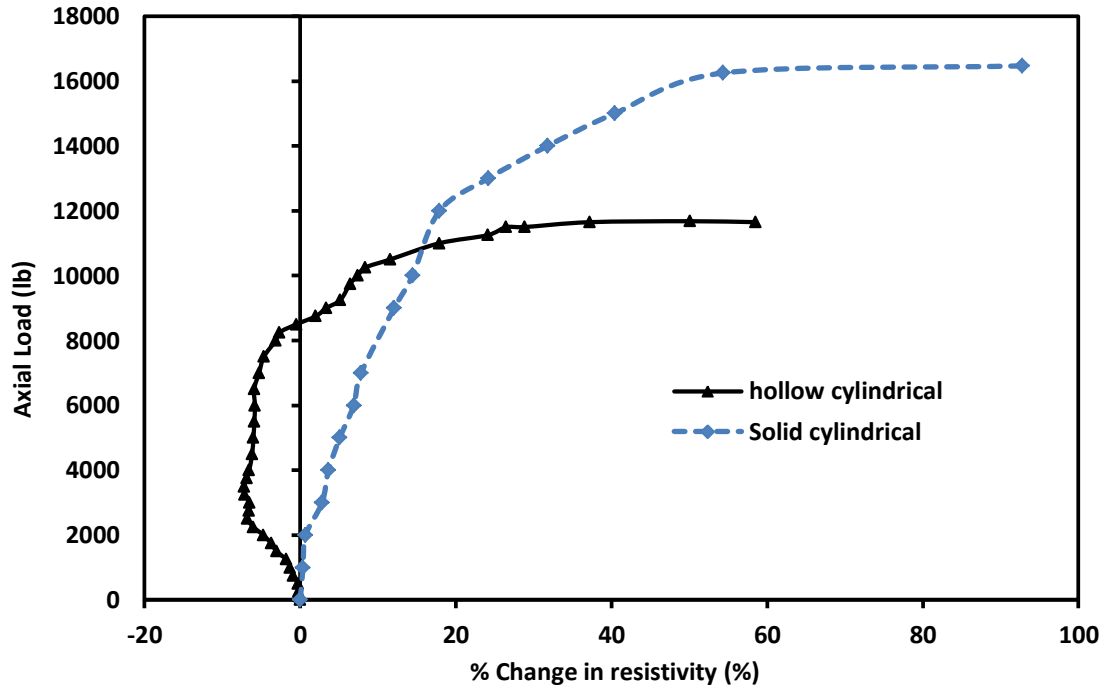


Figure 4-40: Piezoresistive behavior of hollow cylindrical sensor



**Figure 4-41: Comparison of piezoresistive behavior of PRSS**

### Summary

Following conclusions are advanced from the above discussions.

1. Modification of fiber helped to improve the piezoresistive behavior while bringing down the amount of fiber usage. At failure, specimen with modified fiber showed a change of more than 54% while the specimen with short fiber showed a change of 20%.
2. Electrical resistivity was proven as a better indicator than strain. At 50% strength of cement grout, resistivity showed about 40 times more sensitivity than strain.
3. When curing the epoxy grout specimens in water, initial resistance increased by about 30% and leveled off after 10 days. When subjected to elevated temperature (55°C), a sudden increase of more than 100% in resistance was monitored at fourth day.
4. It was observed that initial resistance of cement grout increased by about 20% when water cured at 25°C. Mass of the specimen increased by 3.5%. When the specimens were subjected

- to elevated temperature, an increase of 14% in resistance was monitored as the mass decreased by 6% because of loss of water.
5. Piezoresistive behavior of epoxy grout did not change with age when cured in air even though the strength improved by 20% from 3<sup>rd</sup> day to 28<sup>th</sup> day.
  6. Electrical resistance can be relied upon for monitoring curing of cement grout. Also continuous monitoring of resistance is valuable in order to monitor the health of the structure as formation of cracks was monitored by sudden increase in resistivity.
  7. Fly ash had advantageous effect on improving the conductivity as initial resistance was brought down by 4 times and stability was improved. Also addition of fly ash and carbon fiber improved piezoresistive behavior.
  8. Specially designed cantilever stepped beam configuration was effective in detecting pressure as small as 1.4 kPa (0.2 psi).
  9. Hollow specimen was sensitive at lower load levels, making it as a good structural sensor.

## **CHAPTER 5 CHARACTERIZATION OF COATING MATERIALS**

Cementitious coating materials are being used to maintain and repair aging infrastructure, especially underground structures. Cementitious coatings are used in pipes for waterproofing and protecting interior or exterior surfaces. One such coating was investigated to evaluate the field performance in terms of shrinkage, water absorption and strength characteristics. Tests were performed on the field samples and specimens prepared in laboratory to characterize the cementitious coating material.

### **5.1 Materials and Methods**

#### **5.1.1 Lab Specimens**

The laboratory specimens were tested in three series.

Series-1 Lab- Six numbers of 2\*4 cylinders

Series-2 Lab- Cylindrical specimens of size 3\*6 were prepared in the laboratory, with 3 different water/dry mix (w/d) ratios (0.18, 0.17 and 0.16)

Series-3 Lab- beams of size 12\*2\*2 inches were prepared with the 3 different water/dry mix ratios

##### **5.1.1.1 Compressive Strength**

Compression test was done on 3\*6 cylinders after 1, 3, 7 and 28 days of curing. Sulfur capping was done to make the loading surfaces smooth. Altogether 20 cylinders from series-2 were tested.

##### **5.1.1.2 Tensile Strength**

Splitting tensile test was done on 3\*6 cylinders made in series-2. Tests were performed at 7 and 28 days of curing.

### **5.1.1.3 Pulse Velocity**

A nondestructive testing, ultrasonic pulse (P) wave velocity (PWV) method was used both across the depth and across the diameter of the cylindrical specimens. Transducers having a natural frequency of 150 kHz were used to transmit waves through the specimens. The travel time of the wave between transducers on opposite faces of the specimen was recorded up to an accuracy of 0.1  $\mu$ s. Pulse velocity (P-wave) was calculated by dividing the travel length by the travel time.

### **5.1.1.4 Shrinkage**

Studies were done on lab samples to evaluate the shrinkage potential. Three different water/dry mix ratios were used (0.18, 0.17 and 0.16) and two beams (denoted as #B1 and #B2 for each w/d ratio) of size 12\*2\*2 inches were prepared in each type. Three different pairs of demec points were marked in each beams denoted as #B1 (one beam for each w/d ratio). Change of length between those demec points were monitored for about one month to an accuracy of 0.0005 inches. Mass of the beams also was measured to an accuracy of 0.0001 lbs. After one month of monitoring, those #B1 specimens were kept in 60°C in oven and length and mass were monitored to another two months until they lost all free water in them. On the other hand, specimens denoted as #B2 (one in each w/d ratio) were kept in room temperature until three months.

### **5.1.1.5 Flexural Strength**

All six beam specimens (made for shrinkage studies) were tested for flexural strength under four point loading after the unit weight and ultrasonic pulse wave velocity measurements.

## **5.1.2 Field Samples**

Three series of field samples were investigated which were obtained from coring the failed pipes at various locations.

### **5.1.2.1 Physical properties**

Initially mapping of the thickness of the samples along the circumference was done. The mass and volume of specimens were measured to determine the unit weight. Pulse velocity measurements were taken both across the thickness and diameter of the samples. This is valuable physical characterization for field samples since the pulse velocity is influenced by the elastic properties and unit weight of the material. Also uniformity of the coating in the field can be characterized especially when the coating is applied in layers.

### **5.1.2.2 Water Absorption**

After the initial characterization, field coating samples were immersed in water and change in mass of specimens was monitored for over the period of approximately 14 days (337.5 hours). Surface of specimen was wiped by clean cloth to get surface dry condition and mass was measured to the accuracy of 0.01 grams. After 14 days of water absorption test, specimens were kept in room conditions (70° F) to measure the loss of free water.

## **5.2 Results and Discussion**

### **5.2.1 Laboratory specimens**

#### **5.2.1.1 Physical Characterization**

Series-2 test results on laboratory specimens are summarized in Table 5-1. It was observed that the unit weight and PWV values were less than that of the field samples. Average compressive strength was about 4800 psi after 3 days of curing. Average unit weight of specimens was 129.2 pcf.

**Table 5-1: Characterization of series-2 laboratory coating specimens**

w/d	No	Mass (lb)	Diam. (in)	Height (in)	Unit wt. (pcf)	Pulse Wave Velocity (ft/s)		Strength (psi)		
						Across Diam.	Across depth	Value	Avg.	Remarks
0.18	1	3.2435	3.02	5.965	131.2			2524	2482	1day compressive strength
	2	3.2415	3.01	5.98	131.6			2441		
	3	3.1905	3.01	5.97	129.8			4324	4037	3day compressive strength
	4	3.1835	3.01	5.99	129.1			3751		
	5	3.166	3.01	5.99	128.4		12295	5318	6607	7day comp strength
	6	3.1475	3.01	5.94	128.7		12283	325		7day splitting tension
	7	3.2085	3.02	6.03	128.4	13246	12722	6607		28day comp strength
	8	3.188	3.02	6.01	128	13246	12712	348		28day splitting tension
0.17	1	3.176	3.0	5.9	131.6			2418	2472	1day comp strength
	2	3.1975	3.005	5.94	131.2			2525		
	3	3.123	3.01	5.91	128.3			4174	4175	3day comp strength
	4	3.105	3.015	5.92	126.9			4177		
	5	3.1025	3.0	5.9	128.5		12200	5319	6607	7day comp strength
	6	3.1275	3.02	5.92	127.4		12242	263		7day splitting tension
	7	3.11	3.01	5.9	128.2	13342	12837	5336	5593	28day comp strength
	8	3.1125	3.0	5.92	128.6	13228	12814	5850		
	9	3.0885	3.0	5.9	128.6			365	428	28day splitting tension
	10	3.0895	3.0	5.9	128.6			491		
0.16	1	3.269	3.01	6.01	132.1			2670	2697	1day comp strength
	2	3.264	3.02	6	131.2			2725		
	3	3.1935	3.015	5.95	129.9			4641	4229	3day comp strength
	4	3.204	3.015	6	129.2			3817		
	5	3.1685	3.02	5.94	128.7		12469	6135	6607	7day comp strength
	6	3.2065	3.02	6.02	128.5		12573	310		7day splitting tension
	7	3.1675	3.01	5.91	129.4	13202	12995	6113	6167	28day comp strength
	8	3.184	3.02	6.01	128.5	13458	13043	6221		
	9	3.145	3.01	5.94	128.5			459	412	28day splitting tension
	10	3.1615	3.01	5.98	128.5			366		
<b>Average</b>						<b>13287</b>	<b>12599</b>			
About 43% of 28 day strength was achieved at 1 day.										

Compressive strengths of Series-2 laboratory specimens are compared in Figure 5-1. It was observed that specimens with water/dry mix (w/d) ratio of 0.16 had slightly higher compressive strengths compared to other specimens. Also 41% of the 28 day strength was achieved after 1day by specimens with 0.16 water binder ratio. Third day strength was about 67% of the 28 day strength. Also the compressive strength was higher than 6000 psi in 7 days curing for the mix with w/d of 0.16. In the case of specimens with w/d of 0.18 and 0.17, corresponding numbers were 44%, 75% and 44%, 69% respectively. Altogether, the third day strength was about 70% of the 28 day strength and the specimens gained more than 90% of the strength at 7 days of curing as shown in Figure 5-2.

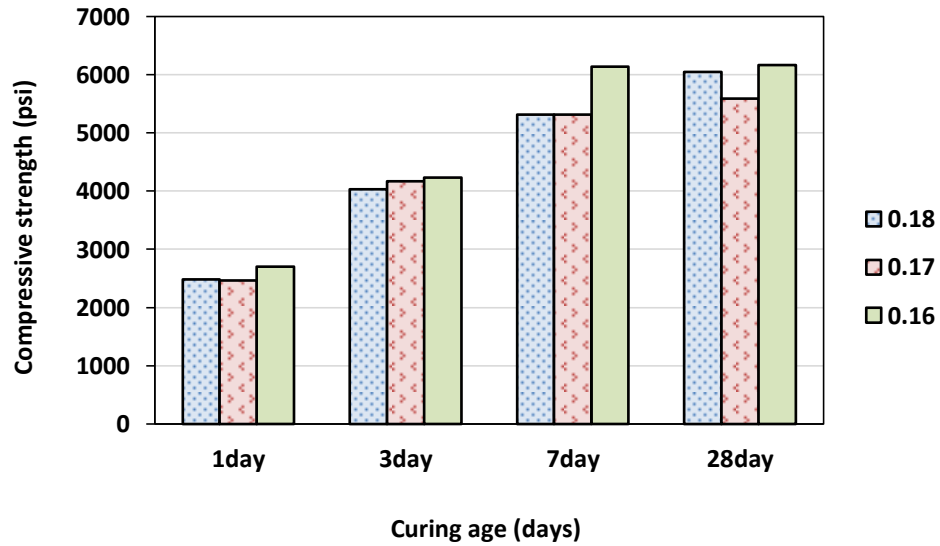


**Figure 5-1: Comparison of compressive strength of series-2 laboratory coating specimens**

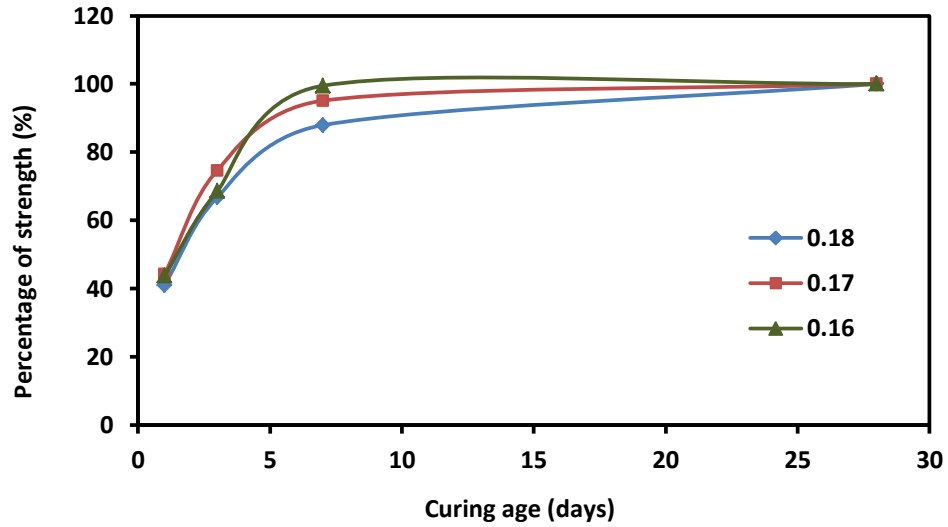


Figure 5-2: Strength gain of coating specimens with curing age

### 5.2.1.2 Shrinkage

As shown in Figure 5-3, beams made in the lab had potential for shrinkage. As the Figure 5-4 indicates, eventually about 8% mass change occurred when the specimens were allowed to loose water.

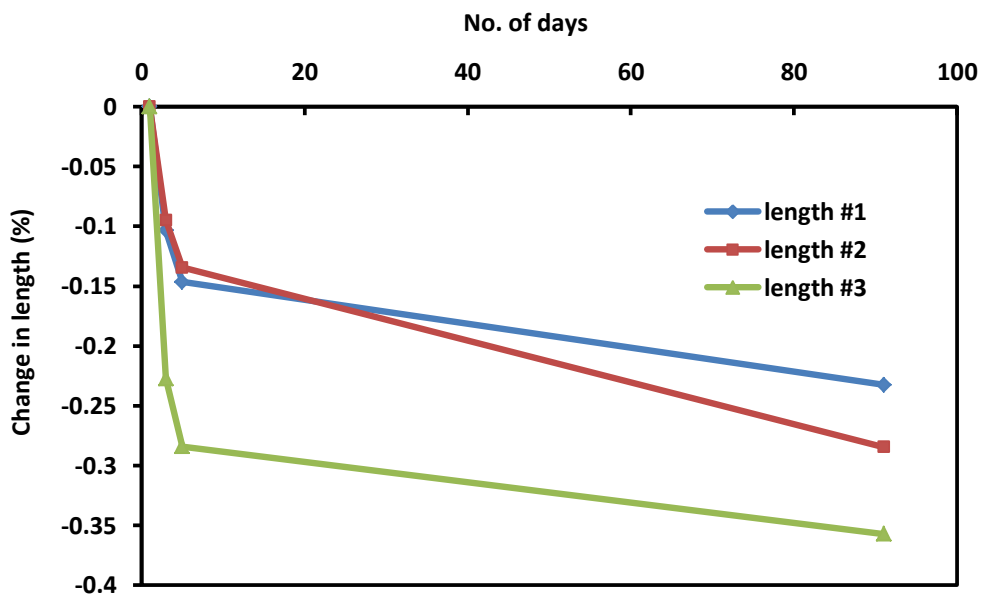
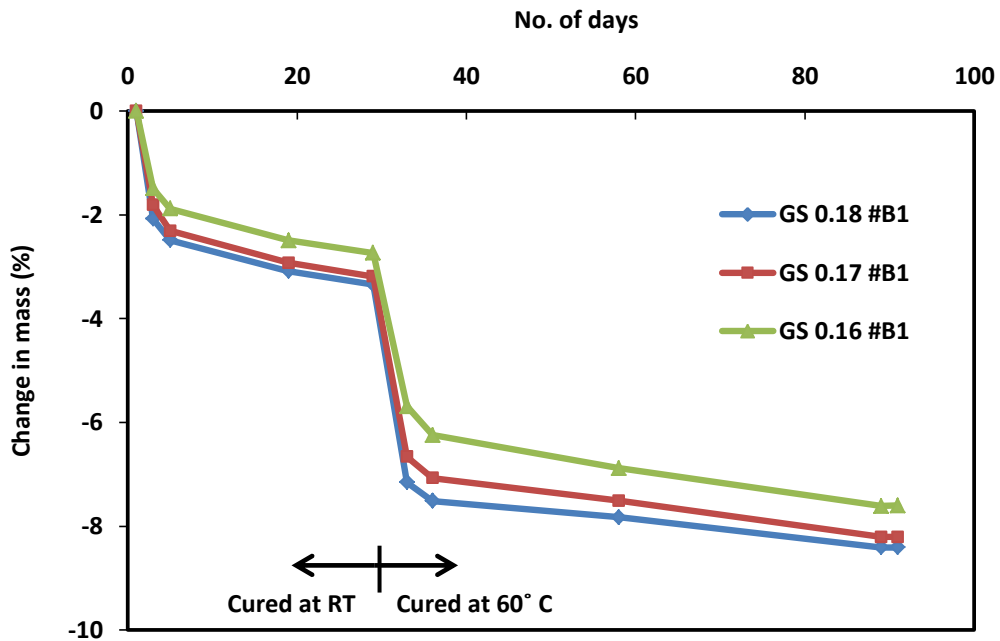


Figure 5-3: Shrinkage measurement on beam (0.17 w/d, #B1)



**Figure 5-4: Monitoring the change in mass of beams made of the coating material**

Table 5-2 and Figure 5-5 show the physical and mechanical properties of beams made of the coating material.

**Table 5-2: Summary of results for test on beams made of the coating material**

Specimen	Initial unit weight (pcf)	final unit weight (pcf)	Pulse Wave Velocity (ft/s)		Flexural strength (psi)
			longitudinal	Across depth	
GS 0.18 #B1	130.8	119.8	12346	12077	810
GS 0.17 #B1	131.1	120.3	12516	11990	799
GS 0.16 #B1	132.9	122.8	12690	12165	1013
GS 0.18 #B2		128.9			731
GS 0.17 #B2		127.4			5623
GS 0.16 #B2		127.7	14245	11737	720

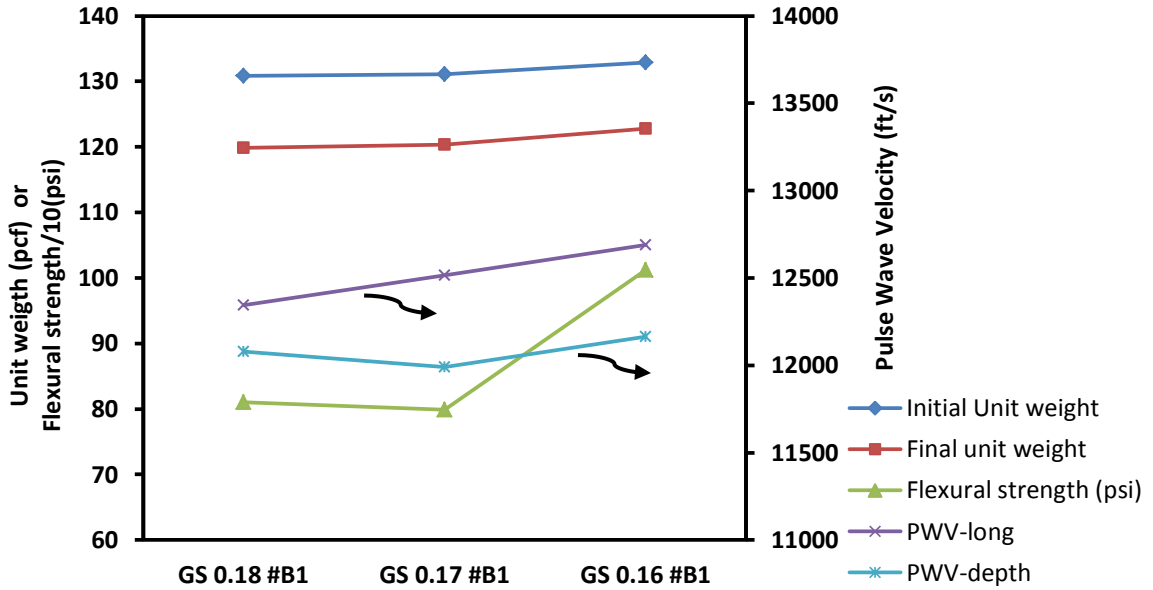


**Figure 5-5: Properties of beams**

Beam specimens which lost the whole free water showed lower PWV values than the ones which were kept in room temperature. Beams with w/d ratio of 0.18 comparatively lost much water and had slightly lower PWV value than its counterparts. Beam with w/d ratio of 0.16 had a flexural strength of 1013 psi. Figure 5-6 shows the failed beams. All the beams failed by splitting parallel to loading direction close to the center.



**Figure 5-6: Failed Geospray beams after subjected to four point flexural loading**

## 5.2.2 Field Samples

### 5.2.2.1 Physical Characterization

Table 5-3 summarizes the average, minimum and maximum thickness of samples, unit weight and pulse wave velocity (PWV) for the Series-1 field samples. Sample B1 was about 1 inch in diameter whereas other samples were about 2 inches in diameter. It was observed that PWV across diameter was slightly higher than the PWV across thickness. It can be attributed to the formation of layers while preparing the coating. The unit weight of the samples varied between 129.7 pcf and 133.6 pcf with an average of 131.6 pcf. Specimen C had the highest thickness and also considerable variation in the thickness compared to the other specimens.

**Table 5-3: Characterization of series-1 field coating samples**

Name	Thickness along circumference (in)			Unit weight measurements			Pulse Wave Velocity (ft/s)	
	Avg.	Min	Max	Mass (lb)	Volume (mL)	Unit wt. (pcf)	Across Diameter	Across thickness
<b>A1</b>	0.604	0.506	0.708	0.1627	34.5	133.6	14301	12083
<b>B1</b>	0.232	0.221	0.251	0.0179	3.9	130.1	17973	13799
<b>C</b>	1.295	1.099	1.516	0.3490	76.2	129.7	15392	13312
<b>D</b>	0.793	0.778	0.814	0.2071	44.0	133.3	15462	11625
<b>E3</b>	0.703	0.612	0.92	0.1819	39.2	131.4	16140	12204
Avg. unit wt.=131.6 pcf, avg. PWV across diameter=15854 ft/s and avg. PWV across thickness=12605 ft/s Thickness of the samples varied from 0.221 to 1.516 inches								

Thickness around the circumference for series 2 field core specimens is mapped in Figure 5-7. It was observed that specimen C#2 had larger variation.

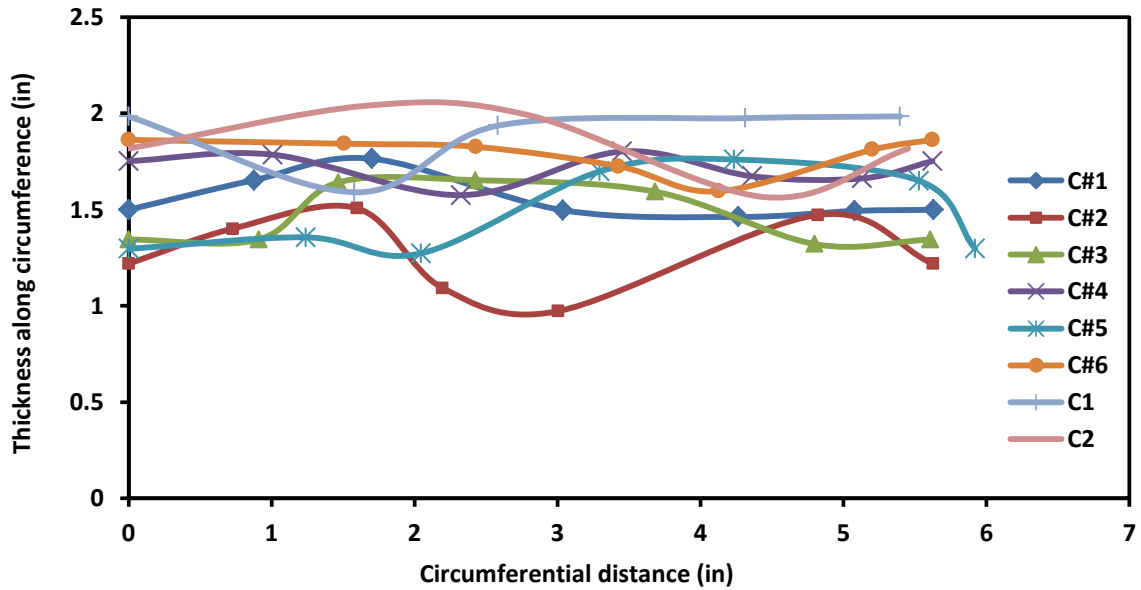


Figure 5-7: Mapping of thickness of series-2 field samples

#### 5.2.2.2 Water Absorption

In Figure 5-8, percentage change in mass of the field coating samples (series#2) when they were subjected to immersion test is shown. It was observed that except C#2, all other samples lost the free water when they were kept in room temperature after subjecting to immersion in water. Specimen C#2 had a change of about 2% in mass after being immersed in water for about 14 days. This showed that the specimen had a lot of pores in it.

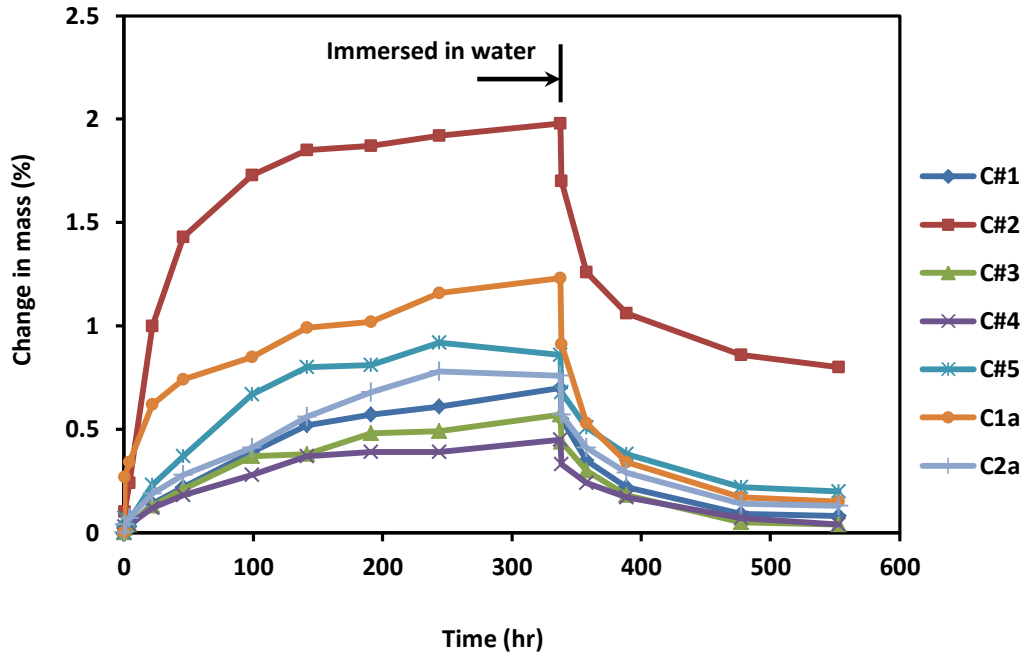


Figure 5-8: Water absorption test for field coating samples (series #2)

### 5.3 Comparison

Figure 5-9 shows the variation of unit weight for all the field specimens and laboratory specimens. It was clear that field samples had higher unit weight than laboratory specimens. Comparison of ultrasonic pulse wave velocities for field and lab specimens are shown in Figure 5-10. Laboratory specimens had almost identical PWV values. PWV measured across depth for field specimens were higher than that of laboratory specimens. Series-2 field specimens had higher pulse velocities than Series-1 and series-3 field specimens when measured across the thickness (Figure 5-9). As shown in Figure 5-11, the pulse velocities were higher in the field specimens because of higher unit weights.

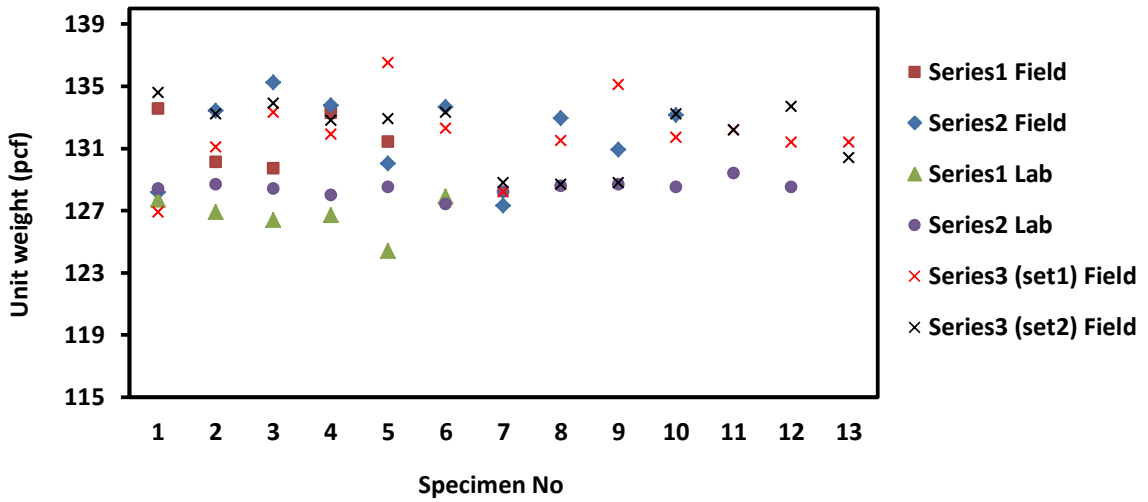


Figure 5-9: Comparison of unit weight of field and lab coating specimens

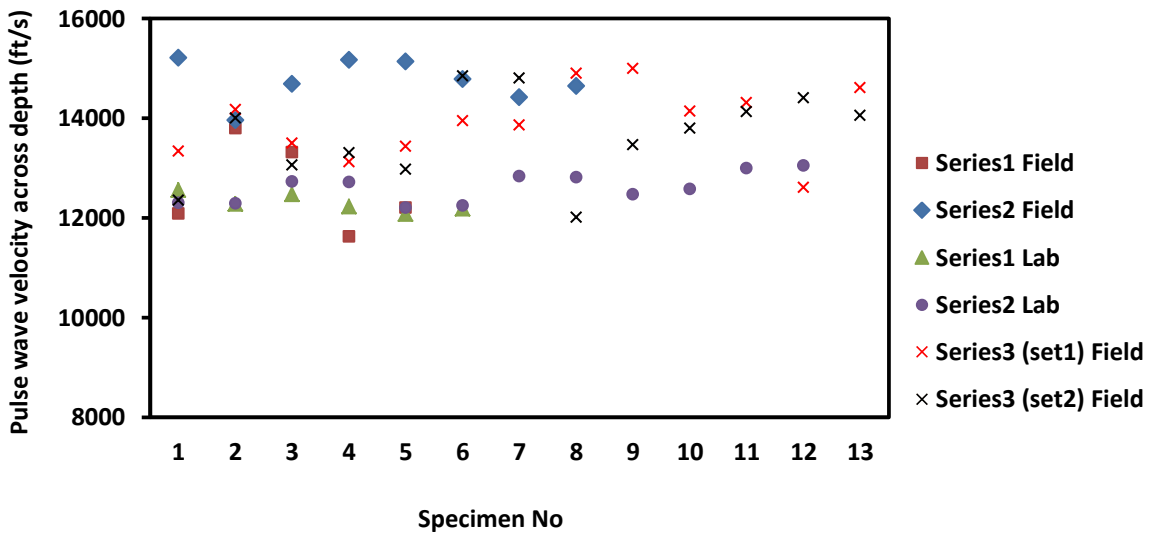
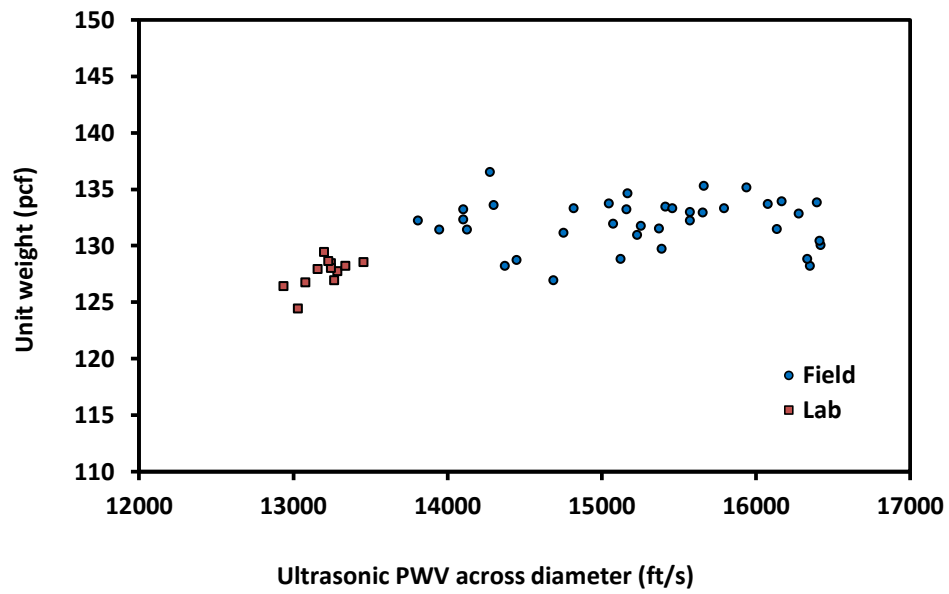


Figure 5-10: Comparison of PWV measured across depth/thickness in coating specimens



**Figure 5-11: Relationship between PWV and unit weight for coating specimens**

**Summary**

Based on the discussions, it can be concluded that the coating material has shrinkage potential.

Hence, material modification needs to be done.

## CHAPTER 6 MODELING THE BEHAVIOR OF REPAIR MATERIALS

### 6.1 Stress-Strain Model

#### 6.1.1 p-q model

A stress-strain model which is known as the ‘p-q model’ was developed by Vipulanandan and Paul (1990) to predict the stress-strain behavior of polymer composite materials. Sett (2003) used the simplified version of the model proposed by Mantrala (1996) to predict the behavior of fiber reinforced polymer concrete. That model is proposed to predict the stress-strain behavior of the epoxy grout material. The proposed model is

$$\sigma = \left[ \frac{\frac{\varepsilon}{\varepsilon_c}}{q + (1-p-q) \frac{\varepsilon}{\varepsilon_c} + p \left(\frac{\varepsilon}{\varepsilon_c}\right)^{\frac{(p+q)}{p}}} \right] \sigma_c, \quad (6-1)$$

where  $\sigma_c$  is the peak stress,  $\varepsilon_c$  is strain at peak stress and  $p, q$  are material parameters. The parameter  $q$  is the ratio between secant and initial tangential moduli. The parameter  $p$  was obtained by minimizing the error in predicting the stress-strain relationship.

When  $q=1$ , it means a linear material up to peak stress. Therefore the lower value of  $q$  represents more non-linear material. On the other hand, the parameter  $p$  controls mainly the post peak behavior, although it has little influence in the pre-peak behavior. Sett (2003) related the parameter  $p$  to toughness of the material.

A typical procedure for optimizing the  $p$  value can be explained using Figure 6-1. Initially  $q$  was calculated by estimating the tangent and secant moduli. Then a value for  $p$  was assumed and stress was predicted using the experimental strain values, calculated  $q$  and assumed  $p$ . The squared error in prediction was calculated. Likewise different  $p$  values were assumed and

corresponding errors were calculated. The value of  $p$  which gave minimum error was selected as the  $p$  for this case, and the stress was predicted by using it in the equation (6-1). However optimization solver tools available in computing packages can be used for the optimization of  $p$ . The model prediction for an epoxy grout mix with 1% fiber is compared to the experimental results in Figure 6-2 and the  $p$  and  $q$  were 0.37 and 0.76 respectively. As seen in the Figure 6-2, the proposed  $p$ - $q$  model predicts the stress-strain behavior very well. It captures the linear behavior and nonlinear behavior very well, especially the post peak strain hardening portion.

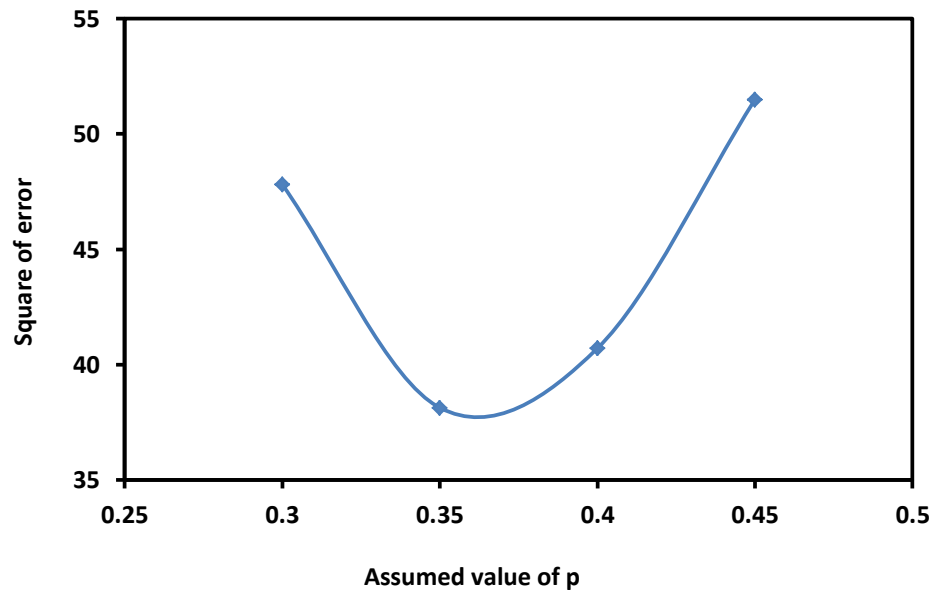


**Figure 6-1: Optimization of parameter  $p$**

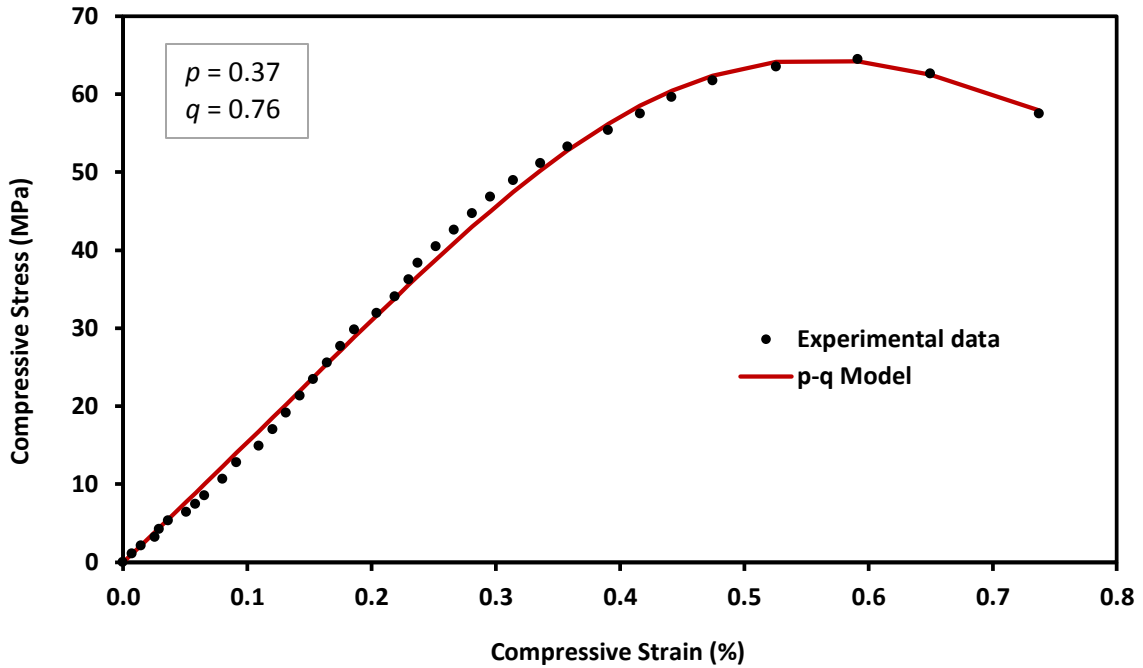


**Figure 6-2: Typical stress-strain prediction for epoxy grout**

### 6.1.2 Stress-Strain Model for Epoxy Grout

Stress-Strain behavior of epoxy grout material which is discussed in chapter 3 was modeled using the proposed p-q model. The model prediction is shown in Figure 6-3 along with the experimental data. As seen in the figure, stress-strain behavior is predicted reasonably well. Especially when the material had higher ductility as in the case with specimen with 0.6% fiber, the behavior was predicted well. Parameter  $q$  for the specimen without fiber was 0.82, while the specimens with 4% and 0.6% fiber had a  $q$  of 0.79 and 0.74 respectively. Likewise the corresponding  $p$  values were 0.12, 0.25 and 0.24. The lower the  $q$  value, more nonlinear was the material. In this case, values of  $q$  for specimens with fibers were comparatively lower which indicates that addition of fiber increased the nonlinear behavior.

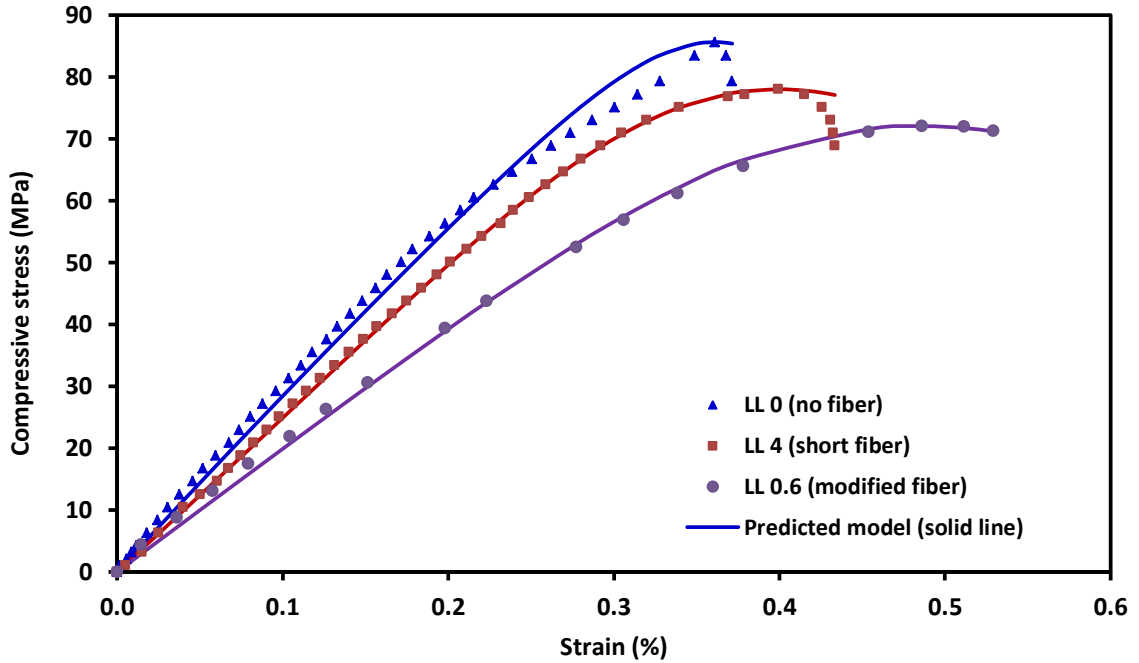


**Figure 6-3: Stress-Strain model for epoxy grout**

Model prediction for stress-strain behavior of six epoxy grout specimens is shown in Figure 6-4.

Model parameters are summarized in Table 6-1. Parameter  $q$  varied between 0.49 and 0.74.

Specimens 1 and 5 had higher values for parameter  $p$  and lower values for parameter  $q$ .

**Table 6-1: Stress-strain model parameters for epoxy grout**

Specimen	Initial tangent modulus (GPa)	$q$	$p$
#1	17.7	0.492	1.405
#2	13.2	0.719	0.337
#3	20	0.741	0.246
#4	20	0.655	0.298
#5	16.7	0.597	1.130
#6	12.5	0.712	0.428

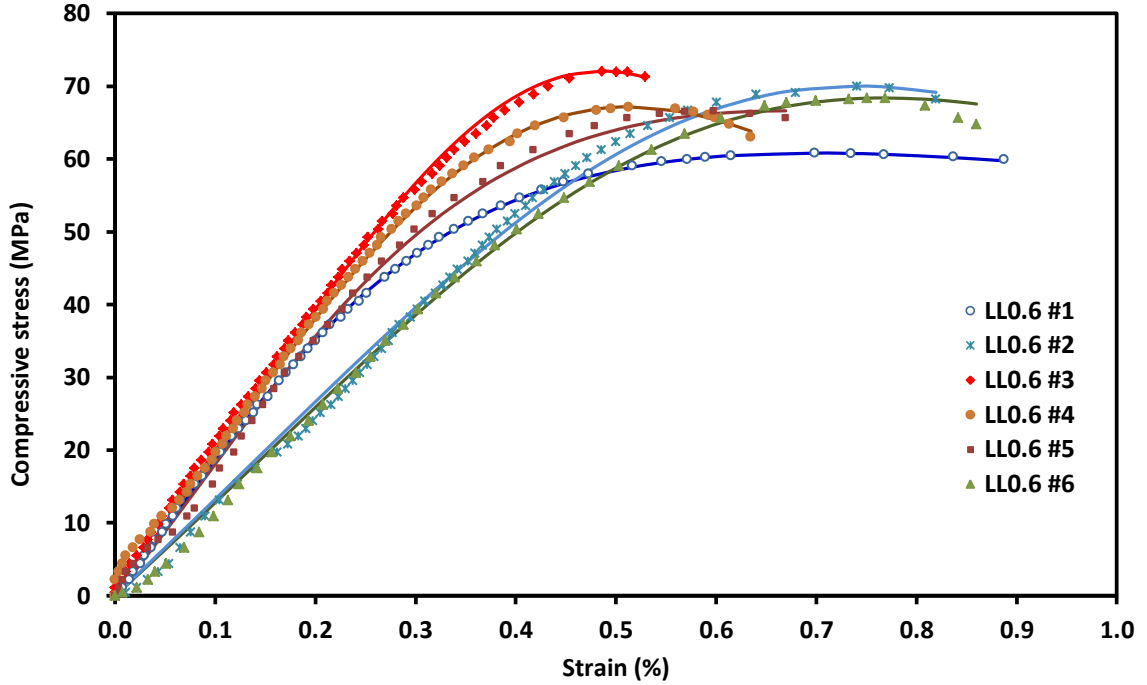


Figure 6-4: Model prediction for stress-strain behavior of epoxy grout

## 6.2 Piezoresistive Model

### 6.2.1 Analytical model (Sett, 2003)

Polymer matrix can be idealized as an insulator at very low concentration of carbon fiber and when the volume fraction of carbon fiber is increased the composite will act as a conductor (Sett, 2003). Composite resistivity of carbon fiber reinforced polymer concrete was described by percolation theory by Carmona et al. (1987). Percolation theory is

$$\rho_i = A \rho^{fiber} (\phi - \phi_{cr})^{-t_i} \quad (6-2)$$

where  $\rho_i$  is the composite resistivity,  $A$  is a pre-factor,  $\rho^{fiber}$  is the resistivity of carbon fiber,  $\phi$  is the volume fraction of the carbon fibers,  $\phi_{cr}$  is the critical volume fraction of the carbon fibers and  $t_i$  is an exponent. Volume fraction of the carbon fibers is represented as

$$\Phi = \frac{V^f}{V^f + V^p + V^s}, \quad (6-3)$$

where  $V^f$ ,  $V^p$ ,  $V^s$  are the volume of conducting fibers, polymer matrix and aggregate respectively. The critical volume fraction of a composite can change due to change in microstructure of the composite which can be caused by externally applied stress. Furthermore it was shown by Sett (2003) that the fractional change in electrical resistivity ( $\partial\rho/\rho_0$ ) is given by

$$\left(\frac{\partial\rho}{\rho_0}\right)_i = \left[ t_i \Phi (\Phi - \Phi_{cr})^{-1} \left[ \left( \frac{1}{K^c \delta_{jk} + B_{jk}^c} \right)_c - \left( \frac{1}{K^f \delta_{jk} + B_{jk}^f} \right)_f \right] + t_i (\Phi - \Phi_{cr})^{-1} Z S_{jk} \right] d\sigma_{jk}. \quad (6-4)$$

Here  $\delta_{jk}$  is the Kronekar delta,  $S_{jk}$  is the deviatoric stress tensor,  $Z$  is the constant of proportionality, and  $B_{jk}$  is the shear parameter. Parameter  $Z$  signifies the rate of change of microstructure while parameter  $B$  quantifies the volume change of the composite/fiber under deviatoric stress. For an isotropic homogeneous and linear elastic material, the coefficient of volume compressibility ( $K$ ) can be written in terms of Young's modulus ( $E$ ) and Poisson's ratio ( $\mu$ ) as

$$K = \frac{E}{3(1-2\mu)}. \quad (6-5)$$

Under uniaxial stress condition, the change in resistivity of linear elastic, isotropic and homogeneous composite can be written in most general form (Sett, 2003) as

$$\left(\frac{\Delta\rho}{\rho_0}\right)_1 = t_1 (\Phi - \Phi_{cr})^{-1} \left[ \Phi \left\{ \frac{1}{\left\{ \left( -\frac{E_c^{PC}}{3(1-2\mu_c^{PC})} \right) + B^{PC} \right\}} - \frac{1}{\left\{ -\frac{E_c^f}{3(1-2\mu_c^f)} \right\} + B^f} \right\} + \frac{2Z\sigma_{11}}{3} \right] \Delta\sigma_{11}. \quad (6-6)$$

Equation 6-6 relates the piezoresistivity of carbon fiber reinforced polymer concrete to the fiber properties ( $E^f$ ,  $\mu^f$  and  $B^f$ ), composite properties ( $E^c$ ,  $\mu^c$ ,  $B^c$ ), microstructure ( $Z$ ), and fiber volume fraction ( $\phi$ ). It is the most general equation of piezoresistivity which can be solved incrementally. Assuming the material is incrementally elastic, in terms of conjugate strain, a common relationship was presented by Sett (2003) as

$$\left(\frac{\Delta\rho}{\rho_0}\right)_i = \Pi_{ijk} \Delta\sigma_{jk} = \Pi_{ijk} C_{jkmn} \Delta\varepsilon_{mn} = M_{ijk} \Delta\varepsilon_{jk} . \quad (6-7)$$

In the Eqn. 6-7, tensor  $\Pi_{ijk}$  is piezoresistivity coefficient,  $C_{jkmn}$  is the elasticity matrix and the tensor  $M_{ijk}$  is the elasto-resistance tensor known as the gage factor. Piezoresistivity coefficient relates the specific change in electrical resistivity to the change in stress tensor whereas gage factor signifies the sensitivity of change in resistivity measurement to strain measurement.

Since resistance in the material is directional (anisotropic), based on the random distribution of the fibers, the resistivity will be represented as a vector. Hence the piezoresistivity coefficient ( $\Pi_{111}$ ) was defined as

$$\left(\frac{\Delta\rho}{\rho_0}\right)_1 = \Pi_{111} \Delta\sigma_{11} . \quad (6-8)$$

Because of Poisson's effect which is given by

$$\varepsilon_{22} = \varepsilon_{33} = -\mu^c \varepsilon_{11} \quad (6-9)$$

the strain-resistivity relationship will be

$$\left(\frac{\Delta\rho}{\rho_0}\right)_1 = (M_{111} - 2\mu^c M_{222}) \Delta\varepsilon_{11} . \quad (6-10)$$

### 6.2.2 Piezoresistive Behavior Model for Epoxy Grout

The incremental nonlinear analytical piezoresistive model presented by Sett (2003) which is given in Eqn. 6-6 was used to model the piezoresistive behavior of epoxy grout. From the manufacturer's data, Young's modulus ( $E$ ) and Poisson's ratio ( $\mu$ ) of the carbon fiber were obtained as 228 GPa and 0.3, respectively. For epoxy grout, modulus was obtained from stress-strain relationship and  $\mu$  was taken as 0.2. Values of  $K_c$  and  $K_f$  were calculated as 8.33 GPa and 190 GPa, respectively.

Piezoresistive behavior of a 0.6% fiber added epoxy grout specimen was modeled and is shown in Figure 6-5 along with experimental data. It can be seen that the incremental model predicted the piezoresistive behavior reasonably well. For 0.6% modified fiber added epoxy grout composite, exponent  $t$  was calculated to be 1.823 using the percolation Eqn. 6-2. Values of shear parameter ( $B$ ) for composite and fiber were found to be 340 GPa and 500 GPa respectively. The parameter  $Z$  which is related to microstructure was found to be  $2.4 \cdot 10^{-6} \text{ m}^4/\text{N}^2$  in this case. Typical piezoresistivity coefficient ( $\Pi_{III}$ ) was calculated as  $5 \cdot 10^{-3}$  and  $10 \cdot 10^{-3} \text{ MPa}^{-1}$  at 20 MPa and 35 MPa stress levels respectively.

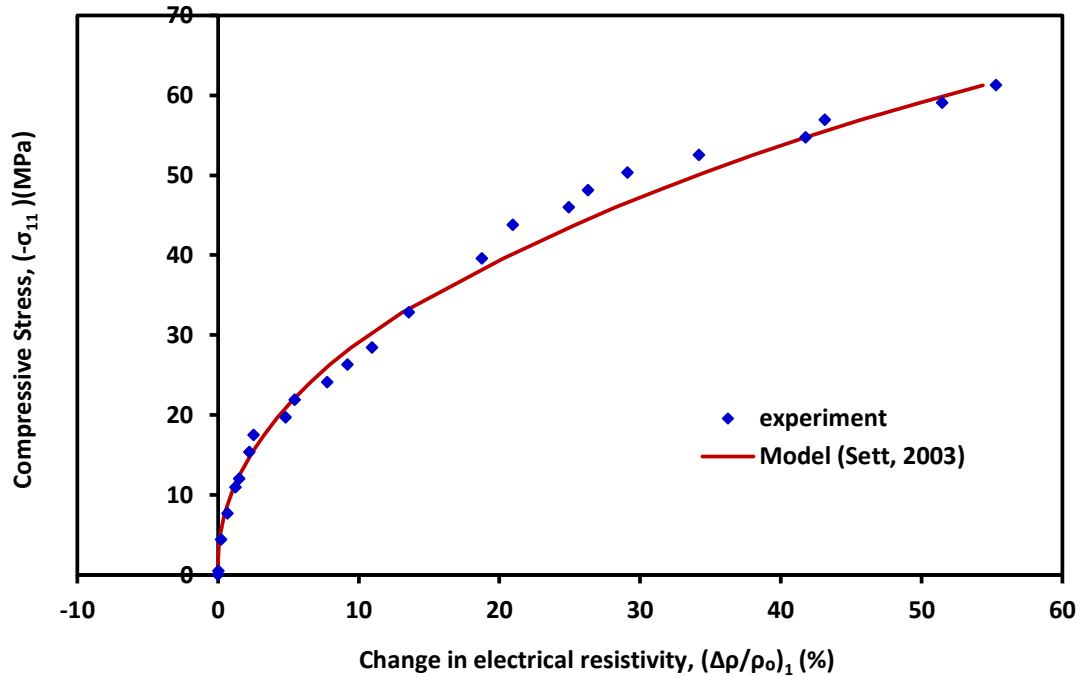


**Figure 6-5: Modeling piezoresistive behavior of epoxy grout**

Piezoresistive behavior of 0.6% (w/w) modified fiber added epoxy grout specimens was modeled and is shown in Figure 6-6. Behavior of two of the specimens is shown in Figure 6-7 along with experimental points. Same model parameters were used except  $Z$ . Piezoresistivity coefficient ( $\Pi_{III}$ ) at two stress levels is summarized in Table 6-2 along with the parameter  $Z$  used for the modeling. As given in Table 6-2, the parameter  $Z$  which is related to microstructure of the composite varied from  $1.1 \cdot 10^{-6}$  to  $4.6 \cdot 10^{-6} \text{ m}^4/\text{N}^2$ . Higher the value for  $Z$ , higher the sensitivity was. Piezoresistive coefficient ( $\Pi_{III}$ ) varied from  $2.5 \cdot 10^{-3}$  to  $9.4 \cdot 10^{-3} \text{ MPa}^{-1}$  at 20 MPa stress level. Likewise, at 35 MPa, it varied from  $4 \cdot 10^{-3}$  to  $23 \cdot 10^{-3} \text{ MPa}^{-1}$ .

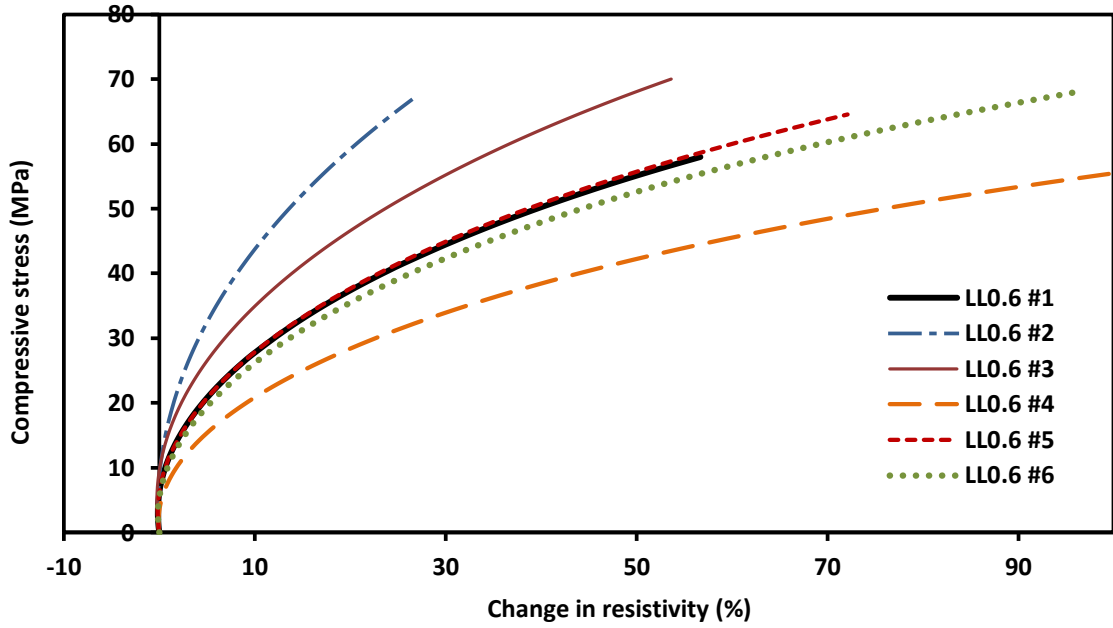


Figure 6-6: Piezoresistive behavior model for epoxy grout

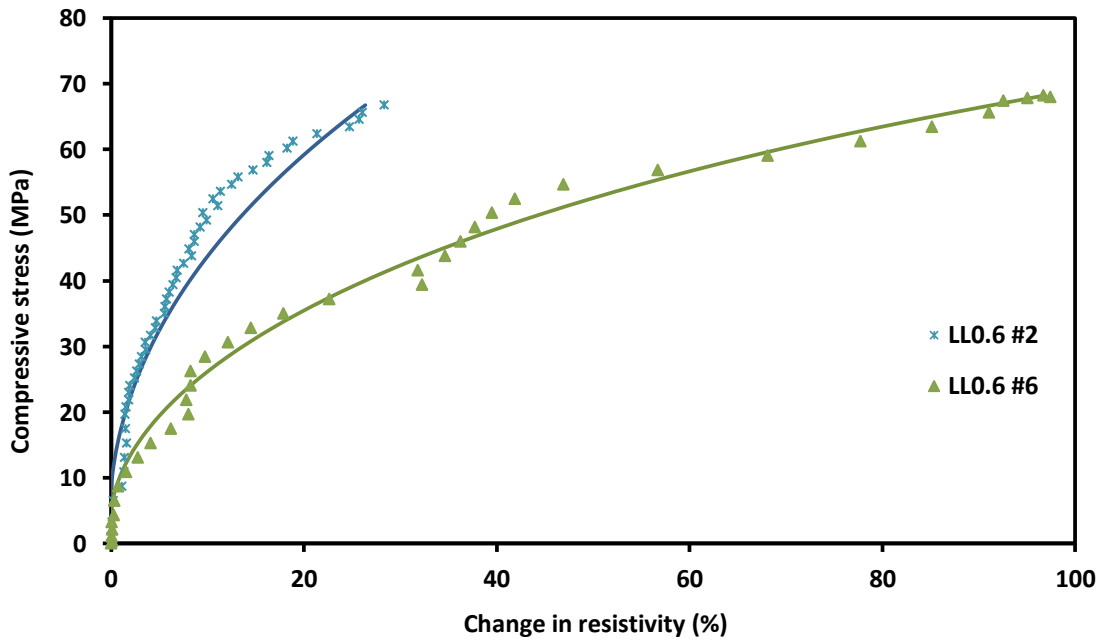


Figure 6-7: Typical piezoresistive behavior model of epoxy grout

**Table 6-2: Piezoresistive coefficients of epoxy grout**

<b>Specimen</b>	<b>Z (m<sup>4</sup>/N<sup>2</sup>)</b>	<b>Π<sub>III</sub> (at 20MPa) (MPa<sup>-1</sup>)</b>	<b>Π<sub>III</sub> (at 35 MPa) (MPa<sup>-1</sup>)</b>
LL 0.6 #1	2.8*10 <sup>-6</sup>	5.5*10 <sup>-3</sup>	11.2*10 <sup>-3</sup>
LL 0.6 #2	1.1*10 <sup>-6</sup>	2.5*10 <sup>-3</sup>	4.0*10 <sup>-3</sup>
LL 0.6 #3	1.9*10 <sup>-6</sup>	3.3*10 <sup>-3</sup>	7.3*10 <sup>-3</sup>
LL 0.6 #4	4.6*10 <sup>-6</sup>	9.4*10 <sup>-3</sup>	23*10 <sup>-3</sup>
LL 0.6 #5	2.7*10 <sup>-6</sup>	5.5*10 <sup>-3</sup>	11.2*10 <sup>-3</sup>
LL 0.6 #6	3.0*10 <sup>-6</sup>	5.9*10 <sup>-3</sup>	13.3*10 <sup>-3</sup>

### **Summary**

Based on the modeling of the behavior,

1. The proposed p-q stress-strain model predicted the stress-strain behavior of grout repair materials very well. It captures the post peak strain hardening portion also.
2. The incremental nonlinear stress-resistivity model predicted the piezoresistive behavior of epoxy grout reasonably well.

## CHAPTER 7 CONCLUSIONS AND RECOMMENDATIONS

### 7.1 Conclusions

This study focused on characterizing the structural and self-monitoring behavior of repair materials. Polymer and cement based structural grouting materials (strengths in the range of 30 to 75 MPa) were modified using carbon fiber to have sensing capabilities. In addition, a real-time application of such smart materials for low stress disaster monitoring was investigated. Also a cementitious repair material typically used in steel pipes as protective coating was investigated to evaluate the field performance in terms of shrinkage, water absorption and strength characteristics. Based on the study the following conclusions can be advanced:

1. Strength of epoxy grout was affected by the addition of carbon fiber. When 0.6% modified fiber was used, strength was reduced by about 15%. On the other hand not much difference was observed in the strength of cement grout with the addition of carbon fiber. Ductility and toughness of both fiber added grouts increased significantly. Failure strain of cement grout doubled with the addition of fiber.
2. Electrical resistivity was a better indicator than engineering strain. At 30 MPa stress level of epoxy grout, resistivity showed a change of 2% while the corresponding change in engineering strain was 0.2%. At half the strength of cement grout, resistivity showed a change of about 6% which is 40 times more than the change in strain. This proved that piezoresistivity was a good self-sensing property of the material. Shape effect on piezoresistivity was studied by testing slab and thin circular disk specimens and it was found that piezoresistive behavior existed despite the shape and size of specimen. When subjected

- to flexural loading resistivity sensed even at small stress levels, which was not evident in the cases for tension or compression.
3. Modification of fiber enabled the reduction in usage of fiber and improved the piezoresistive behavior. At the stress level of 30 MPa, specimen with unmodified fiber showed about 0.3% of change whereas the resistivity of specimen with modified fiber changed by more than 7%. At failure, specimen with modified fiber showed a change of more than 54% while the specimen with short fiber showed a change of 20%.
  4. Piezoresistive behavior of epoxy grout did not change with age when cured in air even though the strength improved by 20% from 3<sup>rd</sup> day to 28<sup>th</sup> day. When subjected to different curing conditions piezoresistive behavior existed but was different than the behavior of air cured specimens. Water cured (25°C) and air cured (at 5°C, 25°C and -15°C) cement grout specimens had almost identical piezoresistive behavior while heat cured (at 55°C) specimens had less sensitivity comparatively.
  5. Concrete material with fly ash showed good piezoresistive behavior and had a clear trend. Comparing the behavior of specimens with class C and class F fly ash, class C fly ash showed more sensitivity with a continuously increasing trend. Addition of class C fly ash with at least 0.5% fiber w/w was efficient and in making the concrete material piezoresistive.
  6. Specially designed cantilever stepped beam configuration was effective in detecting pressure as small as 1.4 kPa (0.2 psi). The cantilever beam internal stresses were magnified by 425 times the applied due to the shape effect so that the change in resistivity in the beam was measurable.

7. A new test protocol was developed to test the cementitious patch material as a tack coat.
  
8. Field coating samples had higher unit weight than laboratory specimens and it was evident from pulse wave velocity measurements also. It was observed that except one, all other samples lost the free water when they were kept at room temperature after subjecting to immersion in water. That particular specimen had a change of about 2% in mass after being immersed in water for about 14 days. This showed that the specimen had a lot of pores in it. Beams specimens made of the same coating material showed potential for shrinkage. Eventually about 8% mass change occurred when the specimens were allowed to loose water. This showed that the material needs modification to avoid the water absorption and shrinkage potential.
  
9. The p-q stress-strain model predicted the stress-strain behavior of grout repair materials very well. It captured the linear behavior and nonlinear behavior very well, especially the post peak strain hardening portion. The incremental nonlinear stress-resistivity model predicted the piezoresistive behavior of epoxy grout reasonably well.

## 7.2 Recommendations

The following suggestions are recommended for future work.

1. Even though piezoresistive characterization was done for the repair materials in this study, more comprehensive study will provide better insights under different loading conditions. It is suggested that tensile and flexural piezoresistive behavior be studied in detail. Also tests at different strain rates should be done as the material, in real time application, might go through different strain rates.
2. Fatigue occurs when a material is subjected to repeated loading and unloading cycles. Since the studied materials also go through such loadings, it is important to study the piezoresistive behavior of those materials under repeated loadings. It is suggested a complete study be done to characterize the piezoresistive behavior under loading unloading cycles.
3. Bonding studies for the patch material showed that bonding is weaker in shear than in tension. Therefore it is recommended that a comprehensive study be done to characterize the shear bonding ability of patch.
4. Mechanical modification of carbon fiber proved to be efficient in bringing down the amount of added fiber and improving the piezoresistive behavior. However there is room for further modification by which the amount of fiber can be reduced further. Also a suitable dispersing agent will improve the uniformity of fiber reinforced composite and might increase the piezoresistive performance. It is suggested that these aspects be studied to make the composites cost effective and efficient self-sensor.

5. As found by the study of cantilever stepped beam, small stresses in the order of 1.4 kPa (0.2 psi) could be sensed by the composite. Different configurations such as a circular disk with extensions (like a ceiling fan) can be tried as different applications suit this.
6. Effect of conductive cable spacing and depth of embedment on the piezoresistive behavior was studied in this work. Also lateral piezoresistive behavior was not studied. It is recommended that those two scenarios be studied to prove that piezoresistive behavior is not affected. Also it is suggested that the effect of nearby metal in piezoresistive behavior of material be studied since it is applicable in areas where grouting is done near the machines.
7. Real-time wireless monitoring was proved as essential for structural health monitoring. There is a need to build a system to get multiple electrical resistance measurements simultaneously in order to get the overall response of a structure. Sometimes measurement at particular locations may be necessary. It is recommended that a monitoring system be designed with minimum instrumentation to get multiple resistance measurements simultaneously while having the options to choose the location remotely.

## REFERENCES

- Abo El-Enein S.A., Kotkata M.F., Hann G.B., Saad M. and Abd El Razek M.M., (1995). "Electrical conductivity of concrete containing silica fume," *Cement and Concrete research*, Vol. 25, No. 8, 1615-1620.
- Al-Qadi I.A., Carpenter S.H., Leng Z., Ozer H. and Trepanier J.S. (2008). "Tack coat optimization for HMA overlays," *Illinois Center for Transportation*, Report ICT-R55.
- American Society of Civil Engineers, (2010). "Minimum Design Loads for Buildings and other Structures". "ASCE 7-10, ISBN: 9780784473283.
- ASTM C496, ASTM Standards, (2004). "Standard Test Method For Splitting Tensile Strength of Cylindrical Concrete Specimens," *Annual Book of ASTM Standards*, Vol: 04.02.
- Basheer P.A.M., Gileece P.R.V., Long A.E. and McCarter W.J., (2002). "Monitoring electrical resistance of concrete containing alternative cementitious materials to assess their resistance to chloride penetration," *Cement & Concrete composites*, 437-449.
- Böger P.L., Wichmann M.H.G., Meyer L.O. and Schulte K., (2008). "Load and health monitoring in glass fiber reinforced composites with an electrically conductive nanocomposite epoxy matrix," *Composites Science and Technology*, Vol. 68, 1886-1894.
- Boschetti-de-Fierro, A., Pardey, R., Savino, V., Muller, A.J., "Piezoresistive Behavior of Epoxy Matrix-Carbon Fiber Composites with Different Reinforcement Arrangements," *Journal of Applied Polymer Science*, Vol. 111, 2009, 2851-2858.
- Carmona F., Canet R. and Delhaes P., (1987). "Piezoresistivity of heterogeneous solids," *Journal of Applied Physics*-61 (7), 2550-2557.
- Chen B., Liu J. and Wu K., (2005). "Electrical responses of carbon fiber reinforced cementitious composites to monotonic and cyclic loading," *Cement & Concrete Research*, Vol. 35, 2183-2191.

- Chen B., Wu K. and Yao W., (2004). "Conductivity of carbon fiber reinforced cement-based composites," *Cement & Concrete composites* 26, 291-297.
- Chen G. and Lin Y. (2004). "Stress-strain-electrical resistance effects and associated state equations for uniaxial rock compression," *International journal of Rock Mechanics & Mining sciences*- Vol. 41, 223-236.
- Choi M.H., Jeon B.H., and Chung I.J., (2000). "The effect of coupling agent on electrical and mechanical properties of carbon fiber/ phenolic resin composites," *Polymer* 41, 3243-3252.
- Chowdhury S. and Basu P.C., (2010). "Strength-Cementitious Material- Water Relationship for proportioning of Fly Ash-Based Concrete," *ACI Materials Journal*, Vol. 107, No. 4, 340-348.
- Chuang Wang, Ke-Zhi Li, He-Jun Li, Geng-Sheng Jiao, Jinhua Lu and Dang-She Hou, (2008). "Effect of carbon fiber dispersion on the mechanical properties of carbon fiber-reinforced cement-based composites," *Materials Science & Engineering* 487, 52-57.
- Chung D.D.L., (1999) "Cement reinforced with short carbon fibers: a multifunctional material," *Composites: Part B: Engineering*, 511-526.
- Chung D.D.L., (2002). "Piezoresistive cement based materials for strain sensing," *Journal of intelligent materials systems and structures*-Vol. 00, 1-11.
- Durand S. and Tellier C., (1996). "Linear and Non-Linear Piezoresistance Coefficients in Cubic Semiconductors. I-Theoretical Formulations," *Journal of Physics III France*- 6, 237-266.
- Hui Li, Hui-gang Xiao, and Jin-ping Ou, (2006). "Effect of compressive strain on electrical resistivity of carbon black-filled cement-based composites," *Cement & Concrete composites* 28, 824-828.
- Kalantari M., Dargahi J., Kovacs J., Mardasi M.G., and Nouri S., "A New Approach for Modeling Piezoresistive Force Sensors Based on Semi-conductive Polymer Composites," *IEEE/ASME Transactions on Mechatronics*-1, 1-10.

- Kawashima S. and Shah S.P., (2011). "Early age autogenous and drying shrinkage behavior of cellulose fiber reinforced cementitious materials," *Cement & Concrete Composites* 33, 201-208.
- Kiremidjian A.S., Straser E.G., Meng T., Law K., and Soon H., (1997). "Structural damage monitoring for Civil Structures," *Structural Health Monitoring: Current Status and Perspectives, edited by Fu-Kuo Chang*, USA.
- Ku-Herrera J.J. and Aviles F., (2012). "Cyclic tension and compression piezoresistivity of carbon nanotube/vinyl ester composites in the elastic and plastic regimes," *Carbon*, Vol. 50, 2592-2598.
- Lian-zhen Xiao, Zong-jin Li and Xizo-sheng Wei, (2007). "Selection of superplasticizer in concrete mix design by measuring the early electrical resistivity of pastes," *Cement & Concrete Composites* 29, 350-356.
- Lim Siong Kang and Mohd Warid Hussin, (2008). "Effect of filler on strength development of Epoxy grout," *Malaysian Journal of Civil engineering*, 38-46.
- Liu J. and Vipulanandan C. (2005). "Tensile bonding strength of epoxy coatings to concrete substrate," *Cement and Concrete Research*, Vol. 35, 1412-1419.
- Manuela Chiarello, and Raffaele Zinno, (2004) "Electrical conductivity of self-monitoring CFRC," *Cement & Concrete composites* 27, 463-469.
- Mason, T.O., Campo, M.A., Hixson, A.D., Woo, L.Y., "Impedance Spectroscopy of Fiber-Reinforced Cement Composites," *Cement and Concrete Composites*, Vol. 24, Issue 5, 2002, 457-465.
- McCarter W.J., Chrisp T.M., Starrs G., Basheer P.A.M. and Blewett J. (2005). "Field monitoring of electrical conductivity of cover-zone concrete," *Cement & Concrete Composites*, Vol. 27, 809-817.

- Mohammad, L. N., Raqib, A. M., Baoshan, H., (2002). "Influence of Asphalt Tack Coat Materials on Interface Shear Strength," *Transportation Research Record 1789*, Paper No. 02-3301, 56-65.
- Narmluk M., and Nawa T. (2011). "Effect of fly ash on the kinetics of portland cement hydration at different curing temperatures," *Cement and Concrete Research* 41, 579-589.
- Ogi K., Inoue H. and Takao Y., (2008). "An electromechanical model for the temperature dependence of resistance and piezoresistance behavior in a CFRP unidirectional laminate," *Composites Science and Technology*-68, 433-443.
- Park J.B., Okabe T., Takeda N., and Curtin W.A., (2002). "Electromechanical modeling of unidirectional CFRP composites under tensile loading condition," *Composites: Part A*, Vol. 33, 267-275.
- Prashanth P. and Vipulanandan C., (2010). "Characterization of Thin Disk Piezoresistive Smart Material for Hurricane Applications," 2009 *THC Conference Proceedings*, [http://egr.uh.edu/hurricane/events/pdf\\_2009conf/pdf\\_poster/PRASHANT.pdf](http://egr.uh.edu/hurricane/events/pdf_2009conf/pdf_poster/PRASHANT.pdf) (accessed May 17, 2012).
- Prashanth P., (2010). "Impedance Spectroscopy Characterization of Piezoresistive Structural Sensors and Microbial Fuel Cells," *MS Thesis-Dept. of Electrical and Computer Eng., University of Houston, Houston, Texas*.
- Reza, F., Batson, G.B., Yamamuro, J.A., Lee, J.S., "Resistance Changes During Compression of Carbon Fiber Cement Composites," *Journal of Materials in Civil Engineering*, Vol. 15, No. 5, 2003, 476-483.
- Robeyst N., Gruyaert E., Grosse C.U., and De Relie N., (2008). "Monitoring the setting of concrete containing blast furnace slag by measuring the ultrasonic p-wave velocity," *Cement & Concrete Research* 2008, 1169-1176.
- Romanoschi, A. S., Metcalf B. J., (2001). "Characterization of Asphalt Concrete Layer Interfaces," *Transportation Research Record 1778*, Paper No. 01-2080.

- Sahin, M. Y., Kirchner, K. and Blackmon W. E., (1987) "Analysis of Asphalt Concrete Layer Slippage and Its Effect on Pavement Performance and Rehabilitation Design," *Proc., 6<sup>th</sup> International Conference on the Structural Design of Asphalt Pavements*, University of Michigan, Ann Arbor.
- Sahmaran M., Lachemi M.X., Hossain K.M.A., and Li V.C. (2009). "Internal curing of engineered cementitious composites for prevention of early age autogenous shrinkage cracking," *Cement & Concrete Research* 39, 893-901.
- Sett K., (2003). "Characterization and Modeling of Structural and Self-Monitoring Behavior of Fiber Reinforced Polymer Concrete," *MS Thesis-Dept. of Civil and Environ. Eng., University of Houston, Houston, Texas*, 52-55 and 99-114.
- Sevkat E., Li J., Liaw B. and Delale F. (2008). "A statistical model of electrical resistance of carbon fiber reinforced composites under tensile loading," *Journal of Composite Science and Technology*-Vol. 68, 2214-2219.
- Sihai Wen and Chung D.D.L., (2007). "Double percolation in the electrical conduction in carbon fiber reinforced cement based material," *Carbon* 45, 263-267.
- Termkhajornkit P., Nawa T., Yamashiro Y., and Saito T., (2009). "Self-healing ability of fly ash-cement systems," *Cement & Concrete composites* - Vol. 31, 195-203.
- Todoroki A., Samejima Y., Hirano Y. and Matsuzaki R., (2009). "Piezoresistivity of unidirectional carbon/epoxy composites for multi-axial loading," *Composites Science and Technology*-69, 1841-1846.
- Vipulanandan C. and Paul E., (1990). "Performance of Epoxy and Polyester Polymer Concrete," *ACI Materials J.*, Vol. 87(3), 241-251.
- Vipulanandan C. and Sett K., (2004). "Development and characterization of piezoresistive smart structural materials," *ASCE Earth & Space*, 656-663.
- Vipulanandan, C. and Parihar, A. (2009). "Bonding Strength of Tack Coat to Cement Concrete Pavement," *Proceedings, ASCE Texas Section*, October 2009.

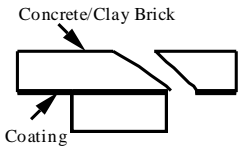
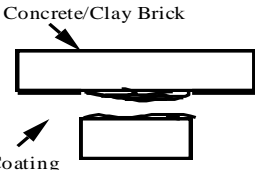
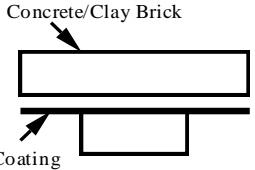
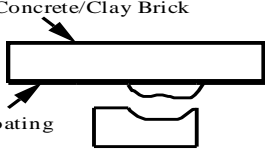
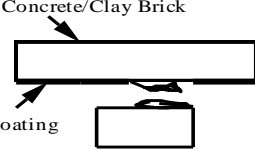
- Waterfall T.L, Johns G.K., Messenger R.K., Jensen B.D., McLain T.W. and Howell L.L. (2008). "Observations of piezoresistivity for polysilicon in bending that are unexplained by linear models," *Sensors and Actuators A*, Vol. 141, 610-618.
- Wen S. and Chung D.D.L. (2007). "Partial replacement of carbon fiber by carbon black in multifunctional cement–matrix composites," *Carbon*, Vol. 45, 505-513.
- Wille K., Naaman A.E. and Parra-Montesinos G.J., (2011). "Ultra-High Performance Concrete with Compressive Strength Exceeding 150 MPa (22 ksi): A Simpler Way," *ACI Materials Journal*, Vol. 108, No. 1, 46-54.
- Xu M.X. Liu W.G., Gao Z.X., Fang L.P. and Yao K.D. (1996). "Correlation of Change in Electrical Resistance with Strain of Carbon Fiber-Reinforced Plastic in Tension," *Journal of Applied Polymer Sciences*-Vol. 60, 1595-1599.
- Yang, C.Q., Wu, Z.S. and Huang, H., (2007). "Electrical properties of different types of carbon fiber reinforced plastics (CFRPs) and hybrid CFRPs," *Carbon-45*, 3027-3035.
- Zhang Dianjun, Wang Qiang, Xu Shilang., (2007) "Experimental study on electrical properties of carbon fiber reinforced concrete," *Journal of Wuhan Univ of technology - Mater.Sci-Ed* vol.22 No.3, 546-550.

## APPENDIX

### A-1 Bonding Failure Modes

Five types of failure modes were observed by Liu and Vipulanandan (2005) in tensile bonding test for coating materials which are summarized in Table A-1.

**Table A-1: Failure modes in tensile bonding strength test (Liu and Vipulanandan, 2005)**

Failure Type	Description	CIGMAT CT-3 Test
Type-1	Substrate Failure	 <p>Concrete/Clay Brick</p> <p>Coating</p>
Type-2	Coating/Mortar Failure	 <p>Concrete/Clay Brick</p> <p>Coating</p>
Type-3	Bonding Failure	 <p>Concrete/Clay Brick</p> <p>Coating</p>
Type-4	Bonding and Substrate Failure	 <p>Concrete/Clay Brick</p> <p>Coating</p>
Type-5	Bonding and Coating/Mortar Failure	 <p>Concrete/Clay Brick</p> <p>Coating</p>

## A-2 Impedance Spectroscopy (IS)

Two-probe method was used in this current study to measure electrical resistance of specimens. Unlike four-probe method, contact resistance is present in two-probe method. However preliminary studies using Impedance Spectroscopy (IS) showed that contact resistance is less than 1% of the bulk resistance and therefore not significant. An approach used by Prashanth (2010) was employed for the investigation.

Prashanth (2010) proposed an equivalent circuit (as shown in Figure A-1) to represent the piezoresistive structural sensor (PRSS) in terms of electrical resistance and capacitance. In the equivalent circuit, the PRSS was represented by a resistor ( $R_m$ ) and the contacts of the embedded electrodes were represented by resistor ( $R_c$ ) and capacitor ( $C_c$ ) in parallel. Impedance ( $Z$ ) of the equivalent circuit system can be given as,

$$Z = R_m + \frac{2R_c}{1 + \omega^2 R_c^2 C_c^2} - j \frac{2\omega R_c^2 C_c}{1 + \omega^2 R_c^2 C_c^2}. \quad (\text{A-1})$$

In Eqn. A-1,  $\omega$  is directly proportional to frequency ( $\omega=2\pi f$ ). When the frequency of the applied signal is very low,  $\omega \rightarrow 0$ ,  $Z = R_m + 2R_c$  and when the frequency is very high,  $\omega \rightarrow \infty$ ,  $Z = R_m$ .

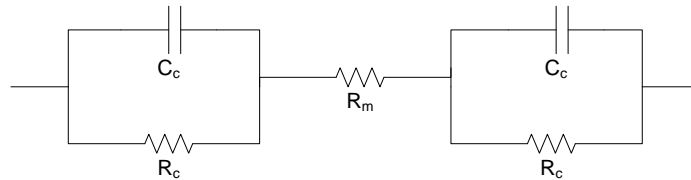


**Figure A-1: Equivalent circuit representing piezoresistive structural sensor**

An arrangement for IS test is shown in the schematic in Figure A-2. Frequencies from 0.1 Hz to 100 kHz can be applied to PRSS using a frequency generator and the resistance values can be measured simultaneously. When low frequency (0.1 Hz) is applied, Ohm meter will read the

bulk resistance plus twice the contact resistance. On the other hand, when higher frequency (100 kHz) is applied to PRSS, only the bulk resistance will be read. From those two measurements, contact resistance of the PRSS can be calculated. By carrying out this procedure, contact resistance was calculated in the current study and it was negligible compared to bulk resistance. Thus, two-probe method was good enough for the intended applications.

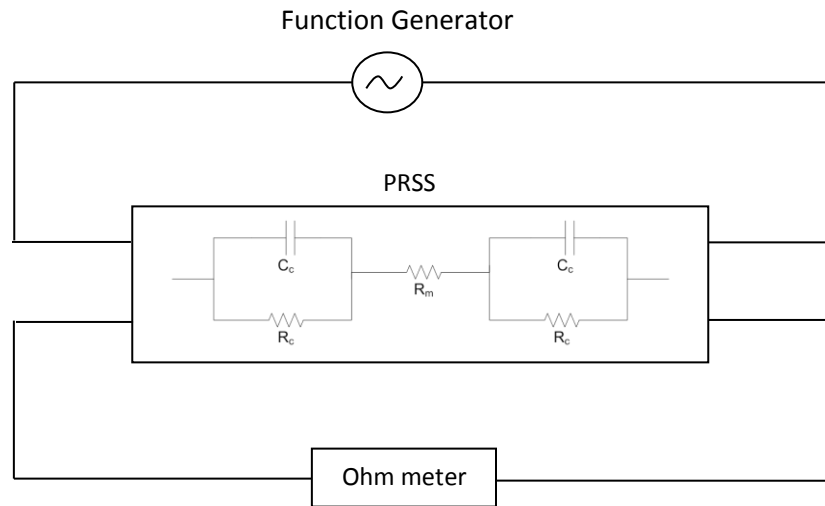


**Figure A-2: Schematic diagram of the IS testing arrangement with ohm meter**

### A-3 Effect of Environmental Conditions on Piezoresistivity

#### (a) Materials and Methods

Cement grout (MM) specimens and epoxy grout (LL) cylindrical specimens (with 1.5” diameter) were prepared with 0.1% and 0.6% (by wt.) carbon fiber loading respectively to study the effect of (i) temperature cycle and (ii) wet-dry cycle on the piezoresistive behavior. During the wet-dry cycles, specimens were subjected to wet condition one day and dry condition the next day. This was continued for 2 weeks. To introduce the wet condition, specimens were immersed in water at room temperature (25°C). Likewise, specimens were air cured at room temperature during dry cycle. For temperature cycles, specimens were cured in air at 60°C and 25°C for a day alternatively. Mass and electrical resistance of the specimens were monitored before beginning the cycles and at the end of each cycle. Table A-2 summarizes the different curing conditions applied to the specimens. Four specimens in each type of grout were subjected to temperature cycle as well as wet-dry cycle. Epoxy grout specimens were cured for 3 days before subjecting to the cycles. Likewise, cement grout specimens were subjected to temperature and wet-dry cycles after 2 days of curing.

**Table A-2: Testing conditions for the piezoresistive grout specimens**

Cycle	Condition	Medium	Temperature	Specimen #
Temperature cycle	Hot	Air	60°C	MM #1, #2, #3, #4
	Room	Air	25°C	LL #1, #2, #3, #4
Wet-Dry cycle	Wet	Water	25°C	MM #5, #6, #7, #8
	Dry	Air	25°C	LL #5, #6, #7, #8
Control specimens		Air	25°C	MM #9, #11 LL #9, #10

#### (b) Testing

In Tables A-3 and A-4, unit weight and initial electrical resistance of LL and MM specimens before piezoresistivity testing is summarized. Also electrical resistance values before testing for piezoresistivity are provided. As summarized in the tables, two (#1 and #2) out of four

specimens subjected to temperature cycles were tested after heat cycles (60°C in air) being the final one. The other two specimens (#3 and #4) were tested after a cool cycle (25°C in air) as the final cycle. In the case of wet-dry cycles, specimens denoted as #5 and #6 were tested after finishing in wet cycles (25°C in water) while specimens #7 and #8 were tested after dry cycle (25°C in air). Two control specimens which were air cured at 25°C throughout the cycling period were also tested for both LL and MM.

**Table A-3: Summary of cement grout (MM) specimens tested for piezoresistivity**

Specimen	#	Applied cycle	Unit weight (kg/m <sup>3</sup> )	Electrical resistance (Ohms)	Comments on piezoresistivity test
Cement grout (MM)	1	Temperature cycle (7 cycles)	1814	343	Final cycle was a heat cycle (60°C in air)
	2		1840	574	
	3		1935	378	Final cycle was a cool cycle (25°C in air)
	4		1857	469	
	5	Wet-Dry cycle (7 cycles)	2044	826	Final cycle was a wet cycle (25°C in water)
	6		2048	581	
	7		2078	905	Final cycle was a dry cycle (25°C in air)
	8		2057	474	
	9	Control	1969	523	Specimens were air cured at 25°C all the time
	11		1960	406	

**Table A-4: Summary of epoxy grout (LL) specimens tested for piezoresistivity**

Specimen	#	Applied cycle	Unit weight (kg/m <sup>3</sup> )	Electrical resistance (Ohms)	Comments on piezoresistivity test
Epoxy grout (LL)	1	Temperature cycle (7 cycles)	2022	5300	Final cycle was a heat cycle (60°C in air)
	2		2094	4593	
	3		2008	1059	Final cycle was a cool cycle (25°C in air)
	4		2105	1315	
	5	Wet-Dry cycle (7 cycles)	2150	722	Final cycle was a wet cycle (25°C in water)
	6		2063	1009	
	7		2073	1216	Final cycle was a dry cycle (25°C in air)
	8		2127	1060	
	9	Control	2065	758	Specimens were air cured at 25°C all the time
	10		2124	796	

**(c) Results**

Compressive strength ( $\sigma$ ) and changes in electrical resistance ( $\Delta R$ ) and mass ( $\Delta M$ ) are summarized in Table A-5 for epoxy grout and cement grout specimens after subjecting them to the test cycles.

**Table A-5: Summary of strength ( $\sigma$ ) and changes in resistance ( $\Delta R$ ) and mass ( $\Delta M$ ) after 7 cycles**

	After temperature cycles				After wet-dry cycles			
	Specimen	$\sigma$ (MPa)	$\Delta R$ (%)	$\Delta M$ (%)	Specimen	$\sigma$ (MPa)	$\Delta R$ (%)	$\Delta M$ (%)
<b>Epoxy grout</b>	LL #1	62.8	41.2	-0.05	LL #5	52.4	1.0	-0.05
	LL #2	65.9	34.7	0.05	LL #6	43.8	15.3	0.18
	LL #3	47.8	64.7	0.00	LL #7	49.4	8.7	0.04
	LL #4	50.8	41.2	-0.10	LL #8	44.6	18.1	0.00
<b>Cement grout</b>	MM #1	28.4	2.3	-8.46	MM #5	30.6	25.9	1.73
	MM #2	27.3	13.4	-8.68	MM #6	32.2	9.6	1.71
	MM #3	24.6	5.0	-8.89	MM #7	32.4	13.4	1.63
	MM #4	17.5	16.2	-8.45	MM #8	30.6	13.1	1.71
<b>Control</b>	<b><math>\sigma</math> of air cured specimens, (MPa)</b>		Epoxy grout (LL) ←		<b><math>\sigma</math> of air cured specimens, (MPa)</b>		Cement grout (MM) ←	
	LL #9	54.0			MM #9	23.0		
	LL #10	52.8			MM #11	34.1		

Variation of mass of the epoxy grout (LL) and cement grout (MM) specimens after temperature cycle and wet-dry cycle are shown in Figures A-3 through A-6. The changes are normalized with respect to the initial values at the beginning of cycles. Day 0 was the start of heat cycle or wet cycle. As shown in Figures A-4 and A-6, minimal changes were observed in the mass of LL specimens under both cycles. However, MM specimens showed increase in mass under wet-dry cycles. After 7 temperature cycles, more than about 8.5% decrease in mass was observed as shown in Figure A-3. Likewise, after 7 wet-dry cycles, more than 1.5% increase in mass was observed in the MM specimens (Figure A-5).

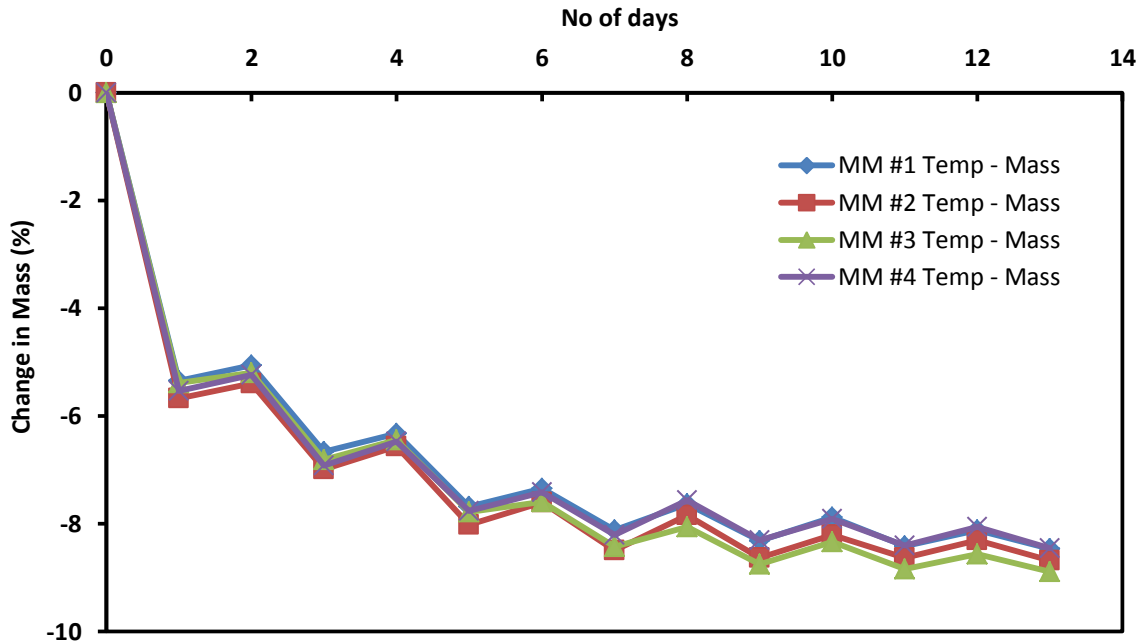


Figure A-3: Variation of Mass in cement grout specimens under temperature cycles

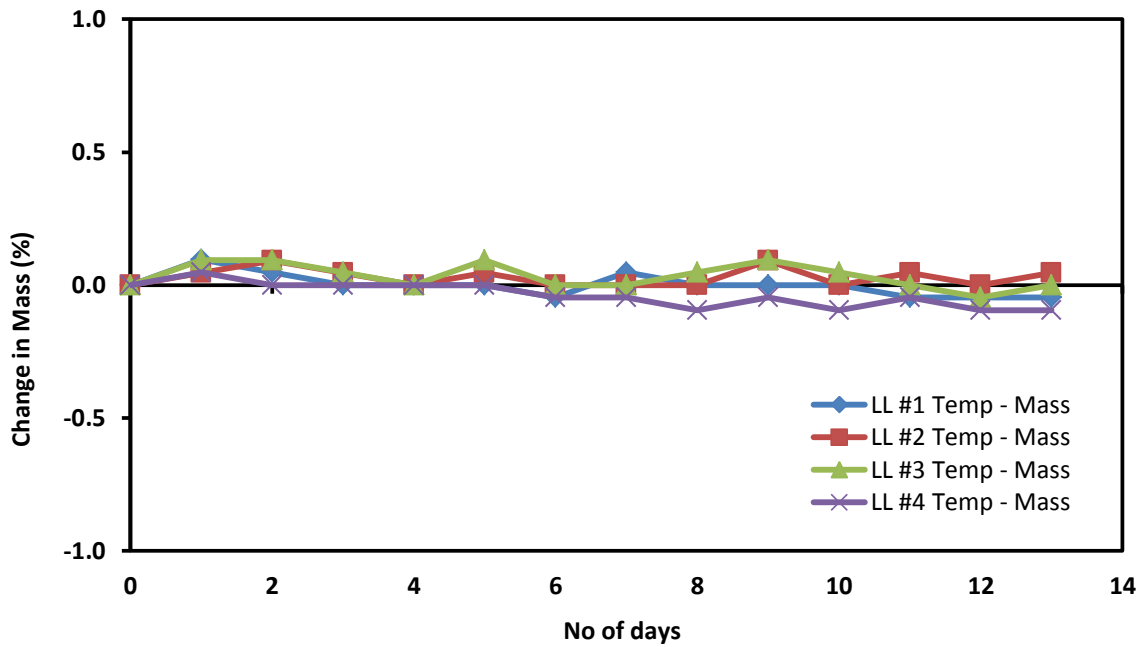


Figure A-4: Variation of Mass in epoxy grout specimens under temperature cycles

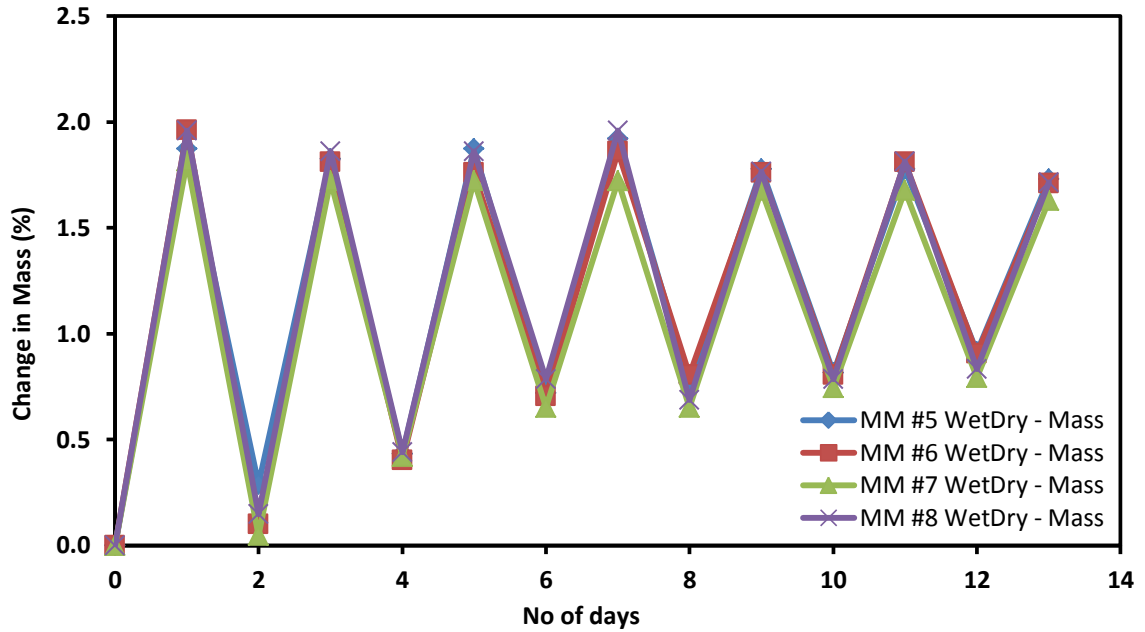


Figure A-5: Variation of Mass in cement grout specimens under wet-dry cycles

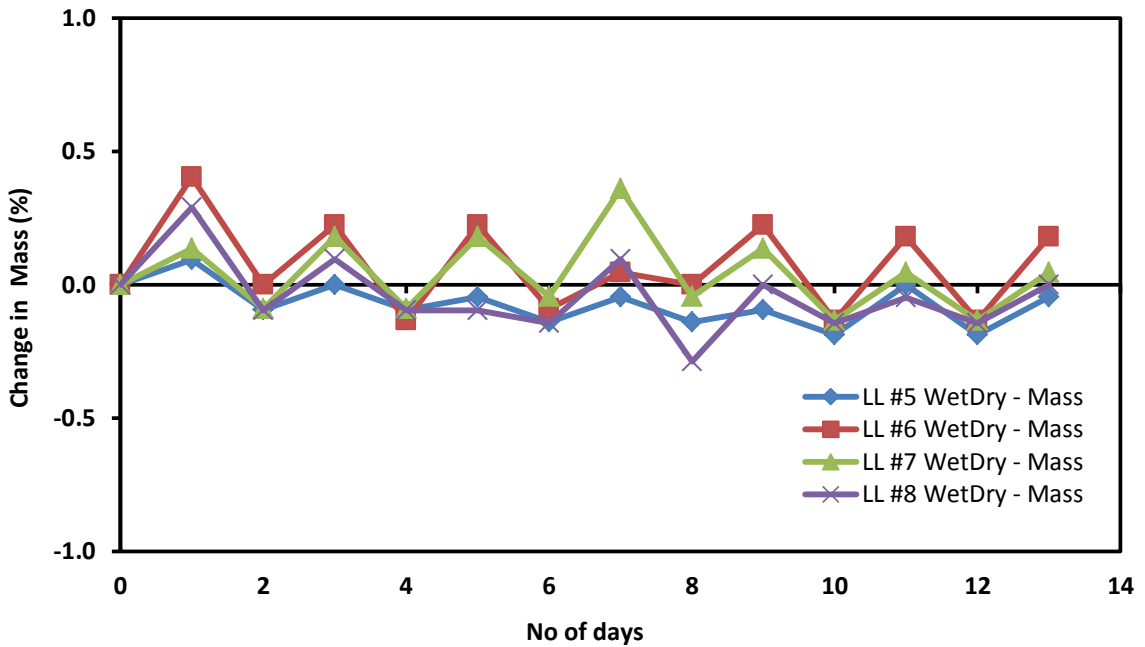
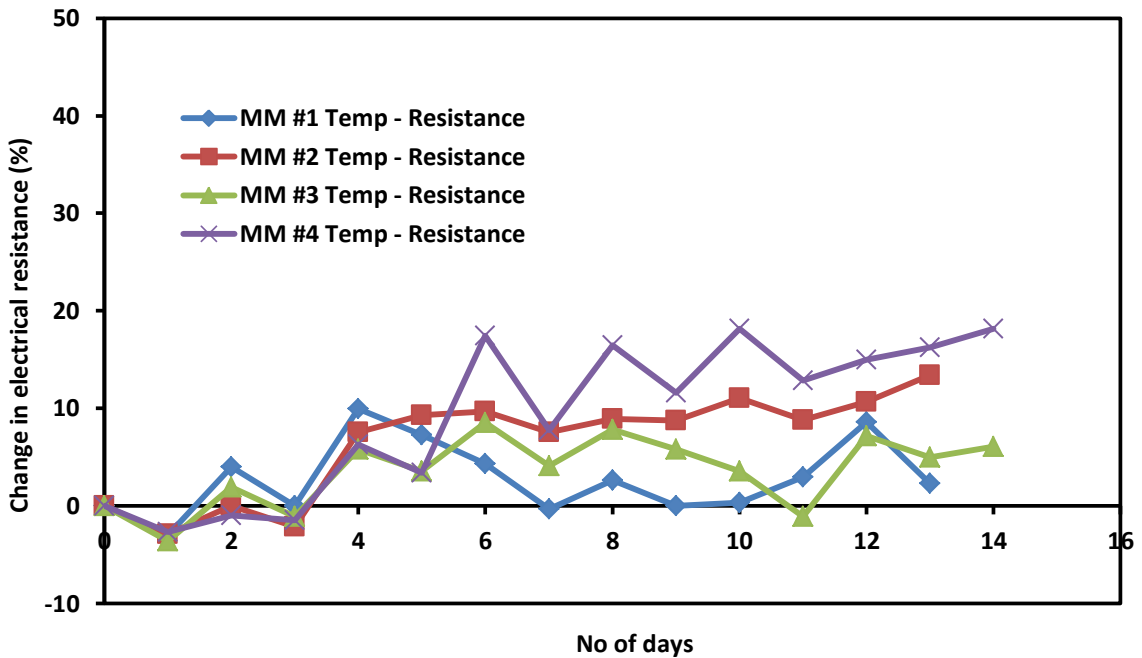


Figure A-6: Variation of Mass in epoxy grout specimens under wet-dry cycles

Variation of electrical resistance of the LL and MM specimens after temperature cycle and wet-dry cycle are shown in Figures A-7 through A-10. The resistance values are normalized

with respect to the initial values at the beginning of cycles. As shown in the figures, both LL and MM specimens were sensitive to the changes occurring inside and outside of them while subjected to different curing conditions. As shown in Figure A-8, LL specimen under temperature cycles showed higher changes in electrical resistance initially before leveling off. A change of more than 60% was monitored after 1st heat cycle. As shown in Figures A-9 and A-10, an increasing and then decreasing trend was monitored for specimens under wet-dry cycles. This indicated that electrical resistivity of specimens is a good measure to sense the changes occurring in the specimens which are subjected to intermittent environmental conditions.



**Figure A-7: Variation of electrical resistance in cement grout specimens under temperature cycles**

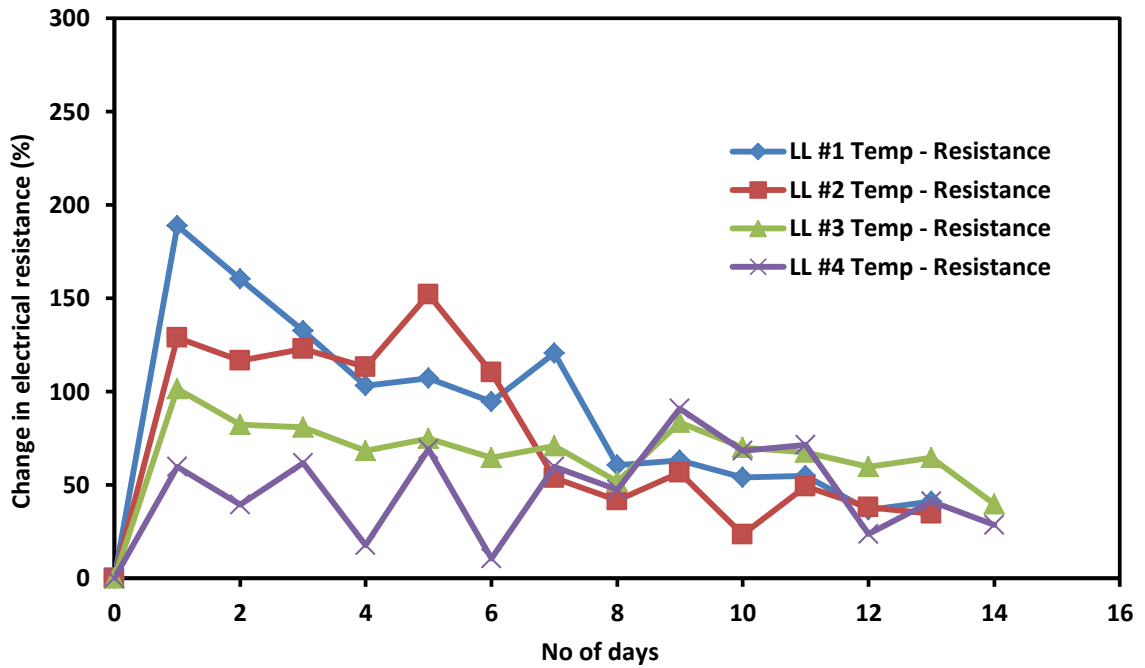


Figure A-8: Variation of electrical resistance in epoxy grout specimens under temperature cycles

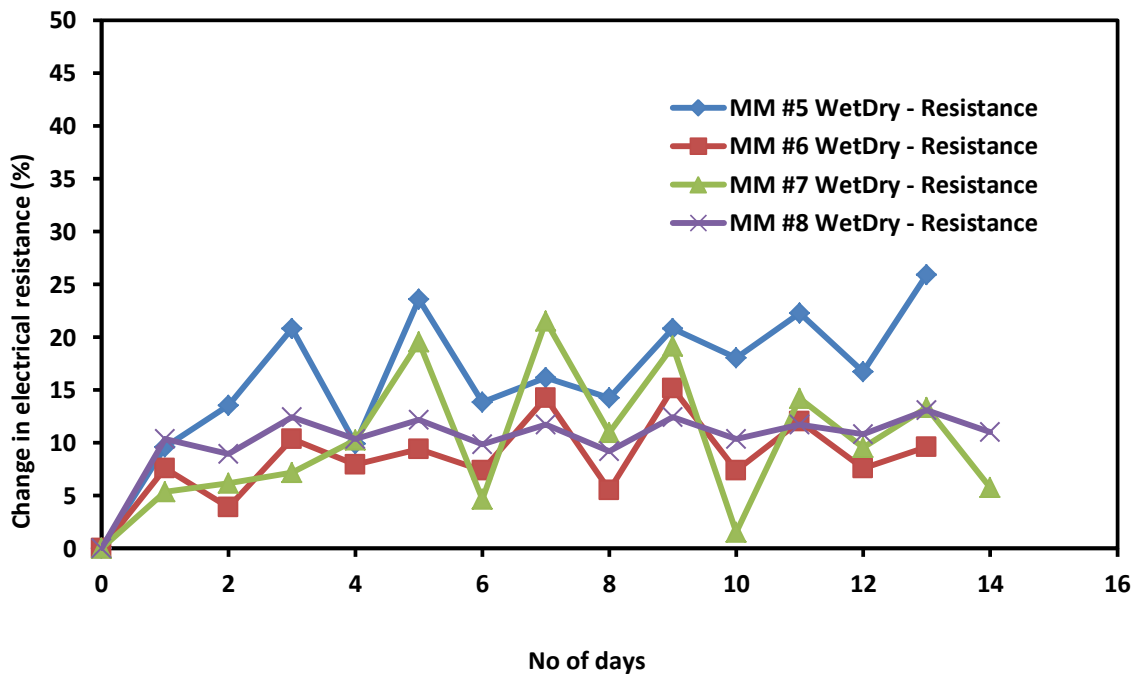
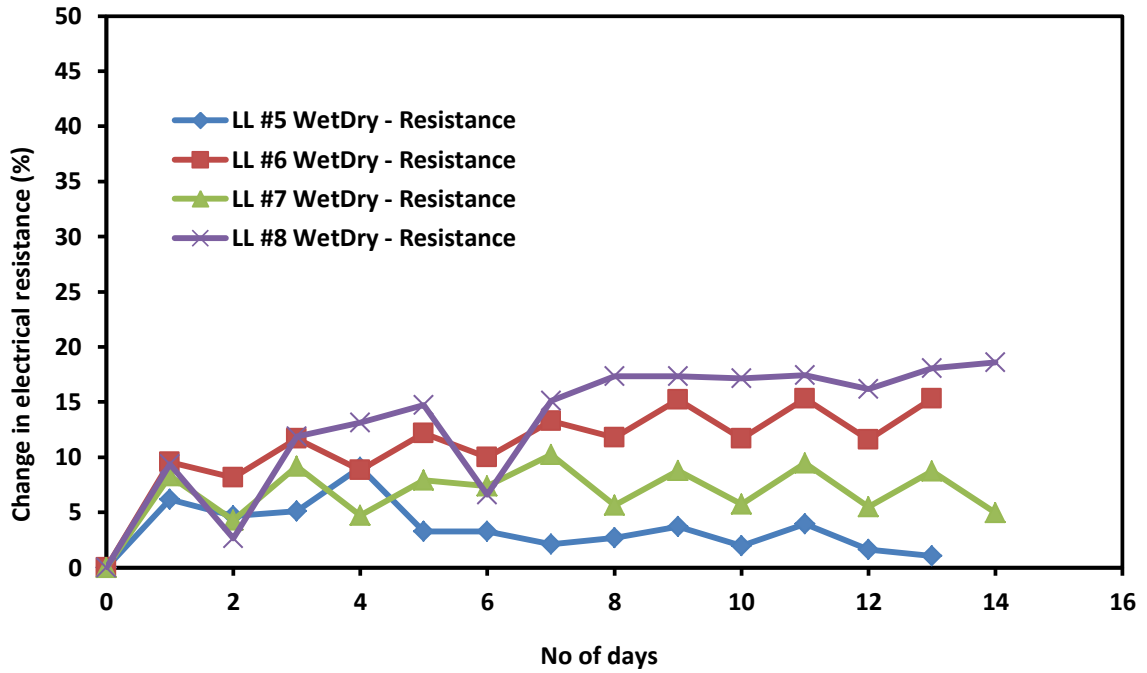
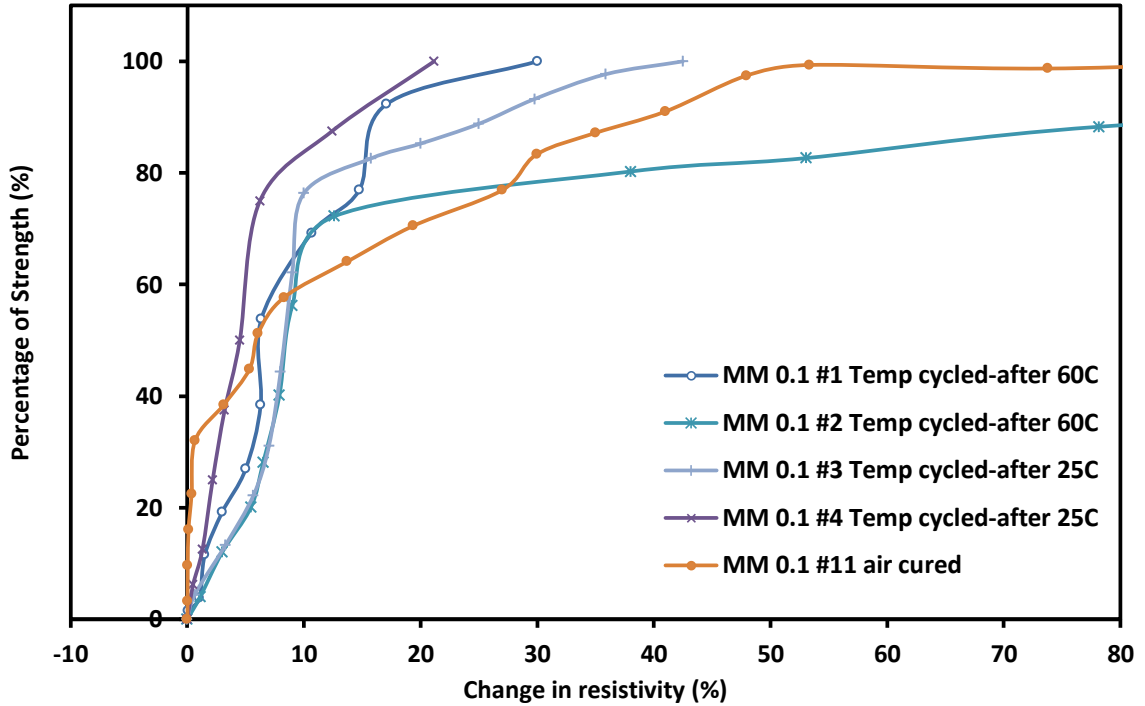


Figure A-9: Variation of electrical resistance in cement grout specimens under wet-dry cycles



**Figure A-10: Variation of electrical resistance in epoxy grout specimens under wet-dry cycles**

Piezoresistive behavior of MM specimens after temperature cycles and wet-dry cycles are shown in Figures A-11 and A-12 respectively. Likewise piezoresistive behaviors of LL specimens are shown in Figures A-13 and A-14. As shown in Figure A-11, MM specimens after temperature cycles showed good piezoresistive behavior. Especially at low stress levels, those specimens were very sensitive compared to the control specimens. At 20% of the strength, electrical resistivity of the specimens changed by more than 2%. Likewise at 60% of the strength, changes over 6% were monitored.



**Figure A-11: Stress-Resistivity relationship for cement grout specimens after temperature cycles**

Piezoresistive behavior of MM specimens after wet-dry cycles is shown in Figure A-12. Specimens had piezoresistive behavior. Two specimens that were tested after final cycle of wetting were more sensitive than the others. Piezoresistive behavior of LL specimens after temperature cycles and wet-dry cycles is shown in Figures A-13 and A-14 respectively. Specimens had piezoresistive behavior after both temperature and wet-dry cycles. As shown in Figure A-13, specimens which were finally heat cured (#1 and #2) showed very good piezoresistive response.

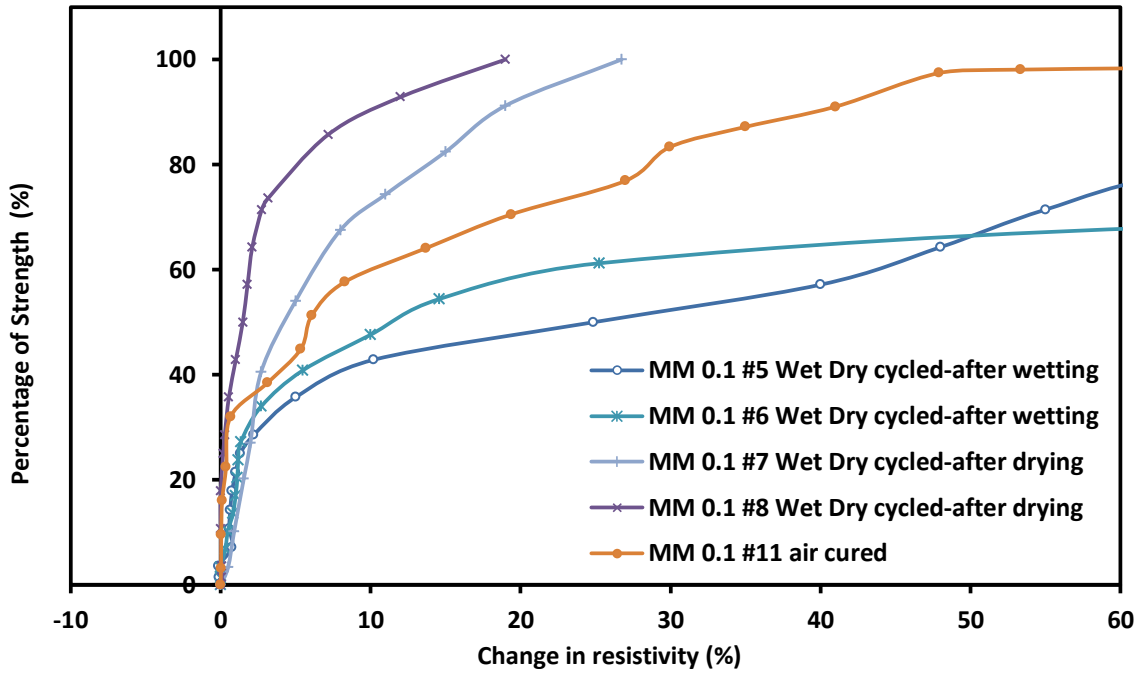


Figure A-12: Stress-Resistivity relationship for cement grout specimens after wet-dry cycles

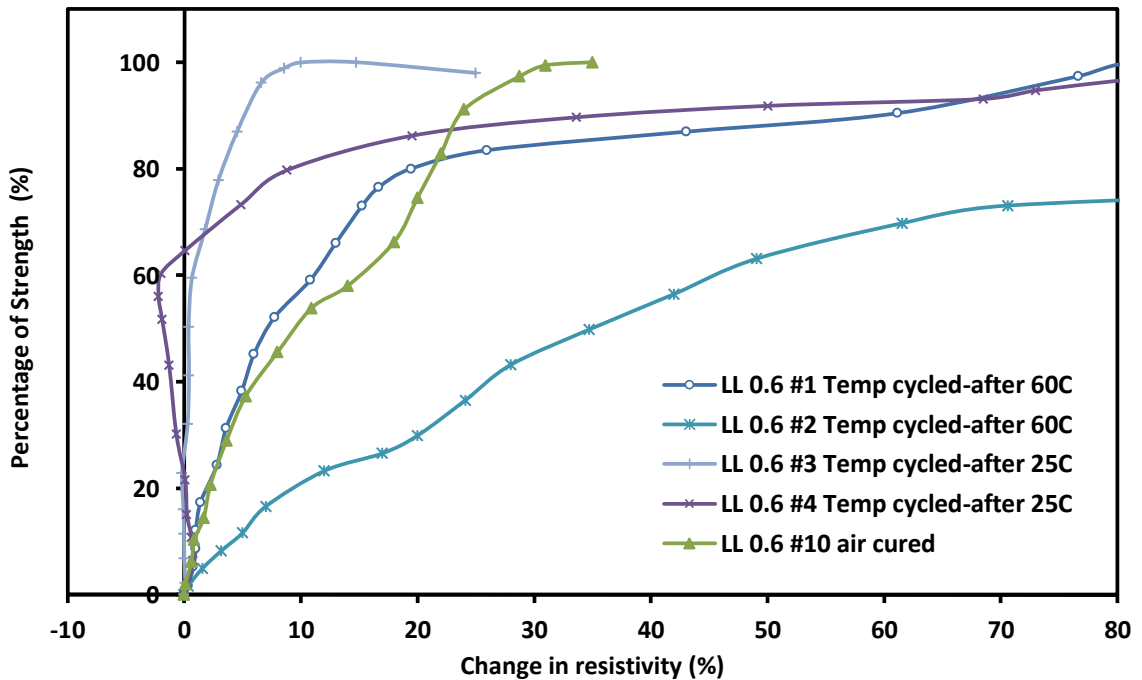
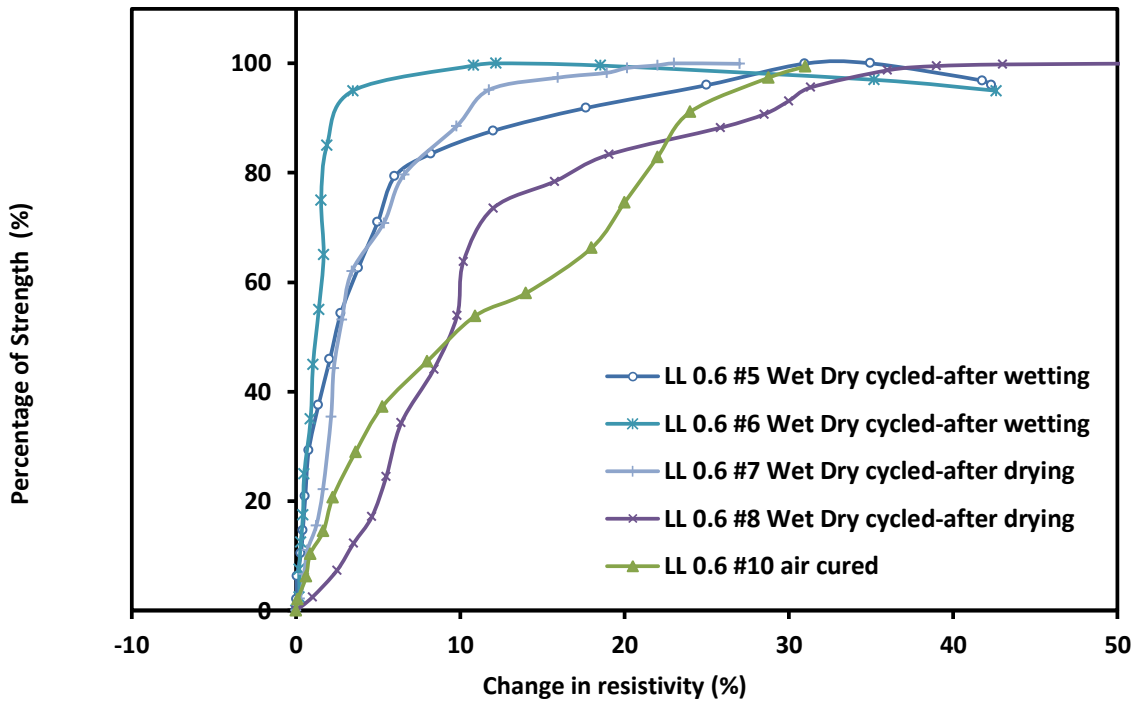


Figure A-13: Stress-Resistivity relationship for epoxy grout specimens after temperature cycles



**Figure A-14: Stress-Resistivity relationship for epoxy grout specimens after wet-dry cycles**

In Table A-6, change in electrical resistivity of epoxy grout and cement grout specimens at selected stress levels are presented. Changes at the following percentage of strength are summarized; 25%, 50%, and 75% of strength, and at failure.

**Table A-6: Change in resistivity ( $\Delta\rho/\rho_0$ ) at certain percentage of strength for epoxy grout and cement grout specimens after subjecting to temperature cycles and wet-dry cycles**

	$(\Delta\rho/\rho_0)$ after temperature cycles, (%)					$(\Delta\rho/\rho_0)$ after wet-dry cycles, (%)				
	% strength	25%	50%	75%	failure	% strength	25%	50%	75%	failure
<b>Epoxy grout</b>	LL #1	3	7	16	82	LL #5	0.5	1.5	5.5	35
	LL #2	14	35	108	575	LL #6	0.5	1.1	1.6	19
	LL #3	-0.5	0.4	2.5	25	LL #7	1.8	2.3	6	23
	LL #4	-0.5	-2	6	80	LL #8	5.5	9.2	13	43
<b>Cement grout</b>	MM #1	4.5	6	14	30	MM #5	1	25	59	185
	MM #2	6	8.5	18	200	MM #6	1	11	160	205
	MM #3	6	8.5	10	42	MM #7	2	4	11	27
	MM #4	2	4.5	6	21	MM #8	0.3	1.5	3.5	19
<b>Control</b>	$(\Delta\rho/\rho_0)$ after air cured at 25°C, (%)					$(\Delta\rho/\rho_0)$ after air cured at 25°C, (%)				
	LL #9	0.5	1	3	5	MM #9	0.3	1	4.5	47
	LL #10	3	9.5	20	35	MM #11	0.5	6	25	104

### Summary

Based on the experimental study, following observations are advanced.

1. Both epoxy grout (LL) and cement grout (MM) showed piezoresistive behavior after the temperature cycle and wet-dry cycle tests.
2. For the epoxy grout, piezoresistivity increased with temperature cycle. Wet-dry cycle did not reduce the piezoresistivity at failure.
3. For the cement grout, piezoresistivity increased with temperature cycle, especially at low stress levels. Also piezoresistivity at failure was higher after wet-dry cycles.